

UC Berkeley
SEMM Reports Series

Title

Stochastic finite element methods and reliability: a state-of-the-art report

Permalink

<https://escholarship.org/uc/item/3d606904>

Authors

Sudret, Bruno

Der Kiureghian, Armen

Publication Date

2000-11-01

Stochastic Finite Element Methods and Reliability

A State-of-the-Art Report

by

Bruno Sudret and Armen Der Kiureghian

A report on research supported by
Electricité de France
under Award Number D56395-T6L29-RNE861

Report No. UCB/SEMM-2000/08
Structural Engineering, Mechanics and Materials
Department of Civil & Environmental Engineering
University of California, Berkeley

November 2000

TA 160
4
R44
2000:8
ENG 1

Acknowledgements

This research was carried out during the post-doctoral stay of the first author at the Department of Civil & Environmental Engineering, University of California, Berkeley.

This post-doctoral stay was supported by *Ecole Nationale des Ponts et Chaussées* (Marne-la-Vallée, France) and by *Electricité de France* under Award Number D56395-T6L29-RNE861 to the University of California at Berkeley. These supports are gratefully acknowledged.

Contents

Part I : Review of the literature	1
1 Introduction	3
1 Classification of the stochastic mechanics approaches	4
2 Outline	5
2 Methods for discretization of random fields	7
1 Generalities	7
1.1 Probability space and random variables	7
1.2 Random fields and related Hilbert spaces	8
2 Point discretization methods	10
2.1 The midpoint method (MP)	10
2.2 The shape function method (SF)	10
2.3 The integration point method	11
2.4 The optimal linear estimation method (OLE)	11
3 Average discretization methods	13
3.1 Spatial average (SA)	13
3.2 The weighted integral method	14
4 Comparison of the approaches	15
5 Series expansion methods	17
5.1 Introduction	17
5.2 The Karhunen-Loève expansion	19

5.2.1	Definition	19
5.2.2	Properties	20
5.2.3	Resolution of the integral eigenvalue problem	21
5.2.4	Conclusion	22
5.3	Orthogonal series expansion	23
5.3.1	Introduction	23
5.3.2	Transformation to uncorrelated random variables	24
5.4	The EOLE method	25
5.4.1	Definition and properties	25
5.4.2	Variance error	26
6	Comparison between KL, OSE, EOLE	26
6.1	Early results	26
6.1.1	EOLE <i>vs.</i> KL	26
6.1.2	OSE <i>vs.</i> KL	27
6.2	Full comparison between the three approaches	28
6.2.1	Definition of a point-wise error estimator	28
6.2.2	Results with exponential autocorrelation function	28
6.2.3	Results with exponential square autocorrelation function	28
6.2.4	Mean variance error <i>vs.</i> order of expansion	29
6.2.5	Conclusions	31
7	Non Gaussian random fields	32
8	Selection of the random field mesh	32
9	Conclusions	34
3	Second moment approaches	37
1	Introduction	37
2	Principles of the perturbation method	38

3	Applications of the perturbation method	39
3.1	Spatial average method (SA)	40
3.2	Shape functions method (SF)	40
4	The weighted integral method	40
4.1	Introduction	40
4.2	Expansion of the response	41
4.3	Variability response functions	41
5	The quadrature method	42
5.1	Quadrature method for a single random variable	43
5.2	Quadrature method applied to mechanical systems	43
6	Advantages and limitations of second moment approaches	44
4	Finite element reliability analysis	47
1	Introduction	47
2	Ingredients for reliability	47
2.1	Basic random variables and load effects	47
2.2	Limit state surface	48
2.3	Early reliability indices	49
2.4	Probabilistic transformation	50
2.5	FORM, SORM	52
2.6	Determination of the design point	54
2.6.1	Early approaches	54
2.6.2	The improved HLRF algorithm(iHLRF)	56
2.6.3	Conclusion	57
3	Gradient of a finite element response	57
3.1	Introduction	57
3.2	Direct differentiation method in the elastic case	58

3.2.1	Sensitivity to material properties	59
3.2.2	Sensitivity to load variables	60
3.2.3	Sensitivity to geometry variables	60
3.2.4	Practical computation of the response gradient	61
3.2.5	Examples	62
3.3	Case of geometrically non-linear structures	62
3.4	Dynamic response sensitivity of elastoplastic structures	63
3.5	Plane stress plasticity and damage	64
4	Sensitivity analysis	65
5	Response surface method	67
5.1	Introduction	67
5.2	Principle of the method	67
5.3	Building the response surface	68
5.4	Various types of response surface approaches	69
5.5	Comparison between direct coupling and response surface methods	71
5.6	Neural networks in reliability analysis	71
5.7	Conclusions	72
6	Conclusions	73
5	Spectral stochastic finite element method	75
1	Introduction	75
2	SSFEM in elastic linear mechanical problems	77
2.1	Introduction	77
2.2	Deterministic two-dimensional finite elements	77
2.3	Stochastic equilibrium equation	77
2.4	Representation of the response using Neumann series	78
2.5	General representation of the response in $\mathcal{L}^2(\Theta, \mathcal{F}, P)$	79

2.6	Post-processing of the results	81
3	Computational aspects	83
3.1	Introduction	83
3.2	Structure of the stochastic stiffness matrix	83
3.3	Solution algorithms	83
3.4	Hierarchical approach	84
4	Extensions of SSFEM	85
4.1	Lognormal input random field	85
4.1.1	Lognormal random variable	86
4.1.2	Lognormal random field	86
4.2	Multiple input random fields	87
4.3	Hybrid SSFEM	88
4.3.1	Monte Carlo simulation	88
4.3.2	Coupling SSFEM and MCS	88
4.3.3	Concluding remarks	89
5	Summary of the SSFEM applications	89
6	Advantages and limitations of SSFEM	90
A.1	Polynomial chaos expansion	93
A.1.1	Definition	93
A.1.2	Computational implementation	94
A.2	Karhunen-Loève expansion of lognormal random fields	96
6	Conclusions	99
1	Summary of the study	99
2	Suggestions for further study	100

Part II : Comparisons of Stochastic Finite Element Methods with MATLAB	101
1 Introduction	103
1 Aim of the present study	103
2 Object-oriented implementation in MATLAB	104
3 Outline	104
2 Implementation of random field discretization schemes	107
1 Introduction	107
2 Description of the input data	107
2.1 Gaussian random fields	107
2.2 Lognormal random fields	109
3 Discretization procedure	109
3.1 Domain of discretization	110
3.2 The Karhunen-Loève expansion	110
3.2.1 One-dimensional case	110
3.2.2 Two-dimensional case	111
3.2.3 Case of non symmetrical domain of definition	111
3.3 The EOLE method	112
3.4 The OSE method	112
3.4.1 General formulation	112
3.4.2 Construction of a complete set of deterministic functions	113
3.5 Case of lognormal fields	115
4 Visualization tools	115
5 Conclusion	117

3	Implementation of SSFEM	119
1	Introduction	119
1.1	Preliminaries	119
1.2	Summary of the procedure	119
2	SSFEM pre-processing	120
2.1	Mechanical model	120
2.2	Random field definition	121
3	Polynomial chaos	122
3.1	Introduction	122
3.2	Implementation of the Hermite polynomials	123
3.3	Implementation of the polynomial basis	123
3.4	Computation of expectation of products	125
3.4.1	Products of two polynomials	125
3.4.2	The product of two polynomials and a standard normal variable	125
3.4.3	Products of three polynomials	126
3.5	Conclusion	127
4	SSFEM Analysis	127
4.1	Element stochastic stiffness matrix	127
4.2	Assembly procedures	128
4.3	Application of the boundary conditions	129
4.4	Storage and solver	130
5	SSFEM post-processing	130
5.1	Strain and stress analysis	130
5.2	Second moment analysis	131
5.3	Reliability analysis	131
5.4	Probability density function of a response quantity	132
6	Conclusions	132

4	Second moment analysis	133
1	Introduction	133
2	Monte Carlo simulation	134
2.1	Introduction	134
2.2	The finite element code FEMRF	134
2.3	Statistical treatment of the response	135
2.4	Remarks on random fields representing material properties	136
3	Perturbation method with spatial variability	136
3.1	Introduction	136
3.2	Derivatives of the global stiffness matrix	137
3.3	Second moments of the response	138
3.4	Remark on another possible Taylor series expansion	138
4	Settlement of a foundation on an elastic soil mass	139
4.1	Deterministic problem statement	139
4.2	Case of homogeneous soil layer	140
4.2.1	Closed form solution for lognormal Young's modulus	140
4.2.2	Numerical results	141
4.3	Case of heterogeneous soil layer	143
4.3.1	Problem statement	143
4.3.2	Numerical results	144
4.4	Efficiency of the approaches	145
5	Conclusions	146
5	Reliability and random spatial variability	147
1	Introduction	147
2	Direct coupling approach : key points of the implementation	148
2.1	Utilization of the finite element code FEMRF	148

2.2	Direct differentiation method for gradient computation	148
3	Settlement of a foundation - Gaussian input random field	150
3.1	Introduction	150
3.2	Influence of the order of expansion	150
3.2.1	Direct coupling	151
3.2.2	SSFEM +FORM	151
3.2.3	Analysis of the results	151
3.3	Influence of the threshold in the limit state function	152
3.4	Influence of the correlation length of the input	155
3.5	Influence of the coefficient of variation of the input	156
3.6	One-dimensional vs. two-dimensional random fields	156
3.7	Evaluation of the efficiency	158
3.8	Application of importance sampling	160
3.8.1	Introduction	160
3.8.2	Numerical results	160
3.9	Probability distribution function of a response quantity	161
3.10	Conclusions	162
4	Settlement of a foundation - Lognormal input random field	164
4.1	Introduction	164
4.2	Influence of the orders of expansion	165
4.3	Influence of the threshold in the limit state function	165
4.4	Evaluation of the efficiency	167
4.5	Conclusions	168
5	Conclusions	169
6	Conclusion	171

Part I

Review of the literature

Chapter 1

Introduction

Modeling a mechanical system can be defined as the mathematical idealization of the physical processes governing its evolution. This requires the definitions of *basic variables* (describing system geometry, loading, material properties), *response variables* (displacement, strain, stresses) and the relationships between these various quantities.

For a long time, researchers have focused their attention on improving structural models (beams, shells, continua, ...) and constitutive laws (elasticity, plasticity, damage theories, ...). With the development of computer science, a great amount of work has been devoted to numerically evaluate approximated solutions of the boundary value problems describing the mechanical system. The finite element method is probably nowadays the most advanced approach for solution of these problems.

However the increasing accuracy of the constitutive models and the constant enhancement of the computational tools does not solve the problem of identification of the model parameters and the uncertainties associated with their estimation. Moreover, in most civil engineering applications, the intrinsic randomness of materials (soil, rock, concrete, ...) or loads (wind, earthquake motion, ...) is such that deterministic models using average characteristics at best lead to rough representations of the reality.

Accounting for randomness and spatial variability of the mechanical properties of materials is one of the tasks of stochastic or probabilistic mechanics, which has developed fast in the last ten years. The aim of this report is to present a state-of-the-art review of the existing methods in this field. Having industrial applications of these methods in mind, attention will be mainly focused on finite element approaches. The literature on this topic has been classified by Matthies *et al.* (1997). A collective state-of-the-art report on computational stochastic mechanics has been published by Schuëller (1997). A recent special issue of *Computer Methods in Applied Mechanics and Engineering* (January 1999) presents the latest developments of various approaches. These three contributions will

be used as a basis for the present report, where only those parts related to the present concerns will be developed¹.

1 Classification of the stochastic mechanics approaches

The existing theories for stochastic mechanics approaches will be classified here with respect to the type of results they primarily yield. Three categories are distinguished :

- the theories aiming at calculating the first two statistical moments of the response quantities, *i.e.* the mean, variance and correlation coefficients. They are mainly based on the *perturbation method*.
- the *reliability methods*, aiming at evaluating the probability of failure of the system. They are based on the definition of a limit state function. As failure is usually associated with rare events, the tails of the probability density functions (PDFs) of response quantities are of interest in this matter.
- the *stochastic finite element methods* aiming at evaluating the global probabilistic structure of the response quantities considered as random processes. We will present in this report the so-called spectral approach (SSFEM).

It has been noted in the reviewed literature that these three categories of approaches are investigated by different communities of researchers having few interactions with each other. We will try to show in this report that the ingredients utilized in these methods have many common features.

Note that the above classification is somewhat subjective. Indeed results obtained as *byproducts* of the main analysis tend to break the walls between these classes, as shown in the following examples, which will be investigated in detail later on :

- By means of sensitivity analysis, it is always possible to compute the PDF of a response quantity after the main reliability analysis.
- The expression of response random processes obtained by SSFEM are generally not used directly. Closed form expressions yield the second-moment statistics, and the PDFs can be obtained by simulation.

¹The book by Haldar and Mahadevan (2000) should be mentioned for the sake of completeness. Due to its recent publication, it could not be reviewed for the present report.

However, it is expected that methods pertaining to one of the above categories will not be efficient in the computation of byproducts. As mentioned before, due to the compartmentalization of the research groups, no significant comparisons have been made so far.

2 Outline

A common ingredient of all the methods mentioned above is the need to represent the spatial variability of the input parameters. This is done by using a random field representation. For computational needs, these random fields have to be discretized in an optimal way. Chapter 2 covers the methods for discretization of random fields.

Chapter 3 deals with second moment methods in the context of finite element analysis. These methods give results in terms of *response variability*. They appear to be the earliest approaches in probabilistic finite element analysis.

Chapter 4 is devoted to *reliability methods* and their coupling with finite element analysis. The ingredients for reliability approaches are first introduced in a general context. Then the specific modifications to be introduced in the finite element context are presented. This approach was first proposed by Der Kiureghian and Taylor (1983).

Chapter 5 is devoted to the spectral stochastic finite element method (SSFEM). This method was introduced by Ghanem and Spanos (1991*a*). The main concepts will be presented as well as a summary of the applications found in the literature.

As a conclusion, we will present a scheme for comparing the SSFEM and the reliability approaches on the problem of evaluating small probabilities of occurrence as well as the PDF of a given response quantity for a specific example. As noticed before, no comparison of this type has been reported in the literature so far.

Chapter 2

Methods for discretization of random fields

The engineering applications in the scope of this report require representation of uncertainties in the mechanical properties of continuous media. The mathematical theory for this is random fields. For definitions and general properties, the reader is referred to Lin (1967) and Vanmarcke (1983).

1 Generalities

The introduction of probabilistic approaches in mechanical problems requires advanced mathematical tools. This section is devoted to the presentation of some of them. Should the reader be already familiar with this material, the following will give him/her at least the notation used throughout the report.

1.1 Probability space and random variables

Classically, the observation of a random phenomenon is called a *trial*. All the possible *outcomes* of a trial form the *sample space* of the phenomenon, denoted hereinafter by Θ . An *event* E is defined as a subset of Θ containing outcomes $\theta \in \Theta$. Probability theory aims at associating numbers to events, *i.e.* their *probability of occurrence*. Let P denote this so-called *probability measure*. The collection of possible events having well-defined probabilities is called the σ -algebra associated with Θ , denoted here by \mathcal{F} . Finally the probability space constructed by means of this notions is denoted by (Θ, \mathcal{F}, P) .

A real *random variable* X is a mapping $X : (\Theta, \mathcal{F}, P) \rightarrow \mathbb{R}$. For continuous random variables, the probability density function (PDF) and cumulative distribution function

(CDF) are denoted by $f_X(x)$ and $F_X(x)$, respectively, the subscript X being possibly dropped when there is no risk of confusion. To underline the random nature of X , the dependency on the outcomes may be added in some cases as in $X(\theta)$. A *random vector* χ is a collection of random variables.

The mathematical expectation will be denoted by $E[\cdot]$. The mean, variance and n -th moment of X are :

$$(2.1-a) \quad \mu \equiv E[X] = \int_{-\infty}^{\infty} x f_X(x) dx$$

$$(2.1-b) \quad \sigma^2 = E[(X - \mu)^2] = \int_{-\infty}^{\infty} (x - \mu)^2 f_X(x) dx$$

$$(2.1-c) \quad E[X^n] = \int_{-\infty}^{\infty} x^n f_X(x) dx$$

Furthermore, the covariance of two random variables X and Y is :

$$(2.2) \quad \text{Cov}[X, Y] = E[(X - \mu_X)(Y - \mu_Y)]$$

Introducing the joint distribution $f_{X,Y}(x, y)$ of these variables, Eq.(2.2) can be rewritten as :

$$(2.3) \quad \text{Cov}[X, Y] = \int_{-\infty}^{\infty} \int_{-\infty}^{\infty} (x - \mu_X)(y - \mu_Y) f_{X,Y}(x, y) dx dy$$

1.2 Random fields and related Hilbert spaces

The vectorial space of real random variables with finite second moment ($E[X^2] < \infty$) is denoted by $\mathcal{L}^2(\Theta, \mathcal{F}, P)$. The expectation operation allows to define an inner product and the related norm as follows :

$$(2.4-a) \quad \langle X, Y \rangle \equiv E[XY]$$

$$(2.4-b) \quad \|X\| = \sqrt{E[X^2]}$$

It can be shown (Neveu, 1992) that $\mathcal{L}^2(\Theta, \mathcal{F}, P)$ is *complete*, which makes it a *Hilbert space*.

A *random field* $H(\mathbf{x}, \theta)$ can be defined as a curve in $\mathcal{L}^2(\Theta, \mathcal{F}, P)$, that is a collection of random variables indexed by a continuous parameter $\mathbf{x} \in \Omega$, where Ω is an open set of \mathbb{R}^d describing the system geometry. This means that for a given \mathbf{x}_o , $H(\mathbf{x}_o, \theta)$ is a random variable. Conversely, for a given outcome θ_o , $H(\mathbf{x}, \theta_o)$ is a *realization* of the field. It is assumed to be an element of the Hilbert space $\mathcal{L}^2(\Omega)$ of square integrable functions over Ω , the natural inner product associated with $\mathcal{L}^2(\Omega)$ being defined by :

$$(2.5) \quad \langle f, g \rangle_{\mathcal{L}^2(\Omega)} = \int_{\Omega} f(\mathbf{x}) g(\mathbf{x}) d\Omega$$

Hilbert spaces have convenient properties to develop *approximate* solutions of boundary value problems, such as the *Galerkin procedure*.

A random field is called *univariate* or *multivariate* depending on whether the quantity $H(\mathbf{x})$ attached to point \mathbf{x} is a random variable or a random vector. It is *one-* or *multidimensional* according to the dimension d of \mathbf{x} , that is $d = 1$ or $d > 1$. For the sake of simplicity, we consider in the following univariate multidimensional fields. In practical terms, this corresponds to the modeling of mechanical properties including Young's modulus, Poisson's ratio, yield stress, etc., as statistically independent fields.

The random field is *Gaussian* if any vector $\{H(\mathbf{x}_1), \dots, H(\mathbf{x}_n)\}$ is Gaussian. A Gaussian field is completely defined by its mean $\mu(\mathbf{x})$, variance $\sigma^2(\mathbf{x})$ and autocorrelation coefficient $\rho(\mathbf{x}, \mathbf{x}')$ functions. Moreover, it is *homogeneous* if the mean and variance are constant and ρ is a function of the difference $\mathbf{x}' - \mathbf{x}$ only, the one-argument function being in this case denoted by $\tilde{\rho}(\cdot)$. The *correlation length* is a characteristic parameter appearing in the definition of the correlation function (see examples Eqs.(2.35)-(2.37)). For one-dimensional homogeneous fields, the *power spectrum* is defined as the Fourier transform of the autocorrelation function, that is :

$$(2.6) \quad S_{HH}(\omega) = \frac{1}{2\pi} \int_{-\infty}^{\infty} \tilde{\rho}(x) e^{-i\omega x} dx$$

A discretization procedure is the approximation of $H(\cdot)$ by $\hat{H}(\cdot)$ defined by means of a *finite set* of random variables $\{\chi_i, i = 1, \dots, n\}$, grouped in a random vector denoted by χ :

$$(2.7) \quad H(\mathbf{x}) \xrightarrow{\text{Discretization}} \hat{H}(\mathbf{x}) = \mathcal{F}[\mathbf{x}, \chi]$$

The main topic here is to define the "best" approximation with respect to some error estimator, that is the one using the minimal number of random variables. The discretization methods can be divided into three groups :

- **point discretization**, where the random variables $\{\chi_i\}$ are *selected values* of $H(\cdot)$ at some given points \mathbf{x}_i .
- **average discretization**, where $\{\chi_i\}$ are *weighted integrals* of $H(\cdot)$ over a domain Ω_e :

$$(2.8) \quad \chi_i = \int_{\Omega_e} H(\mathbf{x}) w(\mathbf{x}) d\Omega$$

- **series expansion methods**, where the field is exactly represented as a series involving random variables and deterministic spatial functions. The approximation is then obtained as a *truncation* of the series.

Reviews of several discretization methods can be found in Li and Der Kiureghian (1993); Ditlevsen (1996); Matthies *et al.* (1997). The main results are collected in the sequel.

2 Point discretization methods

In the context of finite element method, a spatial discretization of the system geometry (the mesh) is utilized for the approximation of the mechanical response of the structure.

2.1 The midpoint method (MP)

Introduced by Der Kiureghian and Ke (1988), this method consists in approximating the random field in each element Ω_e by a single random variable defined as the value of the field at the centroid \mathbf{x}_c of this element :

$$(2.9) \quad \hat{H}(\mathbf{x}) = H(\mathbf{x}_c) \quad , \quad \mathbf{x} \in \Omega_e$$

The approximated field $\hat{H}(\cdot)$ is then entirely defined by the random vector $\chi = \{H(\mathbf{x}_c^1), \dots, H(\mathbf{x}_c^{N_e})\}$ (N_e being the number of elements in the mesh). Its mean μ and covariance matrix $\Sigma_{\chi\chi}$ are obtained from the mean, variance and autocorrelation coefficient functions of $H(\cdot)$ evaluated at the element centroids. Each realization of $\hat{H}(\cdot)$ is piecewise constant, the discontinuities being localized at the element boundaries. It has been shown (Der Kiureghian and Ke, 1988) that the MP method tends to *over-represent* the variability of the random field within each element.

2.2 The shape function method (SF)

Introduced by Liu *et al.* (1986*a, b*), this method approximates $H(\cdot)$ in each element using nodal values \mathbf{x}_i and shape functions as follows :

$$(2.10) \quad \hat{H}(\mathbf{x}) = \sum_{i=1}^q N_i(\mathbf{x}) H(\mathbf{x}_i) \quad \mathbf{x} \in \Omega_e$$

where q is the number of nodes of element e , \mathbf{x}_i the coordinates of the i -th node and N_i polynomial shape functions associated with the element. The approximated field $\hat{H}(\cdot)$ is obtained in this case from $\chi = \{H(\mathbf{x}_1), \dots, H(\mathbf{x}_N)\}$, where $\{\mathbf{x}_i, i = 1, \dots, N\}$ is the set of the nodal coordinates of the mesh.

The mean value and covariance of the approximated field $\hat{H}(\cdot)$ read :

$$(2.11) \quad \mathbb{E} [\hat{H}(\mathbf{x})] = \sum_{i=1}^q N_i(\mathbf{x}) \mu(x_i)$$

$$(2.12) \quad \text{Cov} [\hat{H}(\mathbf{x}), \hat{H}(\mathbf{x}')] = \sum_{i=1}^q \sum_{j=1}^q N_i(\mathbf{x}) N_j(\mathbf{x}') \text{Cov} [H(x_i), H(x_j)]$$

Each realization of $\hat{H}(\cdot)$ is a continuous function over Ω , which is an advantage over the midpoint method.

2.3 The integration point method

This method is mentioned by Matthies *et al.* (1997) referring to Brenner and Bucher (1995). Assuming that every integration appearing in the finite element resolution scheme is obtained from integrand evaluation at *each Gauss point* of each element, the authors discretize the random field by associating a single random variable to each of these Gauss points. This gives accurate results for short correlation length. However the total number of random variables involved increases dramatically with the size of the problem.

2.4 The optimal linear estimation method (OLE)

This method is presented by Li and Der Kiureghian (1993). It is sometimes referred to as the *Kriging method*. It is a special case of the method of *regression on linear functionals*, see Ditlevsen (1996). In the context of point discretization methods, the approximated field $\hat{H}(\cdot)$ is defined by a linear function of nodal values $\chi = \{H(x_1), \dots, H(x_q)\}$ as follows :

$$(2.13) \quad \hat{H}(\mathbf{x}) = a(\mathbf{x}) + \sum_{i=1}^q b_i(\mathbf{x}) \chi_i = a(\mathbf{x}) + \mathbf{b}^T(\mathbf{x}) \cdot \chi$$

where q is the number of nodal points involved in the approximation. The functions $a(\mathbf{x})$ and $b_i(\mathbf{x})$ are determined by minimizing *in each point \mathbf{x}* the variance of the error $\text{Var} [H(\mathbf{x}) - \hat{H}(\mathbf{x})]$ subject to $\hat{H}(\mathbf{x})$ being an unbiased estimator of $H(\mathbf{x})$ in the mean. These conditions write :

$$(2.14) \quad \forall \mathbf{x} \in \Omega, \quad \text{Minimize} \quad \text{Var} [H(\mathbf{x}) - \hat{H}(\mathbf{x})]$$

$$(2.15) \quad \text{with} \quad \mathbb{E} [H(\mathbf{x}) - \hat{H}(\mathbf{x})] = 0$$

Eq.(2.15) requires :

$$(2.16) \quad \mu(\mathbf{x}) = a(\mathbf{x}) + \mathbf{b}^T(\mathbf{x}) \cdot \mathbb{E} [\chi] \equiv a(\mathbf{x}) + \mathbf{b}^T(\mathbf{x}) \cdot \mu_\chi$$

Then the variance error is :

$$(2.17) \quad \text{Var} [H(\mathbf{x}) - \hat{H}(\mathbf{x})] = \text{E} \left[\left(H(\mathbf{x}) - \hat{H}(\mathbf{x}) \right)^2 \right]$$

which turns out to be after basic algebra :

$$(2.18) \quad \text{Var} [H(\mathbf{x}) - \hat{H}(\mathbf{x})] = \sigma^2(\mathbf{x}) - 2 \sum_{i=1}^q b_i(\mathbf{x}) \text{Cov} [H(\mathbf{x}), \chi_i] \\ + \sum_{i=1}^q \sum_{j=1}^q b_i(\mathbf{x}) b_j(\mathbf{x}) \text{Cov} [\chi_i, \chi_j]$$

The minimization problem is solved *point-wise* for $b_i(\mathbf{x})$. Requiring that the partial differential of (2.18) with respect to $b_i(\mathbf{x})$ be zero yields :

$$(2.19) \quad \forall i = 1, \dots, q \quad -\text{Cov} [H(\mathbf{x}), \chi_i] + \sum_{j=1}^q b_j(\mathbf{x}) \text{Cov} [\chi_i, \chi_j] = 0$$

which can be written in a matrix form :

$$(2.20) \quad -\Sigma_{H(\mathbf{x})\chi} + \Sigma_{\chi\chi} \cdot \mathbf{b}(\mathbf{x}) = 0$$

where $\Sigma_{\chi\chi}$ is the covariance matrix of χ . The optimal linear estimation finally writes :

$$(2.21) \quad \hat{H}(\mathbf{x}) = \mu(\mathbf{x}) + \Sigma_{H(\mathbf{x})\chi}^T \cdot \Sigma_{\chi\chi}^{-1} \cdot (\chi - \mu_\chi)$$

Isolating the deterministic part, Eq.(2.21) may be rewritten as :

$$(2.22) \quad \hat{H}(\mathbf{x}) = [\mu(\mathbf{x}) - \Sigma_{H(\mathbf{x})\chi}^T \cdot \Sigma_{\chi\chi}^{-1} \cdot \mu_\chi] + \sum_{i=1}^q \chi_i (\Sigma_{\chi\chi}^{-1} \cdot \Sigma_{H(\mathbf{x})\chi})_i$$

from which it is seen that OLE is nothing but a shape function discretization method where, setting the mean function aside, the shape functions read :

$$(2.23) \quad N_i^{\text{OLE}}(\mathbf{x}) \equiv (\Sigma_{\chi\chi}^{-1} \cdot \Sigma_{H(\mathbf{x})\chi})_i = \sum_{j=1}^q (\Sigma_{\chi\chi}^{-1})_{ij} \sigma(\mathbf{x}) \sigma(\mathbf{x}_j) \rho(\mathbf{x}, \mathbf{x}_j)$$

The variance of the error is (Li and Der Kiureghian, 1993) :

$$(2.24) \quad \text{Var} [H(\mathbf{x}) - \hat{H}(\mathbf{x})] = \sigma^2(\mathbf{x}) - \Sigma_{H(\mathbf{x})\chi}^T \cdot \Sigma_{\chi\chi}^{-1} \cdot \Sigma_{H(\mathbf{x})\chi}$$

The second term in Eq.(2.24) is identical to $\text{Var} [\hat{H}(\mathbf{x})]$. Thus the variance of the error is simply the difference between the variances of $H(\mathbf{x})$ and $\hat{H}(\mathbf{x})$. Since the error variance is

always positive, it follows that $\hat{H}(\mathbf{x})$ always *under-estimates* the variance of the original random field. Moreover it can be proven (Ditlevsen, 1996) that :

$$(2.25) \quad \text{Cov} \left[\hat{H}(\mathbf{x}), H(\mathbf{x}) - \hat{H}(\mathbf{x}) \right] = 0$$

Thus requiring the error variance to be minimized is equivalent to requiring the error and the approximated field to be uncorrelated. Both statements can be interpreted as follows : in the Hilbert space of random variables $\mathcal{L}^2(\Theta, \mathcal{F}, P)$, $\hat{H}(\mathbf{x})$ is the *projection* of $H(\mathbf{x})$ onto the hyperplane mapped by the points $\{\chi_i\}$ (Neveu, 1992).

3 Average discretization methods

3.1 Spatial average (SA)

The spatial average method was proposed by Vanmarcke and Grigoriu (1983), Vanmarcke (1983). Provided a mesh of the structure is available, it defines the approximated field in each element as a *constant* being computed as the average of the original field over the element :

$$(2.26) \quad \hat{H}(\mathbf{x}) = \frac{\int_{\Omega_e} H(\mathbf{x}) d\Omega_e}{|\Omega_e|} \equiv \bar{H}_e, \quad \mathbf{x} \in \Omega_e$$

Vector χ is then defined as the collection of these random variables, that is $\chi^T = \{\bar{H}_e, e = 1, \dots, N_e\}$. The mean and covariance matrix of χ are computed from the mean and covariance function of $H(\mathbf{x})$ as integrals over the domain Ω_e . Vanmarcke (1983) gives results for homogeneous fields and two-dimensional rectangular domains. The case of axisymmetric cylindrical elements is given in Phoon *et al.* (1990). It has been shown that the variance of the spatial average over an element *under-represents* the local variance of the random field (Der Kiureghian and Ke, 1988).

Difficulties involved in this method are reported by Matthies *et al.* (1997) :

- the approximation for non rectangular elements (which can be dealt with by a collection of non overlapping rectangular ones) may lead to a non-positive definite covariance matrix.
- The probability density function of each random variable χ_i is almost impossible to obtain except for Gaussian random fields. For the sake of exhaustivity, recent work from Knabe *et al.* (1998) on spatial averages should be mentioned.

3.2 The weighted integral method

This method was developed by Deodatis (1990, 1991), Deodatis and Shinozuka (1991) and also investigated by Takada (1990 a,b) in the context of stochastic finite elements. It is claimed not to require any discretization of the random field and thus seems to be particularly attractive. In the context of *linear elasticity*, the main idea is to consider the *element stiffness matrices* as basic random quantities. More precisely, using standard finite element notations, the stiffness matrix associated with a given element occupying a volume Ω_e reads :

$$(2.27) \quad \mathbf{k}^e = \int_{\Omega_e} \mathbf{B}^T \cdot \mathbf{D} \cdot \mathbf{B} d\Omega_e$$

where \mathbf{D} denotes the elasticity matrix, and \mathbf{B} is a matrix that relates the components of strains to the nodal displacements.

Consider now the elasticity matrix obtained as a product of a deterministic matrix by a univariate random field (*e.g.* Young's modulus) :

$$(2.28) \quad \mathbf{D}(\mathbf{x}, \theta) = \mathbf{D}_o [1 + H(\mathbf{x}, \theta)]$$

where \mathbf{D}_o is the mean value¹ and $H(\mathbf{x}, \theta)$ is a zero-mean process. Thus Eq.(2.27) can be rewritten as :

$$(2.29) \quad \mathbf{k}^e(\theta) = \mathbf{k}_o^e + \Delta \mathbf{k}^e(\theta) \quad , \quad \Delta \mathbf{k}^e(\theta) = \int_{\Omega_e} H(\mathbf{x}, \theta) \mathbf{B}^T \cdot \mathbf{D}_o \cdot \mathbf{B} d\Omega_e$$

Furthermore the elements in matrix \mathbf{B} are obtained by derivation of the element shape functions with respect to the coordinates. Hence they are polynomials in the latter, say (x, y, z) . A given member of $\Delta \mathbf{k}^e$ is thus obtained after matrix product (2.29) as :

$$(2.30) \quad \Delta \mathbf{k}_{ij}^e(\theta) = \int_{\Omega_e} P_{ij}(x, y, z) H(\mathbf{x}, \theta) d\Omega_e$$

where the coefficients of polynomial P_{ij} are obtained from those of \mathbf{B} and \mathbf{D}_o . Let us write P_{ij} as :

$$(2.31) \quad P_{ij}(x, y, z) = \sum_{l=1}^{\text{NWI}} a_{ij}^l x^{\alpha_l} y^{\beta_l} z^{\gamma_l}$$

where NWI is the number of monomials in P_{ij} , each of them corresponding to a set of exponents $\{\alpha_l, \beta_l, \gamma_l\}$. Substituting for (2.31) in (2.30) and introducing the following *weighted integrals* of random field $H(\cdot)$:

$$(2.32) \quad \chi_l^e(\theta) = \int_{\Omega_e} x^{\alpha_l} y^{\beta_l} z^{\gamma_l} H(\mathbf{x}, \theta) d\Omega_e$$

¹For the sake of clarity, the dependency of random variables on outcomes θ is given in this section.

it follows that :

$$(2.33) \quad \Delta \mathbf{k}_{ij}^e(\theta) = \sum_{l=1}^{\text{NWI}} a_{ij}^l \chi_l^e(\theta)$$

Collecting now the coefficients a_{ij}^l in a matrix $\Delta \mathbf{k}_l^e$, the (stochastic) element stiffness matrix can finally be written as :

$$(2.34) \quad \mathbf{k}^e = \mathbf{k}_o^e + \sum_{l=1}^{\text{NWI}} \Delta \mathbf{k}_l^e \chi_l^e$$

In the above equation, \mathbf{k}_o^e and $\{\Delta \mathbf{k}_l^e, l = 1, \dots, \text{NWI}\}$ are *deterministic* matrices and χ_l^e are random variables. As an example, a truss element requires only 1, a two-dimensional beam element 3, and a plane stress quadrilateral element 3 such weighted integrals and associated matrices.

As pointed out by Matthies *et al.* (1997), the weighted integral method is actually *mesh-dependent* as it can be seen from Eq.(2.32). The original random field is actually projected onto the space of polynomials involved in the \mathbf{B} - matrices, that is basically onto the space spanned by the *shape functions* of the finite elements. This is an implicit kind of discretization similar to the shape function approach (see section 2.2). Moreover, if the correlation length of the random field is small compared to the size of integration domain Ω_e , the accuracy of the method is questionable. Indeed, the shape functions usually employed for elements with constant properties (*e.g.* prismatic beams with constant Young's modulus and cross-section) may not give good results when these properties are rapidly varying in the element. The problem of accuracy of the weighted integrals approach seems not have been addressed in detail in the literature. A comprehensive study including the definition and computation of error estimators would help clarify this issue.

Applications of the weighted integral method for evaluating response variability of the system will be discussed later (Chapter 3, section 4).

4 Comparison of the approaches

Li and Der Kiureghian (1993) carry out an exhaustive comparison of the above discretization methods, *i.e.* MP, SA, SF and OLE. Two-dimensional univariate homogeneous Gaussian random fields were considered, with three different correlation structures, namely

exponential, square exponential, and cardinal sine :

$$(2.35) \quad \rho_A(\mathbf{x}, \mathbf{x}') = \exp\left(-\frac{\|\mathbf{x} - \mathbf{x}'\|}{a}\right)$$

$$(2.36) \quad \rho_B(\mathbf{x}, \mathbf{x}') = \exp\left(-\frac{\|\mathbf{x} - \mathbf{x}'\|^2}{a^2}\right)$$

$$(2.37) \quad \rho_C(\mathbf{x}, \mathbf{x}') = \frac{\sin\left(\frac{2.2 \|\mathbf{x} - \mathbf{x}'\|}{a}\right)}{\frac{2.2 \|\mathbf{x} - \mathbf{x}'\|}{a}}$$

where a is a measure of the correlation length. A square mesh (element size l) is chosen, and the following error estimator is computed on a given element Ω_e as a function of l/a :

$$(2.38) \quad \text{Err}(\Omega_e) = \sup_{\mathbf{x} \in \Omega_e} \frac{\text{Var} [H(\mathbf{x}) - \hat{H}(\mathbf{x})]}{\text{Var} [H(\mathbf{x})]}$$

Applying OLE, four different sets of discretization points are used, namely the nodes of the element under consideration, or the nodes of 3, 5 or 7 adjacent elements respectively.

As far as the *size* of χ in OLE is concerned, results are reported in Figure 2.1. It appears that any point outside the 1×1 grid is non informative for type A correlation model. The error is quite large even for refined mesh ($l/a < 0.2$). For both type B and type C models, the error is negligible as soon as $l/a < 0.5$ (attention should be paid to the different scales on the figures corresponding to correlation type A, B and C respectively).

Comparisons between OLE and the other methods (MP, SA, SF) are reported in figure 2.2 and call for the following comments :

- For type A correlation, the error remains large even for a small element size ($l/a < 0.2$). This is due to the non differentiable nature of the random field in this case (because the autocorrelation function is not differentiable at the origin, see Vanmarcke (1983))
- For type B and C, the error is negligible as soon as $l/a < 0.5$. Thus when the available information about the correlation structure is limited to correlation length a , the choice of type A model should be avoided.
- It is seen that OLE gives better results than SF in all cases. As mentioned before, OLE is basically a SF approach, where the shape functions are not prescribed polynomials, but the "optimal" functions to minimize the variance of the error.
- Other results comparing the approximated correlation structure $\Sigma_{\chi\chi}$ to the initial one is also given by Li and Der Kiureghian (1993). In all cases, OLE leads to better accuracy in the discretization than MP, SA and SF.

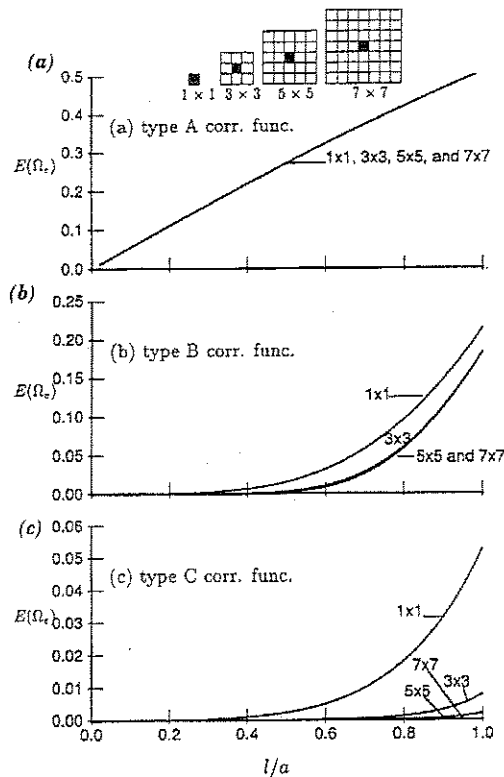


Figure 2.1: Discretization errors for OLE method with varying grid and element size (after Li and Der Kiureghian (1993))

5 Series expansion methods

5.1 Introduction

The discretization methods presented up to now involved a finite number of random variables having a straightforward interpretation : point values or local averages of the original field. In all cases, these random variables can be expressed as *weighted integrals* of $H(\cdot)$ over the volume of the system :

$$(2.39) \quad \chi_i(\theta) = \int_{\Omega} H(\mathbf{x}, \theta) w(\mathbf{x}) d\Omega$$

The weight functions $w(\mathbf{x})$ corresponding to MP, SA, SF and OLE methods are summarized in table 2.1, column #2. In this table, $\delta(\cdot)$ denotes the Dirac function and $\mathbf{1}_{\Omega_e}$ is the *characteristic function* of element e defined by :

$$(2.40) \quad \mathbf{1}_{\Omega_e}(\mathbf{x}) = \begin{cases} 1 & \text{if } \mathbf{x} \in \Omega_e \\ 0 & \text{otherwise} \end{cases}$$

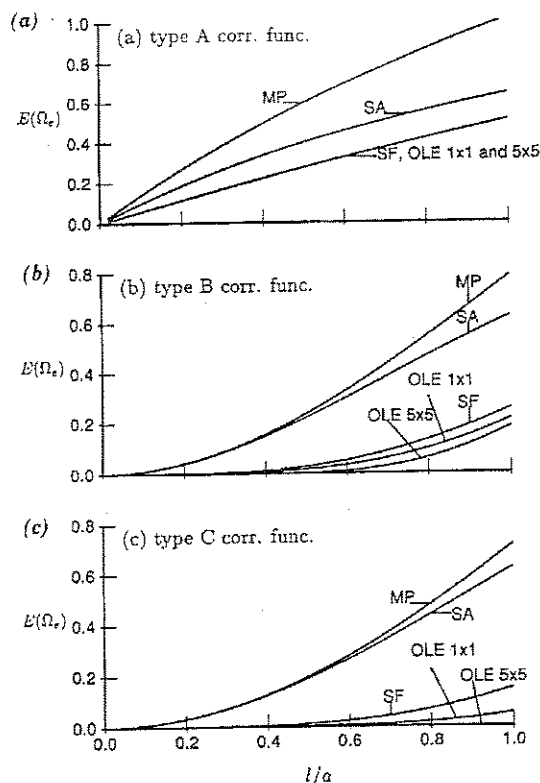


Figure 2.2: Comparison of errors for MP, SA, SF and OLE for varying element size (after Li and Der Kiureghian (1993))

By means of these random variables $\chi_i(\theta)$, the approximated field can be expressed as a finite summation :

$$(2.41) \quad \hat{H}(\mathbf{x}, \theta) = \sum_{i=1}^N \chi_i(\theta) \varphi_i(\mathbf{x})$$

where the deterministic functions $\varphi_i(\mathbf{x})$ are reported in table 2.1, column #3.

Eq.(2.41) can be viewed as the expansion of each realization of the approximated field $\hat{H}(\mathbf{x}, \theta_o) \in \mathcal{L}^2(\Omega)$ over the basis of $\{\varphi_i(\cdot)\}$'s, $\chi_i(\theta_o)$ being the coordinates. From this point of view, the basis used so far are not optimal (for instance, in case of MP, SA and SF, because the basis functions $\{\varphi_i(\cdot)\}$ have a compact support (e.g. each element Ω_e)).

The discretization methods presented in the present section aim at expanding any realization of the original random field $H(\mathbf{x}, \theta_o) \in \mathcal{L}^2(\Omega)$ over a complete set of deterministic functions. The discretization occurs thereafter by *truncating* the obtained series after a finite number of terms.

Table 2.1: Weight functions and deterministic basis unifying MP, SF, SA, OLE methods

Method	weight function $w(\mathbf{x})$	$\varphi_i(\mathbf{x})$
MP	$\delta(\mathbf{x} - \mathbf{x}_c)$	$\mathbf{1}_{\Omega_c}(\mathbf{x})$
SA	$\frac{\mathbf{1}_{\Omega_e}(\mathbf{x})}{ \Omega_e }$	$\mathbf{1}_{\Omega_e}(\mathbf{x})$
SF	$\delta(\mathbf{x} - \mathbf{x}_i)$	polynomial shape functions $N_i(\mathbf{x})$
OLE	$\delta(\mathbf{x} - \mathbf{x}_i)$	"best" shape functions $N_i^{\text{OLE}}(\mathbf{x})$ according to the correlation structure (See Eq.(2.23))

5.2 The Karhunen-Loève expansion

5.2.1 Definition

The Karhunen-Loève expansion of a random field $H(\cdot)$ is based on the *spectral decomposition* of its autocovariance function $C_{HH}(\mathbf{x}, \mathbf{x}') = \sigma(\mathbf{x}) \sigma(\mathbf{x}') \rho(\mathbf{x}, \mathbf{x}')$. The set of deterministic functions over which any realization of the field $H(\mathbf{x}, \theta_o)$ is expanded is defined by the eigenvalue problem :

$$(2.42) \quad \forall i = 1, \dots \quad \int_{\Omega} C_{HH}(\mathbf{x}, \mathbf{x}') \varphi_i(\mathbf{x}') d\Omega_{\mathbf{x}'} = \lambda_i \varphi_i(\mathbf{x})$$

Eq.(2.42) is a Fredholm integral equation. The *kernel* $C_{HH}(\cdot, \cdot)$ being an autocovariance function, it is bounded, symmetric and positive definite. Thus the set of $\{\varphi_i\}$ form a *complete orthogonal basis* of $\mathcal{L}^2(\Omega)$. The set of eigenvalues (spectrum) is moreover *real, positive, numerable*, and has zero as only possible accumulation point. Any realization of $H(\cdot)$ can thus be expanded over this basis as follows :

$$(2.43) \quad H(\mathbf{x}, \theta) = \mu(\mathbf{x}) + \sum_{i=1}^{\infty} \sqrt{\lambda_i} \xi_i(\theta) \varphi_i(\mathbf{x})$$

where $\{\xi_i(\theta), i = 1, \dots\}$ denotes the *coordinates of the realization* of the random field with respect to the set of deterministic functions $\{\varphi_i\}$. Taking now into account all possible realizations of the field, $\{\xi_i, i = 1, \dots\}$ becomes a numerable set of *random variables*.

When calculating $\text{Cov}[H(\mathbf{x}), H(\mathbf{x}')] by means of (2.43) and requiring that it be equal$

to $C_{HH}(\mathbf{x}, \mathbf{x}')$, one easily proves that :

$$(2.44) \quad E[\xi_k \xi_l] = \delta_{kl} \quad (\text{Kronecker symbol})$$

This means that $\{\xi_i, i = 1, \dots\}$ forms a set of *orthonormal* random variables with respect to the inner product (2.4-a). In a sense, (2.43) corresponds to a *separation* of the *space* and *randomness* variables in $H(\mathbf{x}, \theta)$.

5.2.2 Properties

The Karhunen-Loève expansion possesses other interesting properties :

- Due to non accumulation of eigenvalues around a non zero value, it is possible to order them in a descending series converging to zero. Truncating the ordered series (2.43) after the M -th term gives the KL approximated field :

$$(2.45) \quad \hat{H}(\mathbf{x}, \theta) = \mu(\mathbf{x}) + \sum_{i=1}^M \sqrt{\lambda_i} \xi_i(\theta) \varphi_i(\mathbf{x})$$

- The covariance eigenfunction basis $\{\varphi_i(\mathbf{x})\}$ is optimal in the sense that the mean square error (integrated over Ω) resulting from a truncation after the M -th term is minimized (with respect to the value it would take when any other complete basis $\{h_i(\mathbf{x})\}$ is chosen).
- The set of random variables appearing in (2.43) is orthonormal, *i.e.* verifying (2.44), if and only if the basis functions $\{h_i(\mathbf{x})\}$ and the constants λ_i are solution of the eigenvalue problem (2.42).
- Due to the orthonormality of the eigenfunctions, it is easy to get a closed form for each random variable appearing in the series as the following linear transform :

$$(2.46) \quad \xi_i(\theta) = \frac{1}{\sqrt{\lambda_i}} \int_{\Omega} [H(\mathbf{x}, \theta) - \mu(\mathbf{x})] \varphi_i(\mathbf{x}) d\Omega$$

Hence when $H(\cdot)$ is a *Gaussian* random field, each random variable ξ_i is Gaussian. It follows that $\{\xi_i\}$ form in this case a set of *independent* standard normal variables. Furthermore, it can be shown (Loève, 1977) that the Karhunen-Loève expansion of Gaussian fields is almost surely convergent.

- From Eq.(2.45), the error variance obtained when truncating the expansion after M terms turns out to be, after basic algebra :

$$(2.47) \quad \text{Var} [H(\mathbf{x}) - \hat{H}(\mathbf{x})] = \sigma^2(\mathbf{x}) - \sum_{i=1}^M \lambda_i \varphi_i^2(\mathbf{x}) = \text{Var} [H(\mathbf{x})] - \text{Var} [\hat{H}(\mathbf{x})]$$

The righthand side of the above equation is always positive because it is the variance of some quantity. This means that the Karhunen-Loève expansion always *under-represents* the true variance of the field.

5.2.3 Resolution of the integral eigenvalue problem

Eq.(2.42) can be solved analytically only for few autocovariance functions and geometries of Ω . Detailed closed form solutions for triangular and exponential covariance functions for one-dimensional homogeneous fields can be found in Spanos and Ghanem (1989), Ghanem and Spanos (1991*b*), where $\Omega = [-a, a]$. Extension to two-dimensional fields defined for similar correlation functions on a rectangular domain can be obtained as well.

Except in these particular cases, the integral eigenvalue problem has to be solved numerically. A Galerkin-type procedure suggested in Ghanem and Spanos (1991*a*); Ghanem and Spanos (1991*b*, chap. 2) will be now described. Let $\{h_i(\cdot)\}$ be a complete basis of the Hilbert space $\mathcal{L}^2(\Omega)$. Each eigenfunction of $C_{HH}(\mathbf{x}, \mathbf{x}')$ may be represented by its expansion over this basis, say :

$$(2.48) \quad \varphi_k(\mathbf{x}) = \sum_{i=1}^{\infty} d_i^k h_i(\mathbf{x})$$

where d_i^k are the unknown coefficients. The Galerkin procedure aims at obtaining the best approximation of $\varphi_k(\cdot)$ when truncating the above series after the N -th term. This is accomplished by projecting φ_k onto the space \mathcal{H}_N spanned by $\{h_i(\cdot), i = 1, \dots, N\}$. Introducing a truncation of (2.48) in (2.42), the residual reads :

$$(2.49) \quad \epsilon_N(\mathbf{x}) = \sum_{i=1}^N d_i^k \left[\int_{\Omega} C_{HH}(\mathbf{x}, \mathbf{x}') h_i(\mathbf{x}') d\Omega_{\mathbf{x}'} - \lambda_k h_i(\mathbf{x}) \right]$$

Requiring the truncated series being the projection of $\varphi_k(\cdot)$ onto \mathcal{H}_N implies that this residual is orthogonal to \mathcal{H}_N in $\mathcal{L}^2(\Omega)$. This writes :

$$(2.50) \quad \langle \epsilon_N, h_j \rangle \equiv \int_{\Omega} \epsilon_N(\mathbf{x}) h_j(\mathbf{x}) d\Omega = 0 \quad j = 1, \dots, N$$

After some basic algebra, these conditions reduce to a linear system :

$$(2.51) \quad \mathbf{C} \mathbf{D} = \mathbf{\Lambda} \mathbf{B} \mathbf{D}$$

where the different matrices are defined as follows :

$$(2.52-a) \quad \mathbf{B}_{ij} = \int_{\Omega} h_i(\mathbf{x}) h_j(\mathbf{x}) d\Omega$$

$$(2.52-b) \quad \mathbf{C}_{ij} = \int_{\Omega} \int_{\Omega} C_{HH}(\mathbf{x}, \mathbf{x}') h_i(\mathbf{x}) h_j(\mathbf{x}') d\Omega_{\mathbf{x}} d\Omega_{\mathbf{x}'}$$

$$(2.52-c) \quad \mathbf{D}_{ij} = d_i^j$$

$$(2.52-d) \quad \mathbf{\Lambda}_{ij} = \delta_{ij} \lambda_j \quad (\delta_{ij} \text{ Kronecker symbol})$$

This is a discrete eigenvalue problem which may be solved for eigenvectors \mathbf{D} and eigenvalues λ_i . This solution scheme can be implemented using the finite element mesh shape functions as the basis $\{h_i(\cdot)\}$ (see Ghanem and Spanos (1991*b*, chap. 5.3) for the example of a curved plate). Other complete sets of deterministic functions can also be chosen, as described in the next section.

5.2.4 Conclusion

Due to its useful properties, the Karhunen-Loève expansion has been widely used in stochastic finite element approaches. Details and further literature will be given in Chapters 5.

The main issue when using the Karhunen-Loève expansion is to solve the eigenvalue problem (2.42). In most applications found in the literature, the exponential autocovariance function is used in conjunction with square geometries to take advantage of the closed form solution in this case. This poses a problem in industrial applications (where complex geometries will be encountered), because :

- the scheme presented in Section 5.2.3 for numerically solving(2.42) requires additional computations,
- the obtained approximated basis $\{\varphi_i(\cdot)\}$ is no more optimal.

To the author's opinion, it should be possible, for general geometries, to embed Ω in a square-shape volume and use the latter to solve in a closed form (when possible) the eigenvalue problem. Surprisingly, this assertion, earlier made by Li and Der Kiureghian (1993), did not receive attention in the literature.

5.3 Orthogonal series expansion

5.3.1 Introduction

The Karhunen-Loève expansion presented in the above section is an efficient representation of random fields. However, it requires solving an integral eigenvalue problem to determine the complete set of orthogonal functions $\{\varphi_i, i = 1, \dots\}$, see Eq.(2.42). When no analytical solution is available, these functions have to be computed numerically (see Section 5.2.3). The *orthogonal series expansion method* (OSE) proposed by Zhang and Ellingwood (1994) avoids solving the eigenvalue problem (2.42) by selecting *ab initio* a complete set of orthogonal functions. A similar idea had been used earlier by Lawrence (1987).

Let $\{h_i(\mathbf{x})\}_{i=1}^{\infty}$ be such a set of orthogonal functions, *i.e.* forming a basis of $\mathcal{L}^2(\Omega)$. For the sake of simplicity, let us assume the basis is *orthonormal*, *i.e.* :

$$(2.53) \quad \int_{\Omega} h_i(\mathbf{x}) h_j(\mathbf{x}) d\Omega = \delta_{ij} \quad (\text{Kronecker symbol})$$

Let $H(\mathbf{x}, \theta)$ be a random field with prescribed mean function $\mu(\mathbf{x})$ and autocovariance function $C_{HH}(\mathbf{x}, \mathbf{x}')$. Any realization of the field is a function of $\mathcal{L}^2(\Omega)$, which can be expanded by means of the orthogonal functions $\{h_i(\mathbf{x})\}_{i=1}^{\infty}$. Considering now all possible outcomes of the field, the coefficients in the expansion become random variables. Thus the following expansion holds :

$$(2.54) \quad H(\mathbf{x}, \theta) = \mu(\mathbf{x}) + \sum_{i=1}^{\infty} \chi_i(\theta) h_i(\mathbf{x})$$

where $\chi_i(\theta)$ are zero-mean random variables².

Using the orthogonality properties of the h_i 's, it can be shown after some basic algebra that :

$$(2.55-a) \quad \chi_i(\theta) = \int_{\Omega} [H(\mathbf{x}, \theta) - \mu(\mathbf{x})] h_i(\mathbf{x}) d\Omega$$

$$(2.55-b) \quad (\Sigma_{\chi\chi})_{kl} \equiv E[\chi_k \chi_l] = \int_{\Omega} \int_{\Omega} C_{HH}(\mathbf{x}, \mathbf{x}') h_k(\mathbf{x}) h_l(\mathbf{x}') d\Omega_{\mathbf{x}} d\Omega_{\mathbf{x}'}$$

If $H(\cdot)$ is Gaussian, Eq.(2.55-a) proves that $\{\chi_i\}_{i=1}^{\infty}$ are zero-mean Gaussian random variables, possibly *correlated*. In this case, the discretization procedure associated with OSE can then be summarized as follows :

²The notation in this section is slightly different from that used by Zhang and Ellingwood (1994) for the sake of consistency in the present report.

- Choose a complete set of orthogonal functions $\{h_i(\mathbf{x})\}_{i=1}^{\infty}$ (Legendre polynomials were used by Zhang and Ellingwood (1994)) and select the number of terms retained for the approximation, *e.g.* M .
- Compute the covariance matrix $\Sigma_{\chi\chi}$ of the zero-mean Gaussian vector $\chi = \{\chi_1, \dots, \chi_M\}$ by means of Eq.(2.55-b). This fully characterizes χ .
- Compute the approximate random field by :

$$(2.56) \quad \hat{H}(\mathbf{x}, \theta) = \mu(\mathbf{x}) + \sum_{i=1}^M \chi_i(\theta) h_i(\mathbf{x})$$

5.3.2 Transformation to uncorrelated random variables

The discretization of Gaussian random fields using OSE involves correlated Gaussian random variables $\chi = \{\chi_1, \dots, \chi_M\}$. It is possible to transform them into an uncorrelated standard normal vector ξ by performing a spectral decomposition of the covariance matrix $\Sigma_{\chi\chi}$:

$$(2.57) \quad \Sigma_{\chi\chi} \cdot \Phi = \Phi \cdot \Lambda$$

where Λ is the diagonal matrix containing the eigenvalues λ_i of $\Sigma_{\chi\chi}$ and Φ is a matrix whose columns are the corresponding eigenvectors. Random vector χ is related to ξ by :

$$(2.58) \quad \chi = \Phi \cdot \Lambda^{1/2} \cdot \xi$$

Let us denote by $\{\Phi_i^k, i = 1, \dots, M\}$ the coordinates of the k -th eigenvector. From (2.58), each component χ_i of χ is given by :

$$(2.59) \quad \chi_i(\theta) = \sum_{k=1}^M \Phi_i^k \sqrt{\lambda_k} \xi_k(\theta)$$

Hence :

$$(2.60) \quad \begin{aligned} \hat{H}(\mathbf{x}, \theta) &= \mu(\mathbf{x}) + \sum_{i=1}^M \left(\sum_{k=1}^M \Phi_i^k \sqrt{\lambda_k} \xi_k(\theta) \right) h_i(\mathbf{x}) \\ &= \mu(\mathbf{x}) + \sum_{k=1}^M \sqrt{\lambda_k} \xi_k(\theta) \left(\sum_{i=1}^M \Phi_i^k h_i(\mathbf{x}) \right) \end{aligned}$$

Introducing the following notation :

$$(2.61) \quad \varphi_k(\mathbf{x}) = \sum_{i=1}^M \Phi_i^k h_i(\mathbf{x})$$

Eq.(2.60) finally writes :

$$(2.62) \quad \hat{H}(\mathbf{x}, \theta) = \mu(\mathbf{x}) + \sum_{k=1}^M \sqrt{\lambda_k} \xi_k(\theta) \varphi_k(\mathbf{x})$$

The above equation is an approximate Karhunen-Loève expansion of the random field $H(\cdot)$, as seen by comparing with Eq.(2.43).

By comparing the above developments with the numerical solution of the eigenvalue problem associated with the autocovariance function (2.42) (see Section 5.2.3), the following important conclusion originally pointed out by Zhang and Ellingwood (1994) can be drawn : the OSE using a complete set of orthogonal functions $\{h_i(\mathbf{x})\}_{i=1}^{\infty}$ is strictly equivalent to the Karhunen-Loève expansion in the case when the eigenfunctions $\varphi_k(\mathbf{x})$ of the autocovariance function C_{HH} are approximated by using the same set of orthogonal functions $\{h_i(\mathbf{x})\}_{i=1}^{\infty}$.

5.4 The EOLE method

5.4.1 Definition and properties

The *expansion optimal linear estimation* method (EOLE) was proposed by Li and Der Kiureghian (1993). It is an extension of OLE (see section 2.4) using a spectral representation of the vector of nodal variables χ .

Assuming that $H(\cdot)$ is Gaussian, the spectral decomposition of the covariance matrix $\Sigma_{\chi\chi}$ of $\chi = \{H(\mathbf{x}_1), \dots, H(\mathbf{x}_N)\}$ is :

$$(2.63) \quad \chi(\theta) = \mu_{\chi} + \sum_{i=1}^N \sqrt{\lambda_i} \xi_i(\theta) \phi_i$$

where $\{\xi_i, i = 1, \dots, N\}$ are *independent* standard normal variables and (λ_i, ϕ_i) are the eigenvalues and eigenvectors of the covariance matrix $\Sigma_{\chi\chi}$ verifying :

$$(2.64) \quad \Sigma_{\chi\chi} \phi_i = \lambda_i \phi_i$$

Substituting for (2.63) in (2.13) and solving the OLE problem yields :

$$(2.65) \quad \hat{H}(\mathbf{x}, \theta) = \mu(\mathbf{x}) + \sum_{i=1}^N \frac{\xi_i(\theta)}{\sqrt{\lambda_i}} \phi_i^T \Sigma_{H(\mathbf{x})\chi}$$

As in the Karhunen-Loève expansion, the series can be truncated after r terms, the eigenvalues λ_i being sorted first in descending order.

5.4.2 Variance error

The variance of the error for EOLE is :

$$(2.66) \quad \text{Var} [H(\mathbf{x}) - \hat{H}(\mathbf{x})] = \sigma^2(\mathbf{x}) - \sum_{i=1}^r \frac{1}{\lambda_i} (\phi_i^T \Sigma_{H(\mathbf{x})} \chi)^2$$

As in OLE and KL, the second term in the above equation is identical to the variance of $\hat{H}(\mathbf{x})$. Thus EOLE also always *under-represents* the true variance. Due to the form of (2.66), the error decreases monotonically with r , the minimal error being obtained when no truncation is made ($r = N$). This allows to define automatically the cut-off value r for a given tolerance in the variance error.

Remark The truncation of (2.65) after r terms according to the greatest eigenvalues of Σ_{xx} is equivalent to selecting the most important random variables ξ_i in (2.63). This technique of *reduction* is actually general and has been applied in other contexts such as :

- reducing the number of random variables in the shape functions method (Liu *et al.*, 1986b),
- reducing the number of random variables before simulating random field realizations (Yamazaki and Shinozuka, 1990)
- reducing the number of terms in the Karhunen-Loève expansion.

6 Comparison between KL, OSE, EOLE

6.1 Early results

6.1.1 EOLE vs. KL

The accuracy of the KL and EOLE methods has been compared by Li and Der Kiureghian (1993) in the case of one-dimensional homogeneous Gaussian random fields. The error estimator (2.38) was computed for different orders of expansion r . The results are plotted in figure 2.3.

It appears that even when KL is exact (*i.e.* when the exponential decaying covariance kernel is used) the KL maximal³ error is not always smaller than the EOLE error *for a given cut-off number* r . A deeper analysis shows, as pointed out by Li and Der Kiureghian

³Estimator (2.38) is defined as a Sup.

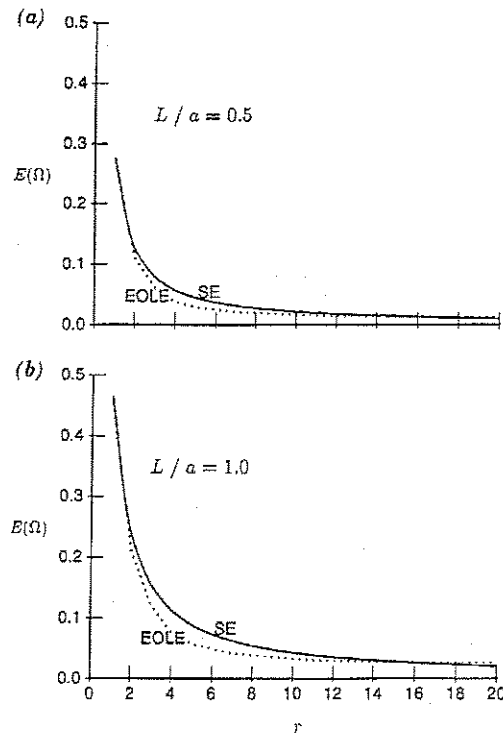


Figure 2.3: Comparison of errors for KL and EOLE methods with type A correlation Eq.(2.35) (after Li and Der Kiureghian (1993))

(1993), that the KL point-wise error variance $\text{Var} [H(x) - \hat{H}(x)]$ for a given r is smaller than the EOLE error *in the interior* of the discretization domain Ω , however larger *at the boundaries*.

6.1.2 OSE vs. KL

Zhang and Ellingwood (1994) applied the OSE method to a one-dimensional Gaussian random field defined over a finite domain $[-a; a]$. The following orthonormal basis $\{h_i(x)\}_{i=0}^{\infty}$ defined by means of the Legendre polynomials was used :

$$(2.67) \quad h_n(x) = \sqrt{\frac{2n+1}{2a}} P_n\left(\frac{x}{a}\right)$$

where P_n is the n -th Legendre polynomial. The authors introduced two error estimators based on the covariance function to evaluate the respective accuracy of KL and OSE methods. To reach a prescribed tolerance, it appears that the number of terms M to be included in OSE is one or two more than the number of terms required by KL.

6.2 Full comparison between the three approaches

To investigate in fuller detail the accuracy of the series expansion methods and allow a full comparison between the three approaches, a MATLAB toolbox for random field discretization has been implemented as part of this study. This implementation is described in detail in Part II, Chapter 2.

6.2.1 Definition of a point-wise error estimator

The following *point-wise* estimator of the error variance is defined :

$$(2.68) \quad \text{err}(\mathbf{x}) = \frac{\text{Var} [H(\mathbf{x}) - \hat{H}(\mathbf{x})]}{\text{Var} [H(\mathbf{x})]}$$

This measure is independent of the mean and standard deviation when $H(\mathbf{x})$ is homogeneous (See Part II, Chapter 2, Section 4). In the following numerical application, a one-dimensional homogeneous Gaussian random field having the following characteristics is chosen :

- Domain $\Omega = [0, 10]$,
- Correlation length $a = 5$.

6.2.2 Results with exponential autocorrelation function

Figure 2.4 represents the estimator (2.68) for the three discretization schemes at different orders of expansion. On each figure, the mean value of $\text{err}(\mathbf{x})$ over Ω is also given. As expected from the properties of the Karhunen-Loève expansion described in Section 5.2.2, the KL approach provides the lowest mean error. The EOLE error is close to the KL error while the OSE error is slightly greater (20 points were chosen for the EOLE discretization, which means that the size of each element in the EOLE-mesh is $L_{RF} \approx a/10$). As already stated by Li and Der Kiureghian (1993), the point-wise variance error at the boundaries of Ω is larger for KL than for EOLE. It is emphasized that the error is still far from zero even when $r = 10$. This is due to the fact that the Gaussian random field under consideration is non differentiable because of the exponential autocorrelation function.

6.2.3 Results with exponential square autocorrelation function

The results for exponential square autocorrelation function (see Eq.(2.36)) are presented in figure 2.5. As there is no analytical solution to the eigenvalue problem associated

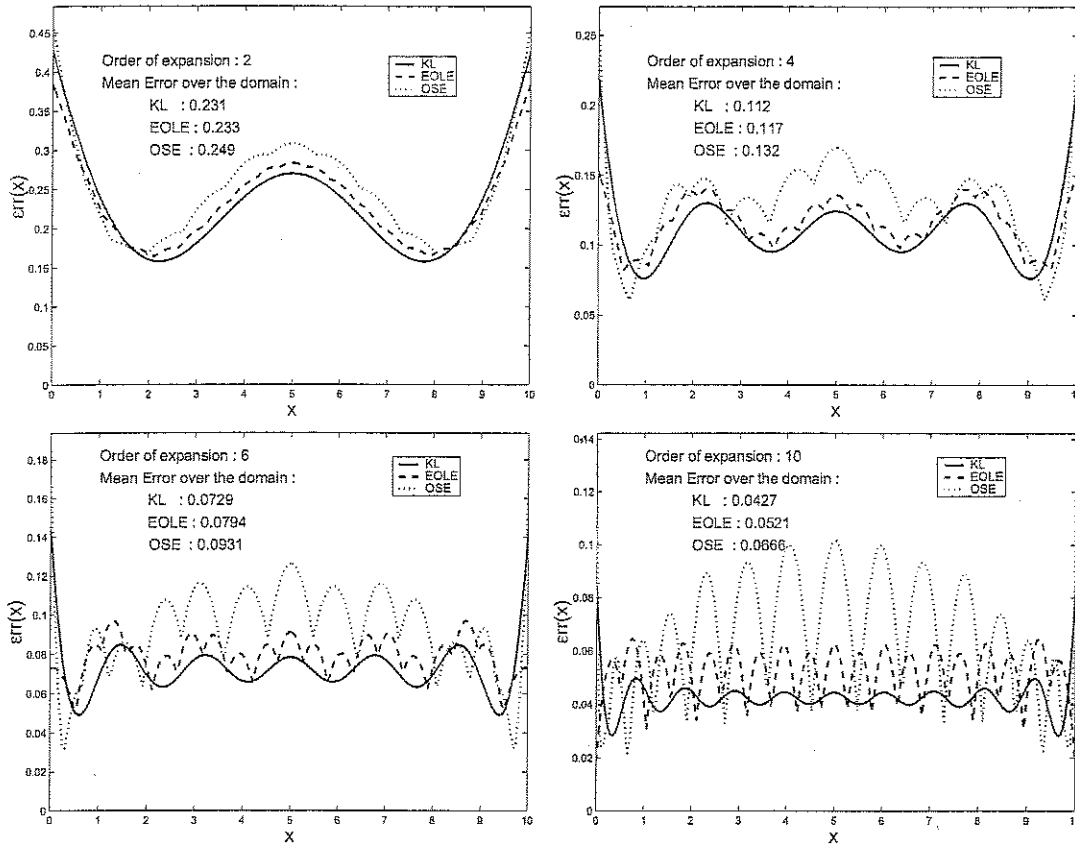


Figure 2.4: Point-wise estimator for variance error, represented for different discretization schemes and different orders of expansion (*exponential autocorrelation function*)

with the Karhunen-Loève expansion in this case, only EOLE and OSE are considered. It appears that EOLE gives better accuracy in this case also.

6.2.4 Mean variance error *vs.* order of expansion

The mean of $err(x)$ over the domain Ω is displayed in figure 2.6 as a function of the order of expansion r for each discretization scheme and for both types of autocorrelation functions.

As expected, at any order of expansion, the smallest mean error is obtained by KL (if applicable). EOLE is almost always better than OSE. The EOLE-mesh refinement necessary to get a fair representation depends strongly on the autocorrelation function, as seen in figure 2.7. If the *exponential* type is considered (figure 2.7-a), EOLE is more accurate than OSE only if $L_{RF}/a \leq 1/6$ in the present example. If the *exponential square*

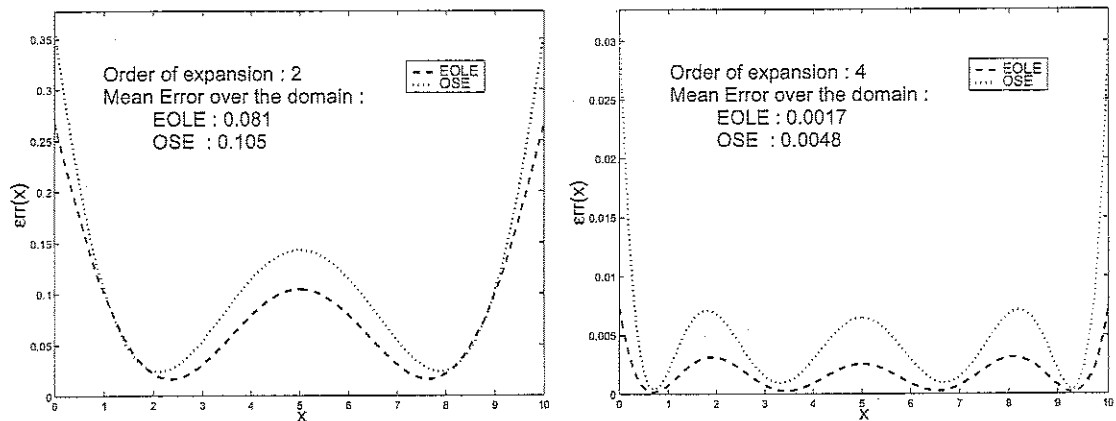
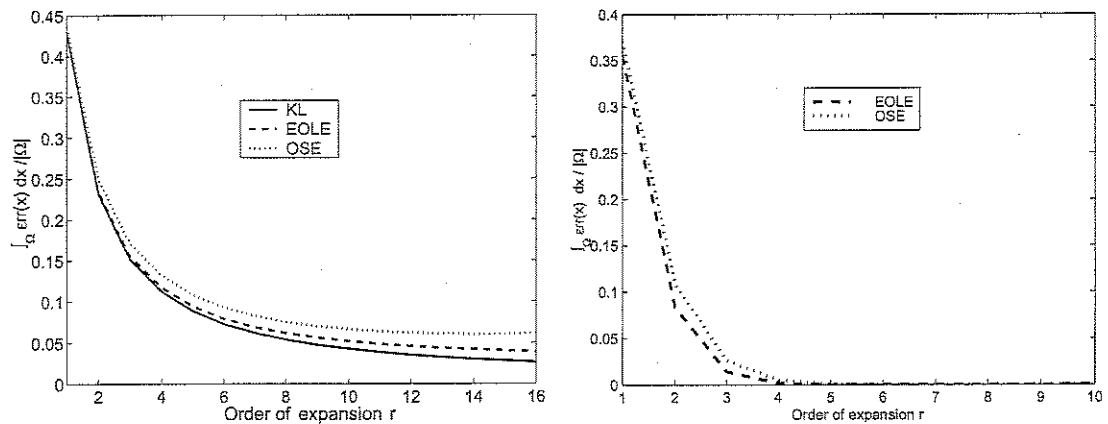


Figure 2.5: Point-wise estimator for variance error, represented for different discretization schemes and different orders of expansion (*exponential square autocorrelation function*)



a - *Exponential autocorrelation function*

b - *Exponential square autocorrelation function*

Figure 2.6: Mean variance error vs. order of expansion for different autocorrelation structures

type is considered (figure 2.7-b), then EOLE is more accurate than OSE whatever the mesh refinement.

It should be noted that, for a given order of expansion r , the variance error obtained in case of the exponential square autocorrelation function is much smaller than that obtained for the exponential autocorrelation function, whatever the discretization scheme. For $r \geq 5$, it is totally negligible for our choice of parameters.

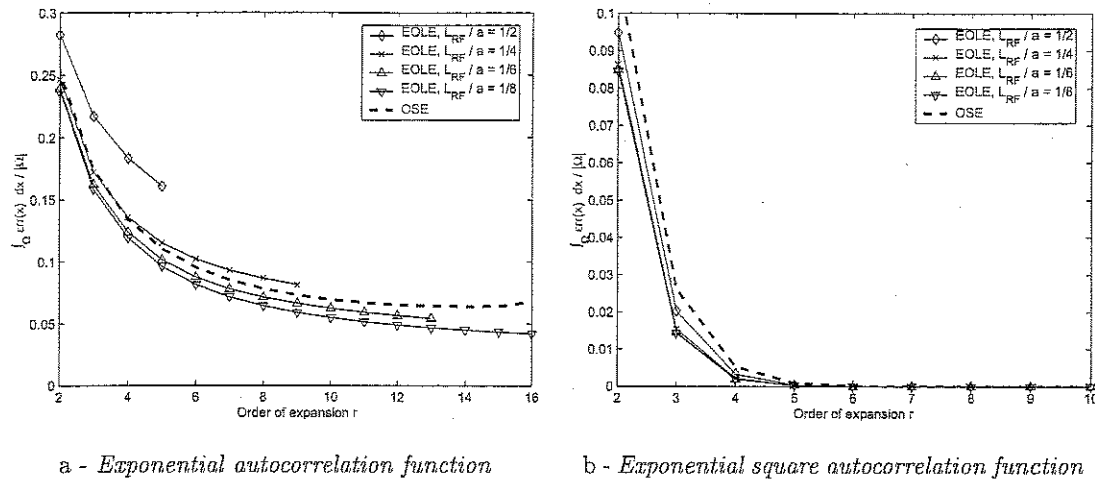


Figure 2.7: Mean variance error *vs.* order of expansion - different EOLE-mesh refinements and OSE

6.2.5 Conclusions

The series expansion discretization schemes (KL, EOLE and OSE) all ensure a rather small variance error as soon as a few terms are included.

When the *exponential* autocorrelation function is used, KL should be selected, since it gives the best accuracy. EOLE is more accurate than OSE if the underlying mesh is sufficiently refined (*i.e.* $L_{RF}/a \leq 1/6$). As already stated by Li and Der Kiureghian (1993), EOLE is more efficient with a fine mesh and a low order of expansion than with a rough mesh and a higher order of expansion.

When the *exponential square* autocorrelation function is used, EOLE is more accurate than OSE whatever the mesh refinement. The ratio $L_{RF}/a \leq 1/2 - 1/3$ is recommended in this case. Generally speaking, the variance error computed with an exponential square autocorrelation function is far smaller than that computed for the exponential case. Thus in practical applications, if there is no particular evidence of the form of the autocorrelation function, the exponential square form should be preferred, since it allows practically an exact discretization (mean variance error $< 10^{-6}$) with only a few terms. This result holds for both EOLE and OSE discretization schemes. Furthermore, this form of autocorrelation function implies a differentiable process, which would be more realistic for most physical processes.

7 Non Gaussian random fields

The case of *non Gaussian fields* has been addressed by Li and Der Kiureghian (1993) in the case when they are defined as a non-linear transformation (also called *translation*) of a Gaussian field :

$$(2.69) \quad H_{\text{NG}}(\cdot) = \mathcal{NL}(H(\cdot))$$

The discretized field is then simply obtained by :

$$(2.70) \quad \hat{H}_{\text{NG}}(\cdot) = \mathcal{NL}(\hat{H}(\cdot))$$

This class of transformations includes the *Nataf transformation* (see details in section 2.4 of Chapter 4). From a practical point of view, it includes the *lognormal random fields*, which are of great importance for modeling material properties due to its non-negative domain.

Although it has not been used in the literature, the translation procedure could be applied with any of the series expansion schemes described in the last section including KL and OSE.

8 Selection of the random field mesh

Several of the methods of discretization presented in this chapter require the selection of a random field mesh, *e.g.* the MP, SA, SF, OLE, EOLE methods. A critical parameter for efficient discretization is the typical size of an element or the grid size.

Several authors including Der Kiureghian and Ke (1988) and Mahadevan and Haldar (1991) have pointed out that the finite element- and the random field meshes have to be designed based upon different criteria. Namely :

- the design of the finite element mesh is governed by the *stress gradients* of the response. Should some singular points exist (crack, edge of a rigid punch, ...), the mesh would have to be locally refined.
- The typical element size L_{RF} in the random field mesh is related to the *correlation length* of the autocorrelation function.

Depending on the discretization method, different recommendations about the element size can be found in the literature :

- Der Kiureghian and Ke (1988) proposed the value :

$$(2.71) \quad L_{RF} \approx \frac{a}{4} \text{ to } \frac{a}{2}$$

by repeatedly evaluating the reliability index of a beam with stochastic rigidity using meshes with decreasing element size.

- This range was confirmed by Li and Der Kiureghian (1993) (see details in section 4) by computing the error estimator (2.38) and by Zeldin and Spanos (1998) by comparing the power spectra of $H(\cdot)$ and $\hat{H}(\cdot)$.
- In the context of reliability analysis (see Chapter 4), Der Kiureghian and Ke (1988) and Mahadevan and Haldar (1991) reported numerical difficulties of the procedure when the length L_{RF} is too small. In this case indeed, the random variables appearing in the discretization are highly correlated and the diagonalization of the associated covariance matrix leads to numerical instabilities.
- As far as the EOLE method is concerned, the short study presented in section 6 allows to conclude that L_{RF} should be taken between $a/10$ and $a/5$ for the exponential autocorrelation function and between $a/4$ and $a/2$ for other cases. However, in contrast to point- and average discretization methods, the fact that L_{RF} is rather small *does not* imply that the number of random variables r used in the discretization is large, since r is prescribed as an independent parameter.

The correlation length being usually constant over Ω , the associated mesh can be constructed on a regular pattern (segment, square, cube). However, in the context of reliability analysis, Liu and Liu (1993) showed that the refinement of the random field mesh should be connected to the *gradient of the limit state function* (see details in Chapter 4). This seems to be a common feature with the finite element mesh : when the response quantities of interest are localized in a specific subdomain of the system, it is possible to choose a coarse mesh in the regions far away from this subdomain.

In the applications, some authors simply construct the random field mesh by *grouping* several elements of the finite element mesh in a single one (see Liu and Der Kiureghian (1991a); Zhang and Der Kiureghian (1993, 1997)). This allows to reduce dramatically the size of the random vector χ . Any realization of $\hat{H}(\cdot)$ is also easily mapped onto the finite element mesh for the mechanical analysis.

To the author's knowledge, no application involving two really independent meshes and a general mapping procedure of the random field realization onto the finite element mesh has been proposed so far. This technique *needs* to be adopted for large industrial applications, where the finite element mesh is generally automatically generated, having variable element size with unprescribed orientation. Indeed, in this case, it would not be practical to define the random field mesh by grouping elements of the finite element mesh.

9 Conclusions

This chapter has presented a review of methods for discretization of random fields that have been used in conjunction with finite element analysis. Comparisons of the efficiency of these methods found in the literature have been reported, and new results regarding the series expansion methods have been presented. The question of the design of the random field mesh has been finally addressed. As a conclusion, advantages and weaknesses of each method are briefly summarized below :

- The point discretization methods described in Section 2 have common advantages : the second order statistics are readily available from those of the field. The marginal PDF of each random variable is the same as that of the field. However, the joint PDF is readily available only when the random field is Gaussian. The number of random variables involved in the discretization increases rapidly with the size of the finite element problem.
- Methods yielding *continuous* realizations of the approximate field (*e.g.* SF, OLE) are preferable to those yielding piecewise constant realizations (*e.g.* MP, SA) since they provide more accurate representations for the same mesh refinement.
- The SA method is practically limited to Gaussian fields since the statistics of the random variables involved in the discretization cannot be determined in any other case. However, it may be extended to non Gaussian fields obtained by translation of a Gaussian field, see Section 7.
- The expansion methods (*e.g.* KL, OSE) do not require a random field mesh. The former is the most efficient in terms of the number of random variables required for a given accuracy. However, it requires the solution of an integral eigenvalue problem. The latter uses *correlated* random variables, which can be transformed into uncorrelated variables by solving a discrete eigenvalue problem. When no closed-form solution of the KL integral eigenvalue problem exists, KL and OSE are equivalent.
- Although applicable to any kind of field, both of these methods are mainly efficient for Gaussian random fields, since the variables involved in the discretization are Gaussian in this case. As an extension, non Gaussian random fields obtained by translation can be dealt with; see Section 7.
- It is possible to reduce the number of random variables involved in a discretization procedure by a spectral decomposition of their covariance matrix. Only those eigenvalues with greatest value are retained in the subsequent analysis. This reduction technique has been applied in conjunction with SF. Coupled with OLE, it yields EOLE.

- Disregarding the analytical KL method (which is only applicable to few correlation structures of the random field and geometry of the system), EOLE and OSE are the most appealing methods.

Both methods provide *analytical* expressions for the realization of the approximate field, involving its autocovariance function or the orthogonal basis functions respectively. These realizations are continuous. In terms of accuracy, EOLE is better than OSE if the random field mesh is sufficiently refined ($L_{RF} \approx a/5 - a/10$, where a is the correlation length).

The covariance matrix of the random variables involved in EOLE is readily available, since these variables correspond to selected points in the domain Ω . Solving an eigenvalue problem is then necessary to achieve the discretization.

Regarding the OSE method, each term of the covariance matrix has to be computed as a weighted integral of the autocovariance function, see Eq.(2.55-b).

Chapter 3

Second moment approaches

1 Introduction

Historically, probability theory was introduced in mechanics in order to estimate the *response variability* of a system, that is the dispersion of the response around a mean value when the input parameters themselves vary around their means. The aim is to understand how uncertainties in the input *propagate* through the mechanical system. For this purpose, second order statistics of the response are to be evaluated.

Suppose the input randomness in geometry, material properties and loads is described by a set of N random variables, each of them being represented as the sum of its mean value and a zero-mean random variable α_i . The input variations around the mean are thus collected in a zero-mean random vector $\boldsymbol{\alpha} = \{\alpha_1, \dots, \alpha_N\}$. In the context of finite element analysis, the second moment methods aim at evaluating the statistics of the nodal displacements, strains and stresses from the mean values of the input variables and the covariance matrix of $\boldsymbol{\alpha}$.

The *perturbation method* introduced in the late 1970's has been employed in a large number of studies. The general formulation is presented in Section 2. Different examples of application in conjunction with random field discretization are presented in Section 3. The *weighted integral method*, which is a combination of a perturbation-based approach with the discretization scheme presented in Chapter 2, Section 3.2 is presented in Section 4. The *quadrature method* proposed recently to compute directly the moments of response quantities is presented in Section 5.

2 Principles of the perturbation method

The perturbation method was applied by many researchers including Handa and Andersson (1981) and Hisada and Nakagiri (1981, 1985) in structural mechanics, Baecher and Ingra (1981) and Phoon *et al.* (1990) for geotechnical problems, and Liu *et al.* (1986*a,b*) for non-linear dynamic problems. It uses a Taylor series expansion of the quantities involved in the equilibrium equation of the system around their mean values. Then the coefficients in the expansions of the left- and right-hand sides are identified and evaluated by perturbation analysis.

In the context of finite element analysis for quasi-static linear problems, the equilibrium equation obtained after discretizing the geometry generally reads :

$$(3.1) \quad \mathbf{K} \cdot \mathbf{U} = \mathbf{F}$$

Suppose the input parameters used in constructing the stiffness matrix \mathbf{K} and the load vector \mathbf{F} are varying around their mean. As a consequence, the three quantities appearing in the above equation will also vary around the values \mathbf{K}_o , \mathbf{U}^o , \mathbf{F}_o they take for these mean values of the input parameters.

The Taylor series expansions of the terms appearing in (3.1) around their mean values read¹ :

$$(3.2) \quad \mathbf{K} = \mathbf{K}_o + \sum_{i=1}^N \mathbf{K}_i^I \alpha_i + \frac{1}{2} \sum_{i=1}^N \sum_{j=1}^N \mathbf{K}_{ij}^{II} \alpha_i \alpha_j + o(\|\alpha\|^2)$$

$$(3.3) \quad \mathbf{U} = \mathbf{U}^o + \sum_{i=1}^N \mathbf{U}_i^I \alpha_i + \frac{1}{2} \sum_{i=1}^N \sum_{j=1}^N \mathbf{U}_{ij}^{II} \alpha_i \alpha_j + o(\|\alpha\|^2)$$

$$(3.4) \quad \mathbf{F} = \mathbf{F}_o + \sum_{i=1}^N \mathbf{F}_i^I \alpha_i + \frac{1}{2} \sum_{i=1}^N \sum_{j=1}^N \mathbf{F}_{ij}^{II} \alpha_i \alpha_j + o(\|\alpha\|^2)$$

where the first (resp. second) order coefficients $(\cdot)_i^I$ (resp. $(\cdot)_{ij}^{II}$) are obtained from the first and second order derivatives of the corresponding quantities evaluated at $\alpha = 0$, *e.g.* :

$$(3.5) \quad \mathbf{K}_i^I = \left. \frac{\partial \mathbf{K}}{\partial \alpha_i} \right|_{\alpha=0}$$

$$(3.6) \quad \mathbf{K}_{ij}^{II} = \left. \frac{\partial^2 \mathbf{K}}{\partial \alpha_i \partial \alpha_j} \right|_{\alpha=0}$$

By substituting (3.2)-(3.4) in (3.1) and identifying the similar order coefficients on both

¹For the sake of simplicity, the dependency of the random variables α_i on the basic outcomes $\theta \in \Theta$ is not written in the sequel.

sides of the equation, one obtains successively :

$$(3.7) \quad U^o = K_o^{-1} \cdot F_o$$

$$(3.8) \quad U_i^I = K_o^{-1} \cdot (F_i^I - K_i^I \cdot U^o)$$

$$(3.9) \quad U_{ij}^{II} = K_o^{-1} \cdot (F_{ij}^{II} - K_i^I \cdot U_j^I - K_j^I \cdot U_i^I - K_{ij}^{II} \cdot U^o)$$

From these expressions, the statistics of U is readily available from that of α . The second order estimate of the mean is obtained from (3.3) :

$$(3.10) \quad E[U] \approx U^o + \frac{1}{2} \sum_{i=1}^N \sum_{j=1}^N U_{ij}^{II} \text{Cov}[\alpha_i, \alpha_j]$$

where the first term U^o is the first-order approximation of the mean. The first order estimate of the covariance matrix reads :

$$(3.11) \quad \text{Cov}[U, U] \approx \sum_{i=1}^N \sum_{j=1}^N U_i^I \cdot (U_j^I)^T \text{Cov}[\alpha_i, \alpha_j] = \sum_{i=1}^N \sum_{j=1}^N \left. \frac{\partial U}{\partial \alpha_i} \right|_{\alpha=0} \left. \frac{\partial U^T}{\partial \alpha_j} \right|_{\alpha=0} \text{Cov}[\alpha_i, \alpha_j]$$

Introducing the correlation coefficients of the random variables (α_i, α_j) :

$$(3.12) \quad \rho_{ij} = \frac{\text{Cov}[\alpha_i, \alpha_j]}{\sigma_{\alpha_i} \sigma_{\alpha_j}}$$

the above equation can be rewritten as :

$$(3.13) \quad \text{Cov}[U, U] \approx \sum_{i=1}^N \sum_{j=1}^N \left. \frac{\partial U}{\partial \alpha_i} \right|_{\alpha=0} \left. \frac{\partial U^T}{\partial \alpha_j} \right|_{\alpha=0} \rho_{ij} \sigma_{\alpha_i} \sigma_{\alpha_j}$$

It is seen that each term of the summation involves the sensitivity of the response to the parameters α_i (partial derivatives of U) as well as the variability of these parameters (σ_{α_i}). Eq.(3.13) thus allows to interpret what quantities are most important with respect to the response variance. The second-order approximation of the covariance matrix can also be derived. It involves up to fourth moments of α and is therefore more intricate to implement and longer to evaluate.

Formulas for the statistics of element strain and stresses have been developed by many authors including Hisada and Nakagiri (1981) and Liu *et al.* (1986b).

3 Applications of the perturbation method

In this section, attention is focused on the use of the perturbation method coupled with random field discretization techniques.

3.1 Spatial average method (SA)

Using the SA method (see Chapter 2, Section 3.1), Baecher and Ingra (1981) obtained the second moment statistics of the settlement of a foundation over an elastic soil mass with random Young's modulus and compared the results with existing one-dimensional analysis.

Vanmarcke and Grigoriu (1983) obtained the first and second order statistics of the nodal displacements of a cantilever beam. Extending the SA formalism to two-dimensional axisymmetric problems, Phoon *et al.* (1990) obtained the first order statistics of the settlement of a pile embedded in an elastic soil layer with random Young's modulus.

3.2 Shape functions method (SF)

Using the SF discretization method (see Chapter 2, Section 2.2), Liu *et al.* (1986*a,b*) applied the perturbation method to static and dynamic non-linear problems, including :

- wave propagation in a one-dimensional elastoplastic bar with random yield stress (Liu *et al.*, 1986*b*);
- static plane stress response of a cantilever beam (same reference);
- static elastoplastic plate with a circular hole, including random cyclic loading and random yield stress (Liu *et al.*, 1986*a*);
- turbine blade (shell element) with random side load and length (same reference).

The results compare fairly well with Monte Carlo simulations. However the coefficient of variation of the random quantities is limited to 10% in all these examples.

4 The weighted integral method

4.1 Introduction

This approach, proposed by Deodatis (1990, 1991), Deodatis and Shinozuka (1991) and Takada (1990*a,b*), couples the perturbation method with the representation of the stochastic stiffness matrix presented in Chapter 2, Section 3.2. This representation can be put in the following form :

$$(3.14) \quad \mathbf{k}^e = \mathbf{k}_o^e + \sum_{l=1}^{NWI} \Delta \mathbf{k}_l^e \chi_l^e$$

where χ_l^e are zero-mean weighted integrals of the random field and Δk_l^e are deterministic matrices. By assembling these contributions over the N elements of the system, a global stochastic stiffness matrix involving $NWI \times N$ random variables is obtained.

4.2 Expansion of the response

In the context of the perturbation method, the following first-order Taylor series expansion of the vector of nodal displacements U is used :

$$(3.15) \quad U = U^o + \sum_{e=1}^N \sum_{l=1}^{NWI} \chi_l^e \left. \frac{\partial U}{\partial \chi_l^e} \right|_{\chi_l^e=0}$$

Assuming deterministic loads, applying (3.7)-(3.8) to this particular case yields :

$$(3.16) \quad U = U^o - \sum_{e=1}^N \sum_{l=1}^{NWI} \chi_l^e K_o^{-1} \cdot \frac{\partial K}{\partial \chi_l^e} \cdot U^o$$

4.3 Variability response functions

From Eq.(3.16) the covariance matrix of the response writes :

$$(3.17) \quad \text{Cov}[U, U] = \sum_{e_1=1}^N \sum_{e_2=1}^N \sum_{l_1=1}^{NWI} \sum_{l_2=1}^{NWI} K_o^{-1} \cdot \frac{\partial K}{\partial \chi_{l_1}^{e_1}} \cdot U^o \cdot U^{oT} \cdot \frac{\partial K^T}{\partial \chi_{l_2}^{e_2}} \cdot (K_o^{-1})^T \cdot \text{Cov}[\chi_{l_1}^{e_1}, \chi_{l_2}^{e_2}]$$

The last term in the above expression is obtained from the definition (2.32) of the weighted integrals. For example, in the one-dimensional case :

$$(3.18) \quad \text{Cov}[\chi_{l_1}^{e_1}, \chi_{l_2}^{e_2}] \equiv E[\chi_{l_1}^{e_1} \chi_{l_2}^{e_2}] = \int_{\Omega_{e_1}} \int_{\Omega_{e_2}} x_1^{\alpha_{l_1}^{e_1}} x_2^{\alpha_{l_2}^{e_2}} E[H(x_1)H(x_2)] dx_1 dx_2$$

where :

$$(3.19) \quad E[H(x_1)H(x_2)] \equiv C_{HH}(x_1 - x_2)$$

is the autocovariance function of $H(\cdot)$. Introducing the power spectral density function $S_{HH}(\omega)$ satisfying :

$$(3.20) \quad C_{HH}(x_1 - x_2) = \int_{\mathbb{R}} S_{HH}(\omega) e^{i\omega(x_1-x_2)} d\omega$$

one finally obtains :

$$(3.21) \quad \begin{aligned} \text{Cov}[\chi_{l_1}^{e_1}, \chi_{l_2}^{e_2}] &= \int_{\mathbb{R}} S_{HH}(\omega) \int_{\Omega_{e_1}} x_1^{\alpha_{l_1}^{e_1}} e^{i\omega x_1} dx_1 \int_{\Omega_{e_2}} x_2^{\alpha_{l_2}^{e_2}} e^{i\omega x_2} dx_2 \\ &= \int_{\mathbb{R}} S_{HH}(\omega) v_{l_1 l_2}^{e_1 e_2}(\omega) d\omega \end{aligned}$$

where $v_{l_1 l_2}^{e_1 e_2}(\omega)$ is defined as :

$$(3.22) \quad v_{l_1 l_2}^{e_1 e_2}(\omega) = \int_{\Omega_{e_1}} x_1^{\alpha_{11}} e^{i\omega x_1} dx_1 \int_{\Omega_{e_2}} x_2^{\alpha_{12}} e^{i\omega x_2} dx_2$$

Substituting (3.21) in (3.17) and gathering the diagonal terms into the vector $\text{Var}[U]$ leads to :

$$(3.23) \quad \text{Var}[U] = \int_{\mathbb{R}} S_{HH}(\omega) \mathbf{V}(\omega) d\omega$$

In the above equation, $\mathbf{V}(\omega)$ is a vector having N components, each of them being the *variability response function* $V_i(\omega)$ at the corresponding degree of freedom. From (3.17),(3.21), it is seen that these functions $V_i(\omega)$ depend on the deterministic stiffness matrices \mathbf{K}_o , $\Delta \mathbf{k}_i^e$, the response mean value \mathbf{U}^o and some functions $v_{l_1 l_2}^{e_1 e_2}(\omega)$ given by Eq.(3.22). These functions can be given closed-form expressions after some algebra in the one-dimensional case (Deodatis, 1990). Each $V_i(\omega)$ gives the contribution of a given scale of fluctuation of the input random field (characterized by ω) to the variance of the nodal displacement U_i .

Deodatis (1990) examined the following upper bound for the variance of U_i . Taking indeed each component of (3.23) separately, the following trivial inequality holds :

$$(3.24) \quad \text{Var}[U_i] \leq \int_{\mathbb{R}} S_{HH}(\omega) \max |V_i(\omega)| d\omega \leq \sigma_H^2 \max |V_i(\omega)|$$

where σ_H^2 is the variance of the input random field, see Eq.(2.28).

The above equation yields an upper bound on the response variance, which is independent of the correlation structure of the input field. This is valuable since this kind of data is difficult to obtain in practice. However, Eq.(3.24) has limited practical use because the quantities $\max |V_i(\omega)|$ are not easily available. In the application of this method to a frame structure, Deodatis (1990) computed these maximum values graphically after plotting the functions $V_i(\omega)$.

5 The quadrature method

An original approach called *quadrature method* has been recently proposed by Baldeweck (1999) to compute the moments of response quantities (*e.g.* nodal displacements) obtained by a finite element code. It is based on the quadrature of the integrals defining these moments.

5.1 Quadrature method for a single random variable

Consider a random variable X whose probability density function (PDF) is denoted by $f_X(x)$ and suppose the moments of $Y = g(X)$ are to be determined. By definition, the i -th moment of Y is given by :

$$(3.25) \quad \mathbb{E}[Y^i] \equiv \mathbb{E}[g^i(X)] = \int_{\mathbb{R}} [g(x)]^i f_X(x) dx$$

The *quadrature* of the above integral is its approximation by a weighted summation of the values of the integrand :

$$(3.26) \quad \mathbb{E}[g^i(X)] \approx \sum_{k=1}^{NP} w_k [g(x_k)]^i$$

where (w_k, x_k) are integration weights and points associated with f_X respectively, and NP is the order of the quadrature scheme. For instance, if X has a uniform distribution over $[-1, 1]$, the integration points in the above equation are the well-known *Gauss points*. More generally, it is possible to compute integration weights and points associated with other PDFs f_X at any order. Baldewck (1999) gives tables for normal and lognormal distributions up to order 10.

5.2 Quadrature method applied to mechanical systems

Suppose the uncertainties of a given mechanical system are described by the vector of basic random variables $\mathbf{X} = \{X_1, \dots, X_N\}$ having a prescribed joint distribution. After a probabilistic transformation (see chapter 4, Section 2.4 for details) it is possible to assume that the X_i 's are uncorrelated standard normal variates. The statistics of a given response quantity S (e.g. nodal displacement, strain- or stress component) is to be determined. The i -th moment of S can be computed as :

$$(3.27) \quad \mathbb{E}[S^i(X_1, \dots, X_N)] = \int_{\mathbb{R}^N} [s(x_1, \dots, x_N)]^i \varphi(x_1) \dots \varphi(x_N) dx_1 \dots dx_N$$

where $\varphi(\cdot)$ is the PDF of a standard normal variate, and $s(x_1, \dots, x_N)$ is usually known in an algorithmic sense, i.e. through a finite element code. Generalizing Eq.(3.26), Eq.(3.27) can be estimated as :

$$(3.28) \quad \mathbb{E}[S^i(X_1, \dots, X_N)] \approx \sum_{k_1=1}^{NP} \dots \sum_{k_N=1}^{NP} w_{k_1} \dots w_{k_N} [s(x_{k_1}, \dots, x_{k_N})]^i$$

It is seen that NP^N evaluations of S (i.e. finite element runs) are needed *a priori*. As stated by Baldewck, the number of evaluations increases exponentially with the

number of random variables. However, some of the weight products $w_{k_1} \dots w_{k_N}$ are totally negligible compared to others, so that some terms in Eq.(3.28) are not computed.

Remark From Eq.(3.27), it is seen that the method is not a “pure” second moment approach, since information about the distributions of the basic random variables is included in the calculation. However, it is presented in this chapter because it gives primarily the moments of the response quantities.

Baldeweck applied the quadrature method to compute the first four moments of the response quantities. From these first moments, a probability distribution function can be fitted (so-called Johnson or Pearson distributions). This PDF can be finally used to get reliability results.

Several examples in structural mechanics, geotechnics and fracture mechanics are presented. In each case, the results obtained with the quadrature method compare well with the other approaches (*e.g.* perturbation method, Monte Carlo simulation). It is noted that non-linear problems can be dealt with as easily as linear problems. However, the limitation on the number of random variables is a severe restriction of this approach (at most 4 were used in the applications described by Baldeweck (1999)).

6 Advantages and limitations of second moment approaches

General formulations and different applications of the perturbation method have been presented in this chapter for linear as well as nonlinear structures. From this analysis, the following conclusions can be drawn :

- Due to its relative simplicity, the first-order perturbation method is practical to get an estimate of the response variance, see Eq.(3.13). It is applicable at low cost to a wide range of problems.
- Due to the Taylor series expansion, accurate results are expected only in case of small variability of the parameters. The upper limit on the coefficient of variation (COV) for which the results are acceptable strongly depends on the degree of nonlinearity of the system. Fair comparisons with Monte Carlo simulations have been obtained for COV up to 20%. However the upper limit may differ a lot with respect to the kind of mechanical problems under consideration. It is important to note that, while the results from perturbation analysis are distribution-free (*i.e.* they only require the second moments of the input variables), the Monte Carlo results by necessity must be obtained for specific distributions. In this sense the comparison is dependent on the assumed distribution in the Monte Carlo analysis.

It is emphasized that the choice of Gaussian distributions is questionable when describing material properties that are positive in nature. In most of the papers referred to in this chapter, Monte Carlo simulations of Gaussian random fields are used as "reference" calculations to assess the validity of the various approaches. No discussion about the possible non physical negative outcomes in the simulation could be found in these papers though.

- the derivatives of K and F have to be derived with respect of each parameter α_i , possibly at the second order level. These derivations are usually performed at the element level before assembling the system. In most situations, they can be done analytically, leading however to intricate formulæ. These calculations can be time consuming, particularly when the second order terms are included. Higher-order approximations are totally intractable.

The weighted integral method described in Section 4 allows to obtain a) second order statistics of the response given a prescribed input random field and b) an upper bound on the response variance which is independent of the correlation structure of the field. It is claimed that the method does not use any particular discretization scheme for the random field. However, as stated in Chapter 2, Section 3.2, the accuracy of the method for problems in which the correlation length is small compared to the size of the structure may not be good. This has been illustrated by Zhang and Der Kiureghian (1997, Chap. 2) on the example of an elastic rod in tension, having constant cross-section and random Young's modulus. Moreover, the following severe limitations of the method have to be recognized :

- it is limited to elastic structures, where the Young's modulus is modeled as a random field. Although extension of the method to nonlinear problems was claimed (Deodatis and Shinozuka, 1991), such a derivation could not be found in the literature.
- by making use of the first-order perturbation method, it is limited to relatively small coefficients of variation of the input.
- the bounds (3.24) on the response variance are difficult to compute in practice, due to the complex expression of the response variability functions $V(\omega)$.
- the number of random variables involved in the computation equals $NWI \times N$ (e.g. NWI is 3 for beam-column elements). The method is thus time consuming for systems having a large number of elements.

Due to its simplicity, the quadrature method is appealing for problems involving a reduced set of random variables. It is neither limited to linear problems nor small coeffi-

icients of variation. However, further exploration of this approach would be necessary to assess its validity in a more general context.

Chapter 4

Finite element reliability analysis

1 Introduction

Reliability methods aim at evaluating the *probability of failure* of a system whose modeling takes into account randomness. Classically, the system is decomposed into components and the system failure is defined by various scenarii about the *joint* failure of components. Thus the determination of the probability of failure of each component is of paramount importance. This chapter will focus on the well-established procedures for evaluating this so-called *component reliability*, first from a general point of view, then in the context of finite element analysis.

2 Ingredients for reliability

2.1 Basic random variables and load effects

Let us denote by \mathcal{X} the set of all *basic* random variables pertaining to the component (*e.g.* a given structure) describing the randomness in geometry, material parameters and loading. If needed, suppose that one of the discretization scheme described in Chapter 2 has been applied to represent random fields as functions of a finite set of random variables. For each realization of \mathcal{X} , the state of the structure is determined by *load effect* quantities, such as displacements, strains, stresses, measures of damage, etc... Let \mathbf{S} denote a vector of such effects, whose values enter in the definition of the failure of the system. These two vectors are related through the *mechanical transformation* :

$$(4.1) \quad \mathbf{S} = \mathcal{S}(\mathcal{X})$$

which is defined, in all but simple situations, in an algorithmic sense, *e.g.* through a finite element computer code.

2.2 Limit state surface

To assess the reliability of a structure, a *limit state function* g depending on load effects is defined as follows :

- $g(\mathbf{S}) > 0$ defines the *safe state* of the structure.
- $g(\mathbf{S}) \leq 0$ defines the *failure state*. In a reliability context, it does not necessarily mean the breakdown of the structure, but the fact that certain requirements of serviceability or safety limit states have been reached or exceeded.

The values of \mathbf{S} satisfying $g(\mathbf{S}) = 0$ define the *limit state surface* of the structure. Examples of limit state functions are :

- $g(\mathbf{S}) = \delta_{\max} - \delta$, if the failure occurs when the displacement δ at a given point exceeds a given threshold δ_{\max} .
- $g(\mathbf{S}) = \sigma_o - J_2(\sigma)$, if the failure occurs when a given point yields (σ_o is the yield stress and $J_2(\sigma)$ the equivalent Von Mises stress).

Let us denote now by $f_{\mathbf{S}}(\mathbf{s})$ the joint probability density function of \mathbf{S} . The probability of failure is then given by :

$$(4.2) \quad P_f = \int_{g(\mathbf{S}) \leq 0} f_{\mathbf{S}}(\mathbf{s}) d\mathbf{s}$$

The above equation contains in itself two major difficulties :

- The joint PDF of the response quantities, $f_{\mathbf{S}}(\mathbf{s})$, is usually not known, the available information being given in terms of the *basic* variables \mathcal{X} .
- The multi-fold integral (4.2) over the failure domain is not easy to compute.

Thus approximate methods have been developed in the last 25 years. Exhaustive presentation of this domain can be found in the monograph by Ditlevsen and Madsen (1996). In the sequel, only the main concepts are summarized.

2.3 Early reliability indices

Early work in structural reliability aimed at determining the failure probability in terms of the second moment statistics of the *resistance* and *demand* variables. Suppose these are lumped into two random variables denoted by R and S respectively. The *safety margin* is defined by :

$$(4.3) \quad Z = R - S$$

Cornell's reliability index (Cornell, 1969) is then defined by :

$$(4.4) \quad \beta_C = \frac{\mu_Z}{\sigma_Z}$$

It can be given the following interpretation : if R and S were to be *jointly normal*, so would be Z . The probability of failure of the system would then be :

$$(4.5) \quad P_f = P(Z \leq 0) = P\left(\frac{Z - \mu_Z}{\sigma_Z} \leq -\frac{\mu_Z}{\sigma_Z}\right) \equiv \Phi(-\beta_C)$$

where $\Phi(\cdot)$ is the standard normal cumulative distribution function. In this case, β_C can be described as a function of the second moment statistics of R and S :

$$(4.6) \quad \beta_C = \frac{\mu_R - \mu_S}{\sqrt{\sigma_R^2 + \sigma_S^2 - 2\rho_{RS}\sigma_R\sigma_S}}$$

Let us consider now a general case where Z is actually a limit state function :

$$(4.7) \quad Z = g(S)$$

the mean μ_S and covariance matrix Σ_{SS} being known. The mean and covariance of Z are not available in the general case where $g(S)$ is non-linear. Using the Taylor expansion around the mean value of S :

$$(4.8) \quad Z = g(\mu_S) + (\nabla_s g)_{S=\mu_S}^T \cdot (S - \mu_S) + o(\| (S - \mu_S)^2 \|)$$

the following first-order approximations are obtained :

$$(4.9) \quad \mu_Z \approx g(\mu_S)$$

$$(4.10) \quad \sigma_Z^2 \approx (\nabla_s g)_{S=\mu_S}^T \cdot \Sigma_{SS} \cdot (\nabla_s g)_{S=\mu_S}$$

This procedure leads to the definition of the so-called *mean value first order second moment reliability index* by using Eqs.(4.9)-(4.10) in (4.4) :

$$(4.11) \quad \beta_{\text{MVFOSM}} = \frac{g(\mu_S)}{\sqrt{(\nabla_s g)_{S=\mu_S}^T \cdot \Sigma_{SS} \cdot (\nabla_s g)_{S=\mu_S}}}$$

The main problem with this reliability index is that it is not *invariant* with respect to changing the limit state function for an equivalent one (for instance by replacing $g(\cdot)$ by $g^3(\cdot)$). Variations can be important in some problems (Ditlevsen and Madsen, 1996, chap. 5).

The problem of invariance was solved by Hasofer and Lind (1974) in a second moment context by recasting the problem in the standard space using a linear transformation of random variables. Essentially, the authors showed that the point of linearization should be selected as the point on the limit state surface nearest to the origin in the standard space, the distance to this point being the first-order second moment reliability index β_{FOSM} . Later, a non-linear probability transformation was employed to account for probability distribution of the variables including non Gaussian distributions. This method is described in the sequel.

2.4 Probabilistic transformation

Consider a transformation of the basic random variables \mathcal{X} :

$$(4.12) \quad \mathbf{Y} = \mathcal{Y}(\mathcal{X})$$

such that \mathbf{Y} is a *Gaussian random vector* with zero mean and unit covariance matrix.

The exact expression of the probability transformation $\mathbf{Y} = \mathcal{Y}(\mathcal{X})$ depends on the joint PDF of \mathcal{X} . Several cases sorted by ascending order of difficulty are listed in the sequel as examples :

- \mathcal{X} is a **Gaussian random vector** with mean $\mu_{\mathcal{X}}$ and covariance matrix $\Sigma_{\mathcal{X}\mathcal{X}}$. The diagonalization of the symmetric positive definite matrix $\Sigma_{\mathcal{X}\mathcal{X}}$ allows to write :

$$(4.13) \quad \mathcal{X} = \mathbf{A} \cdot \mathbf{Y} + \mu_{\mathcal{X}}$$

where \mathbf{A} is obtained by the Cholesky decomposition of $\Sigma_{\mathcal{X}\mathcal{X}}$:

$$(4.14) \quad \Sigma_{\mathcal{X}} = \mathbf{A} \cdot \mathbf{A}^T$$

The probability transformation and its Jacobian then write :

$$(4.15\text{-a}) \quad \mathcal{Y}(\mathcal{X}) = \mathbf{A}^{-1} \cdot (\mathcal{X} - \mu_{\mathcal{X}})$$

$$(4.15\text{-b}) \quad \mathbf{J}_{\mathbf{y},\mathcal{X}} = \mathbf{A}^{-1}$$

- \mathcal{X} is a **vector of independent non normal variables** whose PDF $f_i(x_i)$ and CDF $F_i(x_i)$ are given. The probability transformation in this case is diagonal :

$$(4.16) \quad y_i = \Phi^{-1}[F_i(x_i)], \quad i = 1, \dots, N$$

and its Jacobian reads :

$$(4.17) \quad J_{y,x} = \text{diag} \left(\frac{f(x_i)}{\varphi(y_i)} \right)$$

- \mathbf{X} is a vector of *dependent non normal variables*. In many applications, the *joint* PDF of these random variables is not known. The available information is often limited to the *marginal* distributions (PDF or CDF) and correlation matrix \mathbf{R} , whose coefficients read :

$$(4.18) \quad \rho_{ij} = \frac{\text{Cov}[\chi_i, \chi_j]}{\sigma_i \sigma_j}$$

The problem of constructing joint PDFs *compatible* with given marginal PDFs and correlations was solved by Der Kiureghian and Liu (1986). The authors proposed two different models :

- the *Morgenstern model* : it is limited to small correlations ($|\rho_{ij}| < 0.3$) and the closed form expression for the joint PDF and CDF become tedious to manage when dealing with a large number of random variables.
- the *Nataf model* : it is defined in a convenient closed form for any number of random variables and complies with almost any valid correlation structure.

Due to these characteristics, only the Nataf model is presented now. From the marginal PDF of X_i , the following random vector \mathbf{Z} is defined :

$$(4.19) \quad Z_i = \Phi^{-1}[F_i(\chi_i)]$$

Assuming now that \mathbf{Z} is a Gaussian standard normal vector with yet to be computed correlation matrix \mathbf{R}_o , its joint PDF is given by :

$$(4.20) \quad f_{\mathbf{Z}}(\mathbf{z}) = \varphi_n(\mathbf{z}, \mathbf{R}_o) \equiv \frac{1}{(2\pi)^{n/2} \sqrt{\det \mathbf{R}_o}} \exp \left(-\frac{1}{2} \mathbf{z}^T \cdot \mathbf{R}_o^{-1} \cdot \mathbf{z} \right)$$

Using the inverse transformation of (4.19), the joint PDF of \mathbf{X} then reduces to :

$$(4.21) \quad f_{\mathbf{X}}(\mathbf{X}) = f_1(x_1) \dots f_n(x_n) \frac{\varphi_n(\mathbf{z}, \mathbf{R}_o)}{\varphi(z_1) \dots \varphi(z_n)}$$

To complete the definition, the correlation matrix \mathbf{R}_o should finally be chosen such that the correlation coefficient of any pair (χ_i, χ_j) computed from (4.21) matches the *prescribed* correlation coefficient ρ_{ij} . This condition leads to the following *implicit* equation in $\rho_{o,ij}$:

$$(4.22) \quad \rho_{ij} = \int_{-\infty}^{\infty} \int_{-\infty}^{\infty} \left(\frac{x_i - \mu_i}{\sigma_i} \right) \left(\frac{x_j - \mu_j}{\sigma_j} \right) \varphi_2(z_i, z_j, \rho_{o,ij}) dz_i dz_j$$

Approximate relations for $\rho_{o,ij}(\rho_{ij})$ for a large number of PDF types are given by Der Kiureghian and Liu (1986), Liu and Der Kiureghian (1986), Ditlevsen and Madsen (1996).

From a reliability point of view, assuming the basic variables \mathbf{X} have a Nataf joint PDF, vector \mathbf{Z} defined by (4.19) is Gaussian with zero mean and correlation matrix $\mathbf{R}_o = \mathbf{L}_o \cdot \mathbf{L}_o^T$. The probability transformation to the standard normal space thus writes :

$$(4.23) \quad \begin{aligned} \mathcal{Y}(\mathbf{X}) &= \mathbf{L}_o^{-1} \cdot \mathbf{Z} \\ &= \mathbf{L}_o^{-1} \cdot \{ \Phi^{-1}[F_1(x_1)], \dots, \Phi^{-1}[F_n(x_n)] \}^T \end{aligned}$$

Its Jacobian writes :

$$(4.24) \quad \mathbf{J}_{\mathbf{y},\mathbf{x}} = \mathbf{L}_o^{-1} \cdot \text{diag} \left(\frac{f(x_i)}{\varphi(y_i)} \right)$$

- *The Rosenblatt transformation* introduced by Hohenbichler and Rackwitz (1981) is an alternative possibility when conditional PDFs of \mathbf{X} are known. It is defined as follows :

$$(4.25) \quad \begin{cases} y_1 &= \Phi^{-1}[F(x_1)] \\ y_2 &= \Phi^{-1}[F(x_2|x_1)] \\ &\dots \\ y_n &= \Phi^{-1}[F(x_n|x_1, \dots, x_{n-1})] \end{cases}$$

Unfortunately, it is not invariant by permutation of the variables χ_i (Ditlevsen and Madsen, 1996).

2.5 FORM, SORM

The mapping of the limit state function onto the standard normal space by using the probabilistic transformation (4.12) is described by :

$$(4.26) \quad g(\mathbf{S}) \equiv g(\mathcal{S}(\mathbf{X})) = g(\mathcal{S} \circ \mathcal{Y}^{-1}(\mathbf{Y})) = G(\mathbf{Y})$$

Hence the probability of failure can be rewritten as :

$$(4.27) \quad P_f = \int_{G(\mathbf{y}) \leq 0} \varphi(\mathbf{y}) d\mathbf{y}$$

where $\varphi(\mathbf{Y})$ denotes the *standard normal PDF* of \mathbf{Y} :

$$(4.28) \quad \varphi = \frac{1}{(2\pi)^{n/2}} \exp \left(-\frac{1}{2} \|\mathbf{y}\|^2 \right)$$

This PDF has two interesting properties, namely it is rotationally symmetric and decays exponentially with the square of the norm $\| \mathbf{y} \|$. Thus the points making significant contributions to the integral (4.27) are those with *nearest distance* to the origin of the standard normal space.

This leads to the definition of the *reliability index* β (Ditlevsen and Madsen, 1996), see figure 4.1¹ :

$$(4.29-a) \quad \beta = \boldsymbol{\alpha}^T \cdot \mathbf{y}^*$$

$$(4.29-b) \quad \mathbf{y}^* = \operatorname{argmin} \{ \| \mathbf{y} \| \mid G(\mathbf{y}) \leq 0 \}$$

This quantity is obviously invariant under changes in parametrization of the limit state function, since it has an intrinsic definition, *i.e.* the *distance of the origin to the limit state surface*.

The solution \mathbf{y}^* of the *constrained optimization problem* Eq.(4.29-b) is called the *design point* or the most likely failure point in the standard normal space. When the limit state function $G(\mathbf{y})$ is linear in \mathbf{y} , it is easy to show that :

$$(4.30) \quad P_f = \Phi(-\beta)$$

where $\Phi(\cdot)$ is the standard normal CDF.

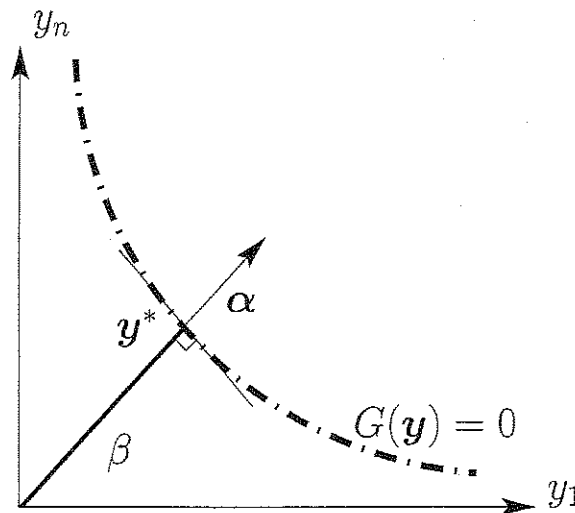


Figure 4.1: Geometrical definition of the design point

When $G(\mathbf{y})$ is non-linear, the *First Order Approximation Method* (FORM) consists in :

¹Rigorously speaking, this definition is only valid when $G(0) > 0$. If 0 lies in the failure domain, β is actually negative, with its absolute value given by Eq.(4.29).

- evaluating the reliability index β by solving (4.29),
- obtaining an approximation of the probability of failure by :

$$(4.31) \quad P_f \approx P_{f_1} = \Phi(-\beta)$$

Geometrically, this is equivalent to replacing the failure domain by the halfspace outside the hyperplane tangent to the limit state surface at $\mathbf{y} = \mathbf{y}^*$. Generally speaking, FORM becomes a better approximation when β is large.

To enhance the precision of Eq.(4.31), *second order approximation methods* (SORM) have been proposed. The idea is to replace the limit state surface by a *quadratic* surface whose probabilistic content is known analytically. Two kinds of approximations are usually used, namely the *curvature fitting* (Breitung, 1984; Der Kiureghian and de Stefano, 1991) which requires the second derivative of $G(\mathbf{y})$ at the design point \mathbf{y}^* and the *point fitting* where semi-paraboloids interpolate the limit state surface at given points around the design point (Der Kiureghian *et al.*, 1987).

Recently, higher order approximation methods (HORM) have been proposed by Grandhi and Wang (1999), where the limit state surface is approximated by higher order polynomials. The amount of computation needed appears to be huge compared to the improvement it yields.

2.6 Determination of the design point

2.6.1 Early approaches

As mentioned earlier, the classical reliability methods (FORM/SORM) require the determination of the *design point*, which is defined as the point on the limit state surface closest to the origin, in the standard normal space. The constrained optimization problem (4.29) is equivalent to :

$$(4.32) \quad \mathbf{y}^* = \operatorname{argmin} \left\{ Q(\mathbf{y}) = \frac{1}{2} \|\mathbf{y}\|^2 \quad | \quad G(\mathbf{y}) \leq 0 \right\}$$

Introducing the Lagrangian of the problem :

$$(4.33) \quad \mathcal{L}(\mathbf{y}, \lambda) = \frac{1}{2} \|\mathbf{y}\|^2 + \lambda G(\mathbf{y})$$

Eq.(4.32) reduces to solving :

$$(4.34) \quad (\mathbf{y}^*, \lambda^*) = \operatorname{argmin} \mathcal{L}(\mathbf{y}, \lambda)$$

Assuming sufficient smoothness of the functions involved, the partial derivatives of \mathcal{L} have to be zero at the solution point. Hence :

$$(4.35) \quad \mathbf{y}^* + \lambda^* \nabla G(\mathbf{y}^*) = 0$$

$$(4.36) \quad G(\mathbf{y}^*) = 0$$

The *positive* Lagrange multiplier λ^* can be obtained from (4.35), then substituted in the same equation. This yields the *first-order optimality conditions* :

$$(4.37) \quad \|\nabla G(\mathbf{y}^*)\| \cdot \mathbf{y}^* + \|\mathbf{y}^*\| \cdot \nabla G(\mathbf{y}^*) = 0$$

This means that the normal to the limit state surface at the design point should point towards the origin.

Hasofer and Lind (1974) suggested an iterative algorithm to solve (4.34), which was later used by Rackwitz and Fiessler (1978) in conjunction with probability transformation techniques. This algorithm (referred to as HLRF in the sequel) generates a sequence of points \mathbf{y}_i from the recursive rule :

$$(4.38) \quad \mathbf{y}_{i+1} = \frac{\nabla G(\mathbf{y}_i)^T \cdot \mathbf{y}_i - G(\mathbf{y}_i)}{\|\nabla G(\mathbf{y}_i)\|} \frac{\nabla G(\mathbf{y}_i)}{\|\nabla G(\mathbf{y}_i)\|}$$

Eq.(4.38) can be given the following interpretation : at the current iterative point \mathbf{y}_i , the limit state surface is linearized, *i.e.* replaced by the trace in the \mathbf{y} -space of the hyperplane tangent to $G(\mathbf{y})$ at $\mathbf{y} = \mathbf{y}_i$. Eq.(4.38) is the solution of this linearized optimization problem, which corresponds to the *orthogonal projection* of \mathbf{y}_i onto the trace of the tangent hyperplane.

As the limit state function and its gradient is usually defined in the original space, it is necessary to make use of a probabilistic transformation such as those described in Section 2.4. The Jacobian of the transformation is used in the following relationship :

$$(4.39) \quad \nabla_{\mathbf{y}} G(\mathbf{y}) = \nabla_{\mathbf{x}} g(\mathbf{x}) \mathbf{J}_{\mathbf{x}, \mathbf{y}}$$

The HLRF algorithm has been widely used due to its simplicity. However it may not converge in some cases, even for rather simple limit state functions. Der Kiureghian and de Stefano (1991) have shown that it certainly diverges when a principal curvature of the limit state surface at the design point satisfies the condition $|\beta \kappa_i| > 1$. Thus several modified versions of this algorithm have been developed (Abdo and Rackwitz, 1990; Liu and Der Kiureghian, 1991b). The latter reference presents a comprehensive review of general purpose optimization algorithms, including the gradient projection method (GP), the augmented lagrangian method (AL), the sequential quadratic programming method (SQP), the HLRF and the modified HLRF (mHLRF). All these algorithms have been implemented in the computer program CALREL (Liu *et al.*, 1989) for comparison

purposes, and tested with several limit state functions. It appears that the most robust as well as efficient methods are SQP and mHLRF.

Although the modified mHLRF was an improvement over the original HLRF, no proof of its convergence could be derived. Thus further work has been devoted in finding an *unconditionally stable* algorithm.

2.6.2 The improved HLRF algorithm(iHLRF)

Zhang and Der Kiureghian (1995, 1997) proposed an *improved* version of HLRF denoted by iHLRF for which unconditional convergence could be proven. It is based on the following recast of the HLRF recursive definition (4.38) :

$$(4.40) \quad \mathbf{y}_{i+1} = \mathbf{y}_i + \lambda_i \mathbf{d}_i$$

$$(4.41) \quad \text{with } \lambda_i = 1$$

$$(4.42) \quad \mathbf{d}_i = \frac{\nabla G(\mathbf{y}_i)^T \cdot \mathbf{y}_i - G(\mathbf{y}_i)}{\|\nabla G(\mathbf{y}_i)\|} \frac{\nabla G(\mathbf{y}_i)}{\|\nabla G(\mathbf{y}_i)\|} - \mathbf{y}_i$$

In the above equations, \mathbf{d}_i and λ_i are the *search direction* and the *step size* respectively. The original HLRF can be improved by computing an optimal step size $\lambda_i \neq 1$.

For this purpose, a *merit function* $m(\mathbf{y})$ is introduced. At each iteration, after computing (4.42), a line search is carried out to find λ_i such that the merit function is minimized, that is :

$$(4.43) \quad \lambda_i = \operatorname{argmin} \{m(\mathbf{y}_i + \lambda \mathbf{d}_i)\}$$

This non-linear problem is not easy to solve. It is replaced by the problem of finding a value λ_i such that the merit function is sufficiently *reduced* (if not minimal). The so-called *Armijo rule* (Luenberger, 1986) is an efficient technique. It reads :

$$(4.44) \quad \lambda_i = \max_{k \in \mathbb{N}} \{b^k \mid m(\mathbf{y}_i + b^k \mathbf{d}_i) - m(\mathbf{y}_i) \leq -ab^k \|\nabla m(\mathbf{y}_i)\|^2\} \quad , \quad a, b > 0$$

Zhang and Der Kiureghian (1995, 1997) proposed the following merit function :

$$(4.45) \quad m(\mathbf{y}) = \frac{1}{2} \|\mathbf{y}\|^2 + c|G(\mathbf{y})|$$

This expression has two properties :

- The HLRF search direction \mathbf{d} (Eq.(4.42)) is a *descent direction* for it, that is \mathbf{d} satisfies : $\forall \mathbf{y}, \quad \nabla m(\mathbf{y})^T \cdot \mathbf{d} \leq 0$ provided $c > \frac{\|\mathbf{y}\|}{\|\nabla G(\mathbf{y})\|}$.
- It attains its minimum at the design point provided the same condition on c is fulfilled.

Both properties are *sufficient* to ensure that the global algorithm defined by Eqs.(4.40),(4.42),(4.44) is unconditionally convergent (Luenberger, 1986).

2.6.3 Conclusion

When the solution of the mechanical problem $\mathcal{S}(\mathcal{X})$ is obtained by a finite element code, each evaluation of $g(\mathcal{S}(\mathcal{X})) \equiv G(\mathbf{y})$ and its gradient $\nabla_{\mathcal{X}}g(\mathcal{X})$ have a non negligible cost (see Section 3 for a detailed presentation). Thus an efficient optimization algorithm for determining the design point should call the smallest number of each evaluation. From this point of view, the iHLRF algorithm is the most efficient algorithm. The reader is referred to Liu and Der Kiureghian (1991b) and Zhang and Der Kiureghian (1997) for detailed cost comparisons.

3 Gradient of a finite element response

3.1 Introduction

As mentioned in the preceding section, the design point is determined by an iterative algorithm which makes use of the gradient of the limit state function in the standard normal space $\nabla_{\mathbf{y}}G(\mathbf{y})$. The limit state function is usually defined in the original space in terms of load effects, which are related to the basic random variables \mathcal{X} . The chain rule of differentiation allows to write :

$$(4.46) \quad \nabla_{\mathbf{y}}G(\mathbf{y}) \equiv \nabla_{\mathbf{y}}g(\mathcal{S}(\mathcal{X}(\mathbf{y}))) = \nabla_{\mathbf{s}}g(\mathbf{s}) \cdot \nabla_{\mathcal{X}}\mathcal{S}(\mathcal{X}) \cdot \mathbf{J}_{\mathcal{X},\mathbf{y}}$$

In this expression, $\nabla_{\mathbf{s}}g(\mathbf{s})$ is usually known analytically, and $\mathbf{J}_{\mathcal{X},\mathbf{y}} = \mathbf{J}_{\mathbf{y},\mathcal{X}}^{-1}$ is given by Eqs.(4.15-b), (4.17), (4.24) depending on the probabilistic transformation. At this point, only the gradient of the mechanical transformation $\nabla_{\mathcal{X}}\mathcal{S}(\mathcal{X})$ remains unknown. Its evaluation however is not an easy task.

Evaluating the gradient of the system response with respect to given input parameters comes under *response sensitivity analysis*. Outside reliability analysis, measures of sensitivity are useful in various applications such as optimal structural design and determination of importance of parameters.

For our purpose of determining the design point, the evaluation of the gradient has to be *efficient* (because of the numerous calls in the iHLRF algorithm) and *accurate* (because its value enters an iterative convergent procedure, which is driven by tolerance checking). The straightforward application of a *finite difference scheme* may be inappropriate in this context. The size of the vector of basic random variables \mathcal{X} being N , one gradient would require at least $N + 1$ complete finite element analysis. The accuracy depends on the size of the finite variation of the parameters and is thus difficult to fix in advance.

A computationally more efficient approach employs the *perturbation method* (Liu *et al.*, 1986b). Recalling the formalism developed in Chapter 3, the first order variation of the

nodal displacement vector U_i^I is given by :

$$(4.47) \quad U_i^I = K_o^{-1} \cdot (F_i^I - K_i^I \cdot U^0)$$

Thus the same *mean value* stiffness matrix K_o is used for evaluating all the components of the displacement gradient vector. This method requires basically one complete finite element analysis and N forward resolutions (4.47), where $i = 1, \dots, N$.

A much more efficient approach called *direct differentiation method* has been proposed to circumvent the drawbacks of the above methods. It is presented in the sequel first for an elastic linear problem. Then the extension to geometrically non-linear structures (Liu and Der Kiureghian, 1989, 1991b), dynamics of J_2 -elastoplastic structures (Zhang and Der Kiureghian, 1993), plane stress elastoplastic damaged structures (Zhang and Der Kiureghian, 1997; Der Kiureghian and Zhang, 1999) will be briefly summarized.

3.2 Direct differentiation method in the elastic case

In the finite element formulation for static problems, the balance between the vector of internal forces R and the vector of external forces F writes :

$$(4.48) \quad R = \bigcup_e \int_{\Omega_e} B^t \cdot \sigma d\Omega_e = \bigcup_e \left\{ \int_{\Omega_e} N^T \cdot \rho_o b_o d\Omega_e + \int_{\partial\Omega_e} N^T \cdot t_o dS_e \right\} = F$$

where \bigcup_e denotes the assembling procedure over all elements, B gives the strain tensor from the nodal displacements, N contains the shape functions, $\rho_o b_o$ and t_o are the body and surface forces respectively.

All these quantities depend on basic random variables. Let χ_m, χ_l, χ_g be those variables representing uncertain material properties, external loads and the geometry of the structure respectively. Let X be the vector of nodal coordinates, U the vector of nodal displacements. In case of small strain linear elastic structures, the following relationships hold :

$$(4.49) \quad X = X[\chi_g]$$

$$(4.50) \quad U = U[X(\chi_g), \chi_m, \chi_l]$$

$$(4.51) \quad R = R[X(\chi_g), U(X(\chi_g), \chi_m, \chi_l), \chi_m]$$

$$(4.52) \quad F = F[X(\chi_g), \chi_l]$$

Thus Eq.(4.48) can be formally rewritten as :

$$(4.53) \quad R[X(\chi_g), U(X(\chi_g), \chi_m, \chi_l), \chi_m] = F[X(\chi_g), \chi_l]$$

To simplify the presentation, it is assumed in this section that the limit state function only depends on the displacement vector U :

$$(4.54) \quad g(\mathcal{S}(\mathcal{X})) \equiv g(U(\mathcal{X}))$$

Thus its gradient becomes :

$$(4.55) \quad \nabla_{\mathcal{X}} g(\mathcal{S}(\mathcal{X})) = \nabla_U g(U) \cdot \nabla_{\mathcal{X}} U$$

To obtain the gradient of the displacement vector U , Eq.(4.53) is differentiated with respect to each set of variables $\mathcal{X}_m, \mathcal{X}_l, \mathcal{X}_g$.

3.2.1 Sensitivity to material properties

Differentiating (4.53) with respect to \mathcal{X}_m yields :

$$(4.56) \quad \frac{\partial R}{\partial U} \nabla_{\mathcal{X}_m} U + \frac{\partial R}{\partial \mathcal{X}_m} = 0$$

Introducing the *stiffness matrix* $K = \frac{\partial R}{\partial U}$ we obtain from the above equation :

$$(4.57) \quad K \cdot \nabla_{\mathcal{X}_m} U = -\frac{\partial R}{\partial \mathcal{X}_m}$$

Differentiating the left hand side of (4.48) with respect to \mathcal{X}_m gives :

$$(4.58) \quad \frac{\partial R}{\partial \mathcal{X}_m} = \bigcup_e \int_{\Omega_e} B^T \cdot \frac{\partial \sigma}{\partial \mathcal{X}_m} d\Omega_e$$

The stresses in element Ω_e are obtained from the nodal displacements u_e by :

$$(4.59) \quad \sigma = D(\mathcal{X}_m) \cdot B \cdot u_e$$

Thus :

$$(4.60) \quad \frac{\partial R}{\partial \mathcal{X}_m} = \bigcup_e \int_{\Omega_e} B^T \cdot \frac{\partial D}{\partial \mathcal{X}_m} \cdot B \cdot u_e d\Omega_e$$

The right hand side of (4.60) is then obtained by evaluating derivative quantities in each element, then assembling them in a global vector exactly as a regular vector of nodal forces.

Examples – Suppose the Young's modulus of the material is represented by a random field and \mathcal{X}_m is the vector of random variables used in its discretization. If the midpoint

method is used, any element χ_m^e of χ_m represents the *constant* Young's modulus in element e . The elasticity matrix in this element thus reduces to :

$$(4.61) \quad D(\chi_m) = D(\chi_m^e) = \chi_m^e D_o$$

Eq.(4.60) then simplifies into :

$$(4.62) \quad \frac{\partial R}{\partial \chi_m} = \bigcup_e \int_{\Omega_e} B^T \cdot D_o \cdot B \cdot u_e d\Omega_e$$

If a series expansion method (*e.g.* KL, OSE, EOLE) is used, the elasticity matrix in each point $x \in \Omega_e$ can be written as

$$(4.63) \quad D(\chi_m, x) = (A_1 + A_2 \cdot \chi_m) \cdot D_o$$

thus depending linearly on the random variables χ (see Eq.(2.65) for the exact expression). In this case, Eq.(4.60) reduces to :

$$(4.64) \quad \frac{\partial R}{\partial \chi_m} = \bigcup_e \int_{\Omega_e} B^T \cdot A_2 \cdot D_o \cdot B \cdot u_e d\Omega_e$$

3.2.2 Sensitivity to load variables

Taking the derivative of Eq.(4.53) with respect to χ_l yields :

$$(4.65) \quad K \cdot \nabla_{\chi_l} U = \frac{\partial F}{\partial \chi_l}$$

where :

$$(4.66) \quad \frac{\partial F}{\partial \chi_l} = \bigcup_e \left\{ \int_{\Omega_e} N^T \cdot \frac{\partial \rho_o b_o}{\partial \chi_l} d\Omega_e + \int_{\partial \Omega_e} N^T \cdot \frac{\partial t_o}{\partial \chi_l} dS_e \right\}$$

Usually χ_l contains load intensity factors for point-wise, surface or body forces. Hence the derivatives in the above equation are analytical.

3.2.3 Sensitivity to geometry variables

Taking the derivative of Eq.(4.53) with respect to χ_g yields :

$$(4.67) \quad \frac{\partial R}{\partial X} \frac{\partial X}{\partial \chi_g} + K \cdot \frac{\partial U}{\partial \chi_g} = \frac{\partial F}{\partial X} \frac{\partial X}{\partial \chi_g}$$

which simplifies in :

$$(4.68) \quad K \cdot \nabla_{\chi_g} U = \left(\frac{\partial F}{\partial X} - \frac{\partial R}{\partial X} \right) \cdot \frac{\partial X}{\partial \chi_g}$$

In this expression, $\frac{\partial \mathbf{X}}{\partial \chi_g}$ is easy to compute since \mathbf{X} is usually an explicit function of χ_g . The difference inside the brackets should however be paid more attention, since the domain of integration Ω_e in (4.48) is dependent on \mathbf{X} . To carry out these derivatives, it is necessary to map the integral domains onto a fixed configuration. Such a mapping is a standard scheme for the so-called isoparametric elements. The derivation of all these quantities for truss and four-node plane elements can be found in Liu and Der Kiureghian (1989).

3.2.4 Practical computation of the response gradient

By compiling Eqs.(4.57),(4.65),(4.68), the response gradient with respect to \mathbf{X} can be written as :

$$(4.69) \quad \mathbf{K} \cdot \nabla_{\mathbf{X}} \mathbf{U} = \frac{\partial \mathbf{F}}{\partial \mathbf{X}} - \frac{\partial \mathbf{R}}{\partial \mathbf{X}}$$

which is simply a set of N linear systems (N being the length of \mathbf{X}) and requires thus N repeated solutions of the following type :

$$(4.70) \quad \nabla_{\chi_i} \mathbf{U} = \mathbf{K}^{-1} \cdot \left[\frac{\partial \mathbf{F}}{\partial \chi_i} - \frac{\partial \mathbf{R}}{\partial \chi_i} \right]$$

However the quantity of interest is not $\nabla_{\mathbf{X}} \mathbf{U}$ in itself, but the product $\nabla_{\mathbf{U}} g(\mathbf{U}) \cdot \nabla_{\mathbf{X}} \mathbf{U}$ (see Eq.(4.55)). The *adjoint method* was proposed (Liu and Der Kiureghian, 1991a) to obtain this quantity directly with a *single* linear system resolution. It consists in solving first for an auxiliary vector Λ :

$$(4.71) \quad \mathbf{K} \cdot \Lambda = \nabla_{\mathbf{U}} g$$

Then the following equality holds :

$$(4.72) \quad \begin{aligned} \nabla_{\mathbf{X}} g(\mathbf{U}(\mathbf{X})) &= \nabla_{\mathbf{U}}^T g \cdot \mathbf{K}^{-1} \cdot \left[\frac{\partial \mathbf{F}}{\partial \mathbf{X}} - \frac{\partial \mathbf{R}}{\partial \mathbf{X}} \right] \\ &= \Lambda^T \cdot \left[\frac{\partial \mathbf{F}}{\partial \mathbf{X}} - \frac{\partial \mathbf{R}}{\partial \mathbf{X}} \right] \end{aligned}$$

This procedure allows to reduce from N to 1 the number of forward substitutions. Note that the *inverse stiffness matrix* used in solving (4.71) is readily available from the initial finite element run.

In summary, the computation of the response gradient requires the partial derivatives $\partial \mathbf{F} / \partial \mathbf{X}$ and $\partial \mathbf{R} / \partial \mathbf{X}$ at the element level, their assembly in a global vector, a forward substitution for an auxiliary vector Λ and finally a matrix product (4.72).

The assumption (4.54) is now relaxed. If strains or stresses appear in the limit state function ($S = U, \sigma, \varepsilon$), they are derived with respect to the parameters as well. For instance, one can write :

$$(4.73) \quad \frac{\partial \sigma}{\partial \chi} = \frac{\partial D}{\partial \chi} \cdot B \cdot u_e + D \frac{\partial B}{\partial \chi} \cdot u_e + D \cdot B \frac{\partial u_e}{\partial \chi}$$

where these expressions have to be expanded for each type of variable (χ_m, χ_l, χ_g). The adjoint method is then used to obtain directly the product $\nabla_{sg} \cdot \nabla_{\chi} S$.

3.2.5 Examples

Der Kiureghian and Ke (1988) considered the reliability of elastic structures, namely a beam with stochastic rigidity and applied load. Both random fields were assumed to be homogeneous and Gaussian. They were discretized by the MP method on the one hand, the SA method on the other hand. These methods respectively over- and under-represent the variance of the original field. Thus they allow to bound the exact results (within the framework of FORM approximations).

Two limit state functions were defined, one in terms of midspan deflection and another in terms of bending moment. The reliability index is computed with different correlation lengths and element sizes. It appears that good accuracy is obtained when the ratio between element size and correlation length is 1/4 to 1/2. The convergence of MP and SA to one another proved the validity of these methods.

Der Kiureghian and Ke (1988) also considered a plate made of two materials with stochastic properties. The limit state function was defined in terms of exceedance of the principal stress in one given point. It appears that the closer the elastic properties to each other, the higher the reliability index.

The orthogonal series expansion method (see Chapter 2, Section 5.3) was applied by Zhang and Ellingwood (1994) to the reliability analysis of fixed-end beam having Gaussian random flexural rigidity EI . The reliability index was computed for various truncated expansions of the field involving an increasing number of terms M . The convergence is attained for $M=6-10$ depending on the choice of the autocovariance function. Using a Karhunen-Loève expansion of the field (with exponentially decaying autocovariance function, *i.e.* analytical expressions for its eigenfunctions), the convergence was obtained using 1 to 2 terms less in the expansion.

3.3 Case of geometrically non-linear structures

Liu and Der Kiureghian (1989) presented exhaustively the response gradient computation for geometrically non-linear structures. In this case, Eqs.(4.51),(4.52) should be

replaced by :

$$(4.74) \quad R = R[X(\chi_g), U(X(\chi_g), \chi_m, \chi_l), \chi_m]$$

$$(4.75) \quad F = F[X(\chi_g), U(X(\chi_g), \chi_m, \chi_l), \chi_l]$$

Included in the above reference is the derivation of all partial derivatives of interest for truss and plane four-node elements. A summary of the procedure can also be found in Liu and Der Kiureghian (1991a). It is emphasized that the non-linearities do not make the gradient computation more expensive, provided the stiffness matrix is replaced by the *tangent stiffness matrix*. The latter is computed during the iterative procedure for solving for the displacements U . Interestingly, the gradient computations do not involve any additional iteration. In conjunction with the gradient method, the gradient response is also obtained by a single forward resolution. However the analytical expressions for the partial derivatives and their coding is much more cumbersome in the non-linear case.

In the above reference, the gradient operators were coded in FEAP (Zienkiewicz and Taylor, 1989). The reliability of a square plate with a hole having random geometry was investigated. The applied load had a random intensity. The elastic material properties (E, ν) were modeled as lognormal and uniform-bounded random fields respectively. As a whole the problem involved 85 random variables, including 30 for each field (30 elements were used for MP discretization), 24 for the coordinates of the hole and 1 for the load intensity. Thus all types of uncertainties were mixed in the same problem. The reliability problem was investigated using FORM and SORM, in conjunction with two limit state functions defined as threshold exceedance of stress and displacements respectively. The CPU was shown to be divided by 100 by using the direct differentiation method rather than finite difference for gradient computation.

3.4 Dynamic response sensitivity of elastoplastic structures

Zhang and Der Kiureghian (1993) extended the direct differentiation method to dynamic problems involving elastoplastic materials. The class of problems considered has the following discretized equation of motion² :

$$(4.76) \quad M(\chi) \ddot{U}(t, \chi) + C(\chi) \dot{U}(t, \chi) + R[U(t, \chi), \chi] = P(t, \chi)$$

where the dots denote the time derivatives. The response gradient with respect to χ is denoted by ;

$$(4.77) \quad V = \frac{\partial U}{\partial \chi}$$

²For the sake of simplicity of the notation, only one sensitivity parameter χ is shown in this section.

By differentiating Eq.(4.76) with respect to χ , the gradient (4.77) turns out to satisfy :

$$(4.78) \quad M \ddot{V} + C \dot{V} + K(U) V = \frac{\partial P}{\partial \chi} - \frac{\partial M}{\partial \chi} \ddot{U} - \frac{\partial C}{\partial \chi} \dot{U} - \frac{\partial R}{\partial \chi} \Big|_{U \text{ fixed}}$$

Eqs.(4.77),(4.78) are solved by using a step-by-step implicit numerical integration method. The following usual linear approximations are used :

$$(4.79) \quad \ddot{U}_{n+1} = \mathcal{L}_1 \left(U_{n+1}, U_n, \dot{U}_n, \ddot{U}_n \right)$$

$$(4.80) \quad \dot{U}_{n+1} = \mathcal{L}_2 \left(U_{n+1}, U_n, \dot{U}_n, \ddot{U}_n \right)$$

When substituting for (4.79), (4.80) in (4.76), a non-linear system of equations is obtained, which is usually solved by a Newton-Raphson scheme. When convergence is achieved, the gradient vector V_{n+1} is obtained by a single forward substitution as in the linear case (see Section 3.2). The matrix used in this substitution is identical to that used for determining U_{n+1} , and is thus readily available in an inverted form.

The quantities appearing in the right hand side contain the derivatives of the internal forces $\partial R / \partial \chi$. In case of non-linear constitutive laws including path dependence (such as plasticity), this derivative is complicated. Zhang and Der Kiureghian (1993) present the complete derivation in the case of J_2 plasticity including isotropic and kinematic hardening.

The first example presented in the above paper is a plane strain analysis of a strip with a circular hole. Cyclic loading under quasi-static conditions was applied. The response gradient with respect to yield stress and hardening parameters was computed using DDM and finite difference with various finite variation size. Convergence from the latter to the former when variation size tends to zero was assessed.

The second example is a truss structure under dynamic loading. Geometrical non-linearities due to large displacements are taken into account. The material of the truss follows J_2 plasticity with linear hardening.

In both cases, the CPU time for the gradient computation is a small fraction of the time required for the response run. This result is applicable to any number of variables provided the adjoint method is used.

3.5 Plane stress plasticity and damage

Zhang and Der Kiureghian (1997) further developed the above formulation for plane stress J_2 plasticity. In this case, the discretized constitutive laws take a special form because of the zero stress constraint. A coupling with the damage model by Lemaitre and Chaboche (1990) is introduced and the sensitivity formulas developed.

As an example, a plate with a hole having initial damage (modeled as a lognormal random field) is investigated. The loading is a periodic traction on a side. The limit state function is defined as the excursion of damage at any point within the plate above a given threshold. Time and space variability is thus introduced in the reliability analysis.

This leads to a *system* reliability problem, the failure modes being related to different locations of the first damage threshold crossing. A similar study is presented by Der Kiureghian and Zhang (1999). It is emphasized that taking into account the spatial variability in reliability dramatically changes the result, *i.e.* the reliability index.

4 Sensitivity analysis

The determination of the design point requires the computation of the gradient of the mechanical response. This can lead to tedious analytical developments and coding when the direct differentiation method is used, but allows for addressing strongly non-linear reliability problems. However, the gradient computation contains information which can be used for *sensitivity analysis*. This is a readily available byproduct of any FORM analysis.

The relative importance of the basic standard normal random variables entering the reliability analysis can be measured by means of the vector α^* defined as :

$$(4.81) \quad \alpha^* = \frac{\mathbf{y}^*}{\|\mathbf{y}^*\|}$$

where \mathbf{y}^* denotes the coordinates of the design point in the standard normal space. Precisely, the ordering of the elements of α^* indicates the relative importance of the random variables in the standard normal space.

Of greatest interest is also the sensitivity of the reliability index β with respect to parameters θ entering the definition of the limit state function ($g(\cdot, \theta_g)$) or the probability distribution function $f_{\mathcal{X}}(\mathcal{X}, \theta_f)$ of the basic random variables \mathcal{X} . In the former case, the sensitivity of β is (Ditlevsen and Madsen, 1996, chap. 8) :

$$(4.82) \quad \frac{d\beta}{d\theta_g} = \frac{1}{\|\nabla_{\mathbf{y}} G(\mathbf{y}^*(\theta_g), \theta_g)\|} \frac{\partial g(\mathcal{X}, \theta_g)}{\partial \theta_g}$$

In the latter case, it involves the partial derivative of the probability transformation (4.12) and turns out to be :

$$(4.83) \quad \frac{d\beta}{d\theta_f} = \alpha^*(\theta_f)^T \cdot \frac{\partial \mathcal{Y}(\mathcal{X}^*(\theta_f), \theta_f)}{\partial \theta_f}$$

where α^* is given by (4.81). The sensitivity of the *probability of failure* to parameters is obtained as :

$$(4.84) \quad \frac{dP_f}{d\theta} = -\varphi(\beta) \frac{d\beta}{d\theta}$$

The papers referred to in Section 3 all include sensitivity analysis of the reliability index, which gives better insight of the problems under consideration.

A special use of the sensitivity analysis is the following. Suppose the limit state function is defined in terms of one load effect, say, one component of displacement u^{i_0} and a threshold :

$$(4.85) \quad g(\mathbf{U}) = u^{i_0} - u$$

Obviously, the probability of failure associated with this limit state function is *identical* to the cumulative distribution function of u^{i_0} evaluated at u . It follows that the PDF of u_i can be computed as the sensitivity of P_f with respect to parameter u . This type of reasoning was applied in Liu and Der Kiureghian (1991a) and Zhang and Der Kiureghian (1997) to determine the complete PDF of a response quantity.

Sensitivity analysis can also be used to identify random variables whose uncertainty has insignificant influence on the reliability index and which can be replaced by deterministic values (*e.g.* the median values of such variables) (Madsen, 1988).

Another interesting application of sensitivity analysis can be found in Mahadevan and Haldar (1991), based on an idea first introduced by Der Kiureghian and Ke (1985). The problem under consideration is to determine whether a parameter representing a distributed load or a material property should be modeled as a random variable or a random field in a reliability study. By first considering all parameters as random variables, the authors determined the importance vector α^* (see Eq.(4.81)). From their numerical investigation, it appears that only those parameters χ_i corresponding to $|\alpha_i^*| > 0.3$ deserve to be modeled as random fields for a better accuracy of the results. The examples considered to determine this empirical value of 0.3 included a clamped beam, a portal frame and a two-dimensional plate with a hole.

To conclude, it is worth mentioning a recent book from Kleiber *et al.* (1997) entirely dedicated to finite element sensitivity analysis of linear and non-linear problems.

5 Response surface method

5.1 Introduction

In the previous sections, ingredients for a *direct coupling* between reliability analysis and finite element computations have been presented. It has been observed that the two most important issues making this “marriage” possible are :

- an unconditionally stable algorithm for the determination of the design point in the standard normal space (e.g. the iHLRF algorithm described in section 2.6),
- a practical method for computing gradients of the limit state function. The *direct differentiation method* described in section 3 turns out to be the most efficient approach. It can be applied to general problems including those involving material as well as geometric non-linearity and dynamics. However, it requires analytical developments that may become cumbersome when non-linear problems are addressed. These developments and the corresponding implementation have to be done from scratch for every class of problems. In contrast, the finite difference approach for gradient computation can be applied without modifying the finite element code, but requires much more computational effort (each gradient requires $(N + 1)$ evaluations of the limit state function, where N is the number of basic random variables).

As a consequence, when a large number of random variables is used together with the finite difference method (for instance, when a commercial finite element code is used, the source code of which not being accessible), the direct approach may eventually be really time consuming (Lemaire, 1998). The *response surface method* offers an alternative in this case.

5.2 Principle of the method

Let $\mathbf{X} = \{X_1, \dots, X_N\}$ be the vector of basic random variables. The basic idea of the response surface method is to approximate the exact limit state function $g(\mathbf{X})$, which is usually known only through an algorithmic procedure, by a polynomial function $\hat{g}(\mathbf{X})$. In practice, quadratic functions are used in the form :

$$(4.86) \quad g(\mathbf{x}) \approx \hat{g}(\mathbf{x}) = a_0 + \sum_{i=1}^N a_i x_i + \sum_{i=1}^N a_{ii} x_i^2 + \sum_{i=1}^N \sum_{j=1, j \neq i}^N a_{ij} x_i x_j$$

where the set of coefficients $\mathbf{a} = \{a_o, a_i, a_{ii}, a_{ij}\}^3$, which correspond to the *constant*, *linear*, *square*, and *cross* terms respectively, are to be determined.

It is argued that a limited number of evaluation of the limit state function (*i.e.* number of finite element runs) is required to build the surface. Then the reliability analysis can be performed by means of the analytical expression (4.86) instead of the true limit state function. This approach is particularly attractive when simulation methods such as importance sampling (Bucher and Bourgund, 1990) are used to get the reliability results.

5.3 Building the response surface

The determination of the unknown coefficients $\mathbf{a} = \{a_o, a_i, a_{ii}, a_{ij}\}$ is performed by the *least-square method*. After choosing a set of fitting points $\{\mathbf{x}^k, k = 1, \dots, \text{NF}\}$, for which the exact value $y^k = g(\mathbf{x}^k)$ is computed, the following error is minimized with respect to \mathbf{a} :

$$(4.87) \quad \text{err}(\mathbf{a}) = \sum_{k=1}^{\text{NF}} (y^k - \hat{g}(\mathbf{x}^k))^2$$

Recasting Eq.(4.86) in the form :

$$(4.88) \quad \hat{g}(\mathbf{x}) = \{1, x_i, x_i^2, x_i x_j\}^T \cdot \{a_o, a_i, a_{ii}, a_{ij}\} \equiv \mathbf{V}^T(\mathbf{x}^k) \cdot \mathbf{a}$$

the least-square problem becomes :

$$(4.89) \quad \text{Find } \mathbf{a} = \text{Argmin} \left\{ \sum_{k=1}^{\text{NF}} (y^k - \mathbf{V}^T(\mathbf{x}^k) \cdot \mathbf{a})^2 \right\}$$

After basic algebra (see for instance Faravelli (1989)), the solution of the above problem turns out to be :

$$(4.90) \quad \mathbf{a} = (\mathcal{V}^T \cdot \mathcal{V})^{-1} \cdot \mathcal{V}^T \cdot \mathbf{y}$$

where \mathcal{V} is the matrix whose rows are the vectors $\mathbf{V}(\mathbf{x}^k)$ (see Eq.(4.88)) and \mathbf{y} is the vector whose components are $y^k = g(\mathbf{x}^k)$.

The various response surface methods proposed in the literature differ only in the terms retained in the polynomial expression (4.86) (*e.g.* with or without cross terms), and the selection of the coordinates of the fitting points $\{\mathbf{x}^k, k = 1, \dots, \text{NF}\}$, *i.e.*, the *experimental design* used in the regression analysis. It is emphasized that $\text{NF} \geq N$ is required to be able to solve (4.90). Furthermore, the fitting points have to be chosen in a consistent way in order to get independent equations, *i.e.* an invertible $\mathcal{V}^T \cdot \mathcal{V}$.

³The subscripts (i, j) vary as described in Eq.(4.86). The variation is not explicitly written here for the sake of simplicity.

5.4 Various types of response surface approaches

Early applications of this method to the analysis of slope stability can be found in Wong (1985). The author employed the so-called *factorial* experimental design. For each random variable X_i , lower and upper values of realizations (x_i^- , x_i^+) are selected. As a whole, 2^N fitting points are defined by all the possible combinations $\{x_1^\pm, x_2^\pm, \dots, x_N^\pm\}$. Wong selected values symmetrically around the mean at a distance of one standard deviation, that is :

$$(4.91) \quad x_i^\pm = \mu_i \pm \sigma_i$$

The number of fitting points increases exponentially with the number of random variables N involved in the reliability problem under consideration.

In order to reduce the number of fitting points in case when N is large, Bucher and Bourgund (1990) proposed a simplified quadratic expression without cross terms, which is defined by only $(2N + 1)$ coefficients $\{a_0, a_i, a_{ii}\}$. In a first step, the mean vector μ_X is chosen as the center point of the response surface. Exactly $(2N + 1)$ fitting points are selected "along the axes" as follows :

$$(4.92) \quad \begin{cases} \mathbf{x}^1 &= \mu_X \\ \mathbf{x}^{2i} &= \mu_X - f \sigma_i \mathbf{e}_i, & i = 1, \dots, N \\ \mathbf{x}^{2i+1} &= \mu_X + f \sigma_i \mathbf{e}_i, & i = 1, \dots, N \end{cases}$$

where σ_i is the standard deviation of the i -th random variable, \mathbf{e}_i is the i -th basis vector of the space of parameters, whose coordinates are $\{0, \dots, 1, 0, \dots\}$, and f is an arbitrary number (set equal to 3 by Bucher and Bourgund (1990)).

From this first response surface, an estimate of the design point \mathbf{x}^* is computed. Then a new center point \mathbf{x}_M is obtained as a linear interpolation between μ_X and \mathbf{x}^* , so that it approximately zeroes the *exact* limit state function :

$$(4.93) \quad \mathbf{x}_M = \mu_X + (\mathbf{x}^* - \mu_X) \frac{g(\mu_X)}{g(\mu_X) - g(\mathbf{x}^*)}$$

A second response surface is then generated around \mathbf{x}_M . As a whole, the approach requires only $(4N + 3)$ evaluations of the limit state function, and can thus be carried out for structural systems involving a great number of random variables. Importance sampling is finally used to get the reliability results.

Rajashekhar and Ellingwood (1993) later considered the approach by Bucher and Bourgund (1990) as the first two steps of an iterative procedure they pushed forward until convergence. They also added cross terms to the response surface definition, obtaining better results in the numerical examples.

Analyzing the three papers presented above, Kim and Na (1997) observed that, in each case, the fitting points are selected around a preselected point (*e.g.* the mean value of the basic random vector) and arranged along the axes or the “diagonals” of the space of parameters, without any consideration on the orientation of the original limit state surface. The authors argued that these procedures may not converge to the true design point in some cases.

Alternatively, they proposed to determine a series of *linear* response surfaces as follows : In each iteration, the fitting points used in the previous step are projected onto the previous response surface, and the obtained projection points (which lie closer to the actual limit state surface) are used for generating the next response surface. In each iteration, an approximate reliability index is readily available, since the response surface is linear. In some sense, this method finds the design point without solving the minimization problem usually associated with FORM. The authors assessed the validity of this so-called *vector projection method* by comparing with Monte Carlo simulation (with 1,000,000 samples), first by using an analytical limit state function, then by studying a frame structure and a truss.

Starting from the paper by Kim and Na (1997), Das and Zheng (2000) recently proposed to enhance the linear response surface by adding square terms. The fitting points defining the final linear response surface are reused to produce the quadratic surface. SORM analysis is then performed.

Lemaire (1997) presents a synthetic summary of the response surface methods (called “adaptive” because of successive refinement until convergence around the design point) and draws the following conclusions :

- it is better to cast the response surface in the standard normal space rather than in the original space for reliability problems. All quantities being adimensional, there is a better control of the regression.
- Provided enough fitting points are used, the choice of the type of experimental design is not fundamental.
- The quality of the response surface has to be checked. Different indicators are proposed to estimate the accuracy, including :
 - the back-transformation of the fitting points from the standard normal space to the original space, in order to exclude non physical points,
 - the conditioning of the experimental matrix $\mathcal{V}^T \cdot \mathcal{V}$ appearing in Eq.(4.90),
 - the quality of the regression measured by a correlation coefficient,
 - the belonging of the obtained design point to the original limit state surface.

In order to reuse at best the finite element results, a data base keeping track of the finite element runs should be constructed.

5.5 Comparison between direct coupling and response surface methods

Few studies have been devoted to the actual comparison of the direct coupling and the response surface methods. A general discussion on their respective advantages can be found in Lemaire (1998).

Lemaire (1997) considers the problem of a hollow sphere submitted to internal pressure. The limit state function is defined analytically and FORM analysis is applied to get the reference results. The response surface method is then applied and gives identical results after three iterations.

Hornet *et al.* (1998) and Pendola *et al.* (2000c) proposed a benchmark problem in non-linear fracture mechanics. Crack initiation in a steel pipe submitted to internal pressure and axial tension is under consideration. Different finite element codes including ANSYS and CODE_ ASTER⁴ are used together with the reliability softwares RYFES⁵ (developed by Lemaire and his colleagues), COMREL (developed by Rackwitz and his colleagues) and PROBAN (developed by Det Norske Veritas). As far as accuracy is concerned, the direct coupling and the response surface method give identical results for probabilities of failure within $[10^{-10}, 10^{-1}]$ (corresponding to an increasing axial tension). As far as efficiency is concerned, Pendola *et al.* (2000c) show that the response surface approach allows to divide by 10 the number of finite element runs for the specific example. However, a finite difference scheme for gradient computation was applied in the direct coupling, which is not optimal. In this example, an axisymmetric non-linear finite element model was used.

A similar comparison has been carried out by Defaux and Heinfling (2000) on the problem of an hyperbolic cooling tower submitted to thermal and wind loading. A linear elastic three-dimensional finite element model using thin shell elements was used. In this case, the direct coupling and the response surface method gave the same results for similar computational cost.

5.6 Neural networks in reliability analysis

Before concluding this section, it is worth mentioning the recent introduction of neural networks in the context of reliability analysis. Basically, neural networks work as powerful

⁴This general purpose finite element code is developed by Electricité de France.

⁵RYFES stands for "Reliability using Your Finite Element Software".

interpolation tools, and can thus be used instead of quadratic response functions to approximate the limit state function. After being trained with a set of input/output data (here realizations of the vector of basic random variables, and corresponding value of the limit state function obtained after a finite element calculation), the neural network can produce reliable output values for any input at low cost.

Hurtado and Alvarez (2000) compare two types of networks called *multi-layer perceptrons* and *radial basis functions* networks. After being trained, the networks are used together with a crude Monte Carlo simulation to get the probability of failure. A system reliability problem associated with the collapse of a frame is considered. It appears that the radial basis functions network provide the best results with a rather small number of training samples.

Pendola *et al.* (2000a) introduce neural networks in conjunction with FORM analysis. The neural network replaces the quadratic response surface obtained after the iterative procedure described in section 5.4. Applying this approach to the benchmark problem described in Pendola *et al.* (2000b), the authors show that the results are identical to those obtained by the response surface method, the number of finite element simulations being however reduced by a factor 2.

5.7 Conclusions

Although the response surface method is an old idea, it seems to have gained new consideration in recent years. The up-to-date approach consists in generating quadratic response surfaces iteratively, where the center point converges to the design point. After convergence, any reliability method can be applied with the response surface, *e.g.* FORM, SORM or importance sampling.

From the few existing comparisons between the direct coupling and the response surface method, it seems that the same accuracy can be obtained by both approaches. When the response surfaces are carefully generated and checked at each step, convergence to the design point is always obtained in these comparisons. However, no proof has been given that this result is general.

As far as efficiency is concerned, the papers dealing with comparison of approaches always conclude that the computational cost of the response surface approach is far less than the direct approach. However all these applications consider a small number of random variables, typically 3-5. If a larger number of random variables were to be considered, the cost of generation of each response surface would probably blow up. Moreover, even for a small number of random variables, the comparisons of efficiency with the direct coupling are not fair, in the sense that gradients are usually computed by finite differences instead of direct differentiation.

As a summary, the response surface method appears to give accurate results for most problems applied, and may be faster than the direct coupling when a small number of random variables is considered, and when it is not possible to implement the direct differentiation method (for instance, when a commercial finite element code is used). Otherwise, the direct coupling will probably require less or equal amount of computation. These conclusions can change in the near future due to the introduction of neural networks in the field of reliability analysis.

6 Conclusions

In this chapter, methods coupling reliability and finite element analysis have been presented. The classical approach of reliability (FORM/SORM) has been summarized. The need of computing response gradients was emphasized. For this purpose, the direct differentiation method has been presented. It allows sensitivity analysis for general problems including material and geometrical non-linearities and dynamics. Using this approach, the computational cost of the gradient is a small increment over the cost of the non-linear response itself.

It has been shown that reliability analysis allows for obtaining PDFs of any response quantity. It should be noticed that this approach will give accurate results only for the tails of the PDF. Indeed it is based on FORM, which may be inaccurate for low reliability indices (large probabilities).

The response surface method has been presented as an alternative to direct coupling. It is also applicable to the most general problems and does not require the implementation of gradients in the finite element code. Whether one method is more efficient than the other depends fundamentally on the number of random variables included in the analysis and the way gradients are computed.

Chapter 5

Spectral stochastic finite element method

1 Introduction

The *spectral stochastic finite element method* (SSFEM) was proposed by Ghanem and Spanos (1990, 1991a) and presented in a comprehensive monograph by Ghanem and Spanos (1991b). It is an extension of the deterministic finite element method (FEM) for boundary value problems involving random material properties.

To understand what kind of discretization is introduced in SSFEM, let us come back for a while in the deterministic world, and consider a mechanical system Ω with deterministic geometry, material properties and loading. The evolution of such a system is governed by a set of partial differential equations (PDE) and associated boundary conditions and initial state. When no closed-form solution to these equations exists, a discretization procedure has to be applied in order to handle the problem numerically. In the usual finite element method, the geometry Ω is replaced by a set of points $\{\mathbf{x}_i, i = 1, \dots, N\}$ that are the nodes of the finite element mesh. Correspondingly the response of the system, *i.e.* the displacement field $\mathbf{u}(\mathbf{x})$ is approximated by means of nodal displacements $\{u^i, i = 1, \dots, N\}$ gathered into a vector \mathbf{U} . The set of PDE can then be transformed to a system of equations in $\{u^i\}_{i=1}^N$.

If a material property such as the Young's modulus is now modeled as a random field, the system will be governed by a set of *stochastic* PDE, and the response will be the displacement random field $\mathbf{u}(\mathbf{x}, \theta)$, where θ denotes a basic outcome in the space of all possible outcomes Θ^1 . A *spatial* discretization procedure such as that described in the

¹See notation in Chapter 2, Section 1.1.

above paragraph results in approximating the response as a *random vector of nodal displacements* $\mathbf{U}(\theta)$, each component being a random variable $u^i(\theta)$ yet to be characterized.

A random variable is completely determined by the value it takes for all possible outcomes $\theta \in \Theta$. Adopting the same kind of discretization as for the spatial part would result in selecting a finite set of points $\{\theta_1, \dots, \theta_Q\}$ in Θ . The Monte Carlo simulation of the problem corresponds to this kind of strategy. The realizations θ_i have to be selected with some rules to ensure that the space Θ is correctly sampled. It is however well known that an accurate description of the response would require a large value for Q .

SSFEM aims at discretizing the “random dimension” in a more efficient way using series expansions. Two different procedures are used.

- the input random field is discretized using the truncated Karhunen-Loève expansion presented in Chapter 2, Section 5.2.
- Each random nodal displacement $u^i(\theta)$ is represented by its coordinates in an appropriate basis of the space of random variables $\mathcal{L}^2(\Theta, \mathcal{F}, P)$, namely the *polynomial chaos*.

The outline of this chapter will be the following :

- SSFEM will be first developed in Section 2 for elastic two-dimensional problems involving a Gaussian random field for modeling the Young’s modulus of the material.
- Computational issues regarding the peculiar system of equations eventually obtained will be addressed in Section 3.
- Extensions of SSFEM to problems involving non Gaussian input random fields or multiple random fields will be presented in Section 4, as will the so-called *hybrid SSFEM*.
- A list of applications found in the literature will be given in Section 5.
- Finally advantages and limitations of SSFEM will be discussed in Section 6.

Some technical developments including the definition of the polynomial chaos and the additional tools related to the discretization of lognormal random field are gathered in an appendix at the end of this chapter.

2 SSFEM in elastic linear mechanical problems

2.1 Introduction

Rather than presenting SSFEM in a general, thus intricate way, the main ideas are first developed in this section on a simple example, namely the accounting of the spatial variability of the Young's modulus in an elastic mechanical system. In this case, the deterministic finite element method is assumed to be well-known. Hence only the approximated solution "in the random dimension" is developed.

2.2 Deterministic two-dimensional finite elements

Using classical notations, the finite element method in linear elasticity eventually yields a linear system of size $N \times N$ (N being the number of degrees of freedom) :

$$(5.1) \quad \mathbf{K} \cdot \mathbf{U} = \mathbf{F}$$

where the *global stiffness matrix* \mathbf{K} is obtained after assembling the *element stiffness matrices* \mathbf{k}^e :

$$(5.2) \quad \mathbf{k}^e = \int_{\Omega_e} \mathbf{B}^T \cdot \mathbf{D} \cdot \mathbf{B} d\Omega_e$$

In the above equation, \mathbf{D} stands for the elasticity matrix and \mathbf{B} is the matrix that relates the components of strain to the element nodal displacements.

2.3 Stochastic equilibrium equation

Suppose now that the material Young's modulus is a Gaussian² random field. The elasticity matrix in point \mathbf{x} can thus be written as :

$$(5.3) \quad \mathbf{D}(\mathbf{x}, \theta) \equiv H(\mathbf{x}, \theta) \mathbf{D}_o$$

where \mathbf{D}_o is a constant matrix. The Karhunen-Loève expansion of $H(\cdot)$ writes (Eq.(2.43)) :

$$(5.4) \quad H(\mathbf{x}, \theta) = \mu(\mathbf{x}) + \sum_{i=1}^{\infty} \sqrt{\lambda_i} \xi_i(\theta) \varphi_i(\mathbf{x})$$

²This assumption, which is not realistic, will be relaxed later.

Substituting for (5.3),(5.4) in (5.2) yields :

$$(5.5) \quad k^e(\theta) = k_o^e + \sum_{i=1}^{\infty} k_i^e \xi_i(\theta)$$

where k_o^e is the mean element stiffness matrix and k_i^e are *deterministic matrices* obtained by :

$$(5.6) \quad k_i^e = \sqrt{\lambda_i} \int_{\Omega_e} \varphi_i(x) B^T \cdot D_o \cdot B d\Omega_e$$

Assembling the above element contributions eventually gives the stochastic counterpart of the equilibrium equation (5.1) (assuming a deterministic load vector F) :

$$(5.7) \quad \left[K_o + \sum_{i=1}^{\infty} K_i \xi_i(\theta) \right] \cdot U(\theta) = F$$

In the above equation, K_i are *deterministic matrices* obtained by assembling k_i^e in a way similar to the deterministic case.

2.4 Representation of the response using Neumann series

The vector of nodal displacements $U(\theta)$ is formally obtained by inverting (5.7). However no closed-form solution for such an inverse exists. An early strategy adopted by Ghanem and Spanos (1991b) consists in using a Neumann series expansion of the inverse stochastic stiffness matrix to get an approximate response. Eq.(5.7) can be rewritten as :

$$(5.8) \quad K_o \cdot \left[I + \sum_{i=1}^{\infty} K_o^{-1} \cdot K_i \xi_i(\theta) \right] \cdot U(\theta) = F$$

which leads to :

$$(5.9) \quad U(\theta) = \left[I + \sum_{i=1}^{\infty} K_o^{-1} \cdot K_i \xi_i(\theta) \right]^{-1} \cdot U^0, \quad U^0 = K_o^{-1} \cdot F$$

The Neumann series expansion of the above equation has the form :

$$(5.10) \quad U(\theta) = \sum_{k=0}^{\infty} (-1)^k \left[\sum_{i=1}^{\infty} K_o^{-1} \cdot K_i \xi_i(\theta) \right]^k \cdot U^0$$

whose first terms explicitly write :

$$(5.11) \quad U(\theta) = \left[I - \sum_{i=1}^{\infty} K_o^{-1} \cdot K_i \xi_i(\theta) + \sum_{i=1}^{\infty} \sum_{j=1}^{\infty} K_o^{-1} \cdot K_i \cdot K_o^{-1} \cdot K_j \xi_i(\theta) \xi_j(\theta) + \dots \right] \cdot U^0$$

Truncating both the Karhunen-Loève and the Neumann expansions (indices i and k in Eq.(5.10), respectively) yields an approximate solution for $U(\theta)$.

2.5 General representation of the response in $\mathcal{L}^2(\Theta, \mathcal{F}, P)$

From (5.11) it is seen that each random displacement $u^i(\theta)$ can be represented as a series of polynomials in the standard normal variables $\{\xi_k(\theta)\}_{k=1}^{\infty}$. Reordering all terms by means of a single index j , this representation formally writes :

$$(5.12) \quad u^i(\theta) = \sum_{j=0}^{\infty} u_j^i \mathcal{P}_j \left(\{\xi_k(\theta)\}_{k=1}^{\infty} \right)$$

where $\mathcal{P}_0 \equiv 1$ and $\mathcal{P}_j \left(\{\xi_k(\theta)\}_{k=1}^{\infty} \right)$ are polynomials in standard normal variables, e.g. :

$$(5.13) \quad \mathcal{P}_j \left(\{\xi_k(\theta)\}_{k=1}^{\infty} \right) = \xi_{i_1}^{\alpha_1} \xi_{i_2}^{\alpha_2} \cdots \xi_{i_p}^{\alpha_p}$$

The set of $\{\mathcal{P}_j\}_{j=0}^{\infty}$ in Eq.(5.13) forms a *basis* of the space of all random variables $\mathcal{L}^2(\Theta, \mathcal{F}, P)$, and the coefficients u_j^i are interpreted as the coordinates of $u^i(\theta)$ in this basis.

Referring to the inner product defined in $\mathcal{L}^2(\Theta, \mathcal{F}, P)$ by Eq.(2.4-a), the above basis is however *not orthogonal*. For instance, $\xi_1(\theta)$ and $\xi_1^3(\theta)$ are two basis random variables whose inner product is $E[\xi_1^4] = 3$. For further exploitation of the response, such as computing its moments, an orthogonal basis appears more appealing.

The *polynomial chaos*³ proposed by Ghanem and Spanos (1991b) possesses this property. The details of its construction are quite technical and not essential to the understanding of SSFEM. Thus they are given in Appendix A.1 at the end of this chapter.

To proceed, let us assume that any random variable $u(\theta)$ element of $\mathcal{L}^2(\Theta, \mathcal{F}, P)$ can be given the following representation :

$$(5.14) \quad u(\theta) = \sum_{j=0}^{\infty} u_j \Psi_j(\theta)$$

where $\{\Psi_j(\theta)\}_{j=0}^{\infty}$ is a complete set of orthogonal random variables defined as polynomials in $\{\xi_k(\theta)\}_{k=1}^{\infty}$, satisfying⁴ :

$$(5.15-a) \quad \Psi_0 \equiv 1$$

$$(5.15-b) \quad E[\Psi_j] = 0 \quad j > 0$$

$$(5.15-c) \quad E[\Psi_j(\theta)\Psi_k(\theta)] = 0 \quad j \neq k$$

³Also referred to as Wiener chaos from the name of the mathematician who derived it first.

⁴Eq.(5.14) has been preferred to a more detailed notation such as $u(\theta) = \sum_{j=0}^{\infty} u_j \Psi_j \left(\{\xi_k(\theta)\}_{k=1}^M \right)$ for the sake of simplicity.

The expansion of the nodal displacements vector is consequently written as :

$$(5.16) \quad U(\theta) = \sum_{j=0}^{\infty} U_j \Psi_j(\theta)$$

the “coordinates” U_j being *deterministic* vectors having N components. Note that the first term U_0 in the above equation is *different* from the first term in the Neumann expansion (5.11). The latter, denoted by U^0 , is that obtained by a perturbation approach (see Chapter 3, Section 2).

By denoting $\xi_0(\theta) \equiv 1$ and substituting the above equation in (5.7), one gets :

$$(5.17) \quad \left(\sum_{i=0}^{\infty} K_i \xi_i(\theta) \right) \cdot \left(\sum_{j=0}^{\infty} U_j \Psi_j(\theta) \right) - F = 0$$

For computational purposes, the series involved in (5.17) are truncated after a finite number of terms, precisely $(M+1)$ for the stiffness matrix expansion (Karhunen-Loève expansion) and P for the displacements vector expansion. As a result, the residual in (5.17) due to the truncation reads :

$$(5.18) \quad \epsilon_{M,P} = \sum_{i=0}^M \sum_{j=0}^{P-1} K_i \cdot U_j \xi_i(\theta) \Psi_j(\theta) - F$$

The best approximation of the exact solution $U(\theta)$ in the space \mathcal{H}_P spanned by $\{\Psi_k\}_{k=0}^{P-1}$ is obtained by *minimizing* this residual in a mean square sense. In the Hilbert space $\mathcal{L}^2(\Theta, \mathcal{F}, P)$, this is equivalent to requiring that this residual be orthogonal to \mathcal{H}_P , which yields :

$$(5.19) \quad E[\epsilon_{M,P} \cdot \Psi_k] = 0 \quad k = 0, \dots, P-1$$

Let us introduce the following notation :

$$(5.20) \quad c_{ijk} = E[\xi_i \Psi_j \Psi_k]$$

$$(5.21) \quad F_k = E[\Psi_k F]$$

Note that F_k is zero for $k > 0$ in the case of deterministic loading considered in this report. Using (5.18), Eq.(5.19) can be rewritten as :

$$(5.22) \quad \sum_{i=0}^M \sum_{j=0}^{P-1} c_{ijk} K_i \cdot U_j = F_k \quad k = 0, \dots, P-1$$

For the sake of simplicity, let us define :

$$(5.23) \quad K_{jk} = \sum_{i=0}^M c_{ijk} K_i$$

Hence Eq.(5.22) rewrites :

$$(5.24) \quad \sum_{j=0}^{P-1} \mathbf{K}_{jk} \cdot \mathbf{U}_j = \mathbf{F}_k \quad k = 0, \dots, P-1$$

In the above equations, each \mathbf{U}_j is a N -dimensional vector, each \mathbf{K}_{jk} a matrix of size $N \times N$. The P different equations can be cast in a linear system of size $NP \times NP$ as follows :

$$(5.25) \quad \begin{bmatrix} \mathbf{K}_{00} & \dots & \mathbf{K}_{0,P-1} \\ \mathbf{K}_{10} & \dots & \mathbf{K}_{1,P-1} \\ \vdots & & \vdots \\ \mathbf{K}_{P-1,0} & \dots & \mathbf{K}_{P-1,P-1} \end{bmatrix} \cdot \begin{bmatrix} \mathbf{U}_0 \\ \mathbf{U}_1 \\ \vdots \\ \mathbf{U}_{P-1} \end{bmatrix} = \begin{bmatrix} \mathbf{F}_0 \\ \mathbf{F}_1 \\ \vdots \\ \mathbf{F}_{P-1} \end{bmatrix}$$

which may formally be rewritten as :

$$(5.26) \quad \mathcal{K} \cdot \mathcal{U} = \mathcal{F}$$

After solving this system for $\mathcal{U} = \{\mathbf{U}_k, k = 0, \dots, P-1\}$, the best approximation of $\mathbf{U}(\theta)$ in the subspace \mathcal{H}_P spanned by $\{\Psi_k\}_{k=0}^{P-1}$ is given by :

$$(5.27) \quad \mathbf{U}(\theta) = \sum_{j=0}^{P-1} \mathbf{U}_j \Psi_j(\theta)$$

As reported in Appendix A, Section A.1.2, the dimension P of \mathcal{H}_P is usually 10-35 in application. This means that any nodal displacement is characterized as a random variable by 15-35 coefficients. The amount of computation required for solving the linear system (5.26) is thus much greater than that required for the deterministic analysis of the same problem.

2.6 Post-processing of the results

The coefficients in Eq.(5.27) do not provide a clear interpretation of the response randomness in themselves. The following useful quantities are however readily obtained.

- The *mean* nodal displacement vector $\mathbb{E}[\mathbf{U}]$ is the first term of the expansion, namely \mathbf{U}_0 , since $\mathbb{E}[\Psi_j(\theta)] = 0$ for $j > 0$.
- The *covariance matrix* of the components of vector \mathbf{U} is :

$$(5.28) \quad \text{Cov}[\mathbf{U}, \mathbf{U}] = \sum_{i=1}^{P-1} \mathbb{E}[\Psi_i^2] \mathbf{U}_i \cdot \mathbf{U}_i^T$$

the coefficients $\mathbb{E}[\Psi_i^2]$ being easily computed due to the definition of the Ψ_i 's (See Appendix A.1).

- The probability density function of any component U^i of the nodal displacement vector can be obtained by simulating the basis random variables $\Psi_j(\theta)$, then using Eq.(5.27). In the case when this equation is limited to quadratic terms (second order polynomial chaos), a closed-form expression for the *characteristic function* of U has been given by Ghanem (1999a), which can be then numerically Fourier-transformed to obtain the required PDF.
- Reliability analysis has been claimed a straightforward byproduct of SSFEM in Ghanem and Spanos (1991b). However no such application could be found in the literature.

It seems possible to couple the general reliability tools developed in Chapter 4, Section 2 with SSFEM. Let us consider for instance a limit state function of the following form :

$$(5.29) \quad g(\mathbf{U}(\theta)) = u - u^{i_0}$$

where u^{i_0} is a nodal displacement under consideration and u is a prescribed threshold. Substituting the i_0 -th component of the vectorial equation (5.27) in (5.29) yields the following *analytical* polynomial expression of the limit state function :

$$(5.30) \quad g(\mathbf{U}(\theta)) = u - \sum_{j=0}^{P-1} u_j^{i_0} \Psi_j(\{\xi_k(\theta)\}_{k=1}^{\infty})$$

This limit state function is already cast in the standard normal space due to the definition of the polynomials $\Psi_j(\{\xi_k(\theta)\}_{k=1}^{\infty})$. Moreover, its gradient with respect to the basic random variables can easily be obtained in closed-form as well. Determining the design point and associated probability of failure should thus be straightforward.

Of course, this approach requires having solved (5.25) beforehand and it is probably not efficient when a single reliability problem is to be solved. In contrast, it might be interesting when the probability density function of a response quantity is to be determined by sensitivity analysis after repeated FORM analyses (see Chapter 4, Section 4), or when *system* reliability is under consideration (in the latter case, a number of previous component reliability analyses is required as well).

In any case, the accuracy of this approach has to be checked. Especially the accuracy in representing the tails of the PDF of the response should be carefully evaluated (these tails are essential in reliability analysis). It may happen that an acceptable accuracy requires a large number of terms P in the expansion of the response. This approach must eventually be compared to the classical finite element reliability approach developed in chapter 4 in terms of accuracy and efficiency.

3 Computational aspects

3.1 Introduction

As it can be seen in Eq.(5.25), the size of the linear system resulting from the SSFEM approach increases rapidly with the series cut-off number P . Whenever classical direct methods are used to solve the system, the computational time may blow up rapidly. This is the reason why early applications of SSFEM were limited to a small number of degrees of freedom N . Only in recent papers was the problem of computational efficiency of SSFEM addressed (Ghanem and Kruger, 1996; Pellissetti and Ghanem, 2000). The main results are reported in this section.

3.2 Structure of the stochastic stiffness matrix

Eqs.(5.23)-(5.24) suggest that the global matrix \mathcal{K} is completely determined by the matrices \mathbf{K}_i and the coefficients c_{ijk} . Storing \mathcal{K} as these building blocks \mathbf{K}_i along with the c_{ijk} coefficients reduces the required amount of memory considerably. Ghanem and Kruger (1996) took the example of a 4-term KL expansion. Using a second (resp. third) order polynomial chaos, the proposed method requires 11 times (resp. 33 times) less memory compared to the classical global storage. It turns out that a large number of coefficients c_{ijk} are zero (see the tables in Ghanem and Spanos (1991b, chap. 3)).

It is recalled that \mathbf{K}_0 corresponds to the stiffness matrix of a system having the *mean* material properties. In the same way, \mathbf{K}_i , $i > 0$, can be viewed as the stiffness matrix corresponding to a certain spatial fluctuation of the material properties given by the eigenfunction $\varphi_i(\boldsymbol{x})$. Since the mean of these fluctuations is zero, and if they are bounded within a certain range, the entries of \mathbf{K}_0 are expected to be dominant in magnitude. Furthermore, it is easily seen from (5.20) that $c_{ojk} \propto \delta_{jk}$ since $\xi_o \equiv 1$ and the Ψ_j 's are orthogonal to one another. Examining now (5.23), this means that \mathbf{K}_0 has a contribution only in the \mathbf{K}_{jj} blocks that are on the main diagonal of \mathcal{K} . These arguments tend to prove a diagonal dominance in \mathcal{K} which should be taken advantage of in the solution scheme. Finally the matrices \mathbf{K}_i all have the same non-zero structure, which can simplify the storage.

3.3 Solution algorithms

To take advantage of the proposed storage scheme, it is necessary that the solution method not require explicit assembling of \mathcal{K} . Iterative methods such as the *conjugate gradient method* are well suited to this situation, since they only require matrix-vector

products. It is thus sufficient to compute the matrices K_{jk} by means of Eq.(5.23) each time they are operated on. Since only a small number of coefficient c_{ijk} is non zero, this is not a time-consuming task.

In the context of iterative algorithms for solving linear systems, the spectral condition number of the matrix (the ratio between its largest and smallest eigenvalues) is of paramount importance. These algorithms rapidly converge when the condition number is low. To enhance the convergence, *preconditioning techniques* (see Demmel (1997) for a state-of-the-art review) have been proposed. They essentially replace the original system $K \cdot U = F$ by :

$$(5.31) \quad M^{-1} K \cdot U = M^{-1} \cdot F$$

where the condition number of $M^{-1} K$ is much lower than that of K .

The Jacobi preconditioner ($M = \text{diag}(K)$) and incomplete factorization preconditioners ($M = L^{\text{inc}} U^{\text{inc}}$, L^{inc} and U^{inc} being the incomplete triangular factors of K) are usually employed in the context of deterministic finite elements.

Due to the properties mentioned in Section 3.2, the following preconditioning matrix was proposed by Ghanem and Kruger (1996) for efficient solution of the SSFEM linear system :

$$(5.32) \quad M = \text{diag} \{ \hat{K}_{jj} \} \equiv \begin{bmatrix} \hat{K}_{00} & 0 & \dots & 0 \\ 0 & \hat{K}_{11} & 0 & 0 \\ \vdots & & & \vdots \\ 0 & 0 & \dots & \hat{K}_{P-1,P-1} \end{bmatrix} \quad \text{where} \quad \hat{K}_{jj} = c_{0jj} L_{K_o}^{\text{inc}} U_{K_o}^{\text{inc}}$$

Applying this approach to a system with $N = 264$ degrees of freedom and $P = 5, 15$, the authors showed that the proposed preconditioner allows to divide the number of iterations by 12-15 compared to the Jacobi preconditioner. Moreover, the former leads to a number of iterations independent of the coefficient of variation of the input field whereas the latter does not⁵.

3.4 Hierarchical approach

The polynomial chaos basis is called *hierarchical* because increasing the dimension of the functional space (*i.e.* P) does not change the lower-order basis functions. This leads to the following solution strategy. Suppose the linear system (5.26) is partitioned as

⁵The larger the coefficient of variation, the larger the condition number of K .

follows :

$$(5.33) \quad \begin{bmatrix} K_{ll} & K_{lh} \\ K_{hl} & K_{hh} \end{bmatrix} \cdot \begin{bmatrix} U_l \\ U_h \end{bmatrix} = \begin{bmatrix} F_l \\ F_h \end{bmatrix}$$

where $()_l$ and $()_h$ stand for *lower* and *higher* order terms, respectively.

If the lower-order solution $\tilde{U}_l = K_{ll}^{-1} \cdot F_l$ was obtained with sufficient accuracy, it can be expected to be close to U_l appearing in (5.33). Thus an approximate solution of (5.33) is :

$$(5.34) \quad U_l = \tilde{U}_l$$

$$(5.35) \quad U_h = K_{hh}^{-1} (F_h - K_{hl} \cdot \tilde{U}_l)$$

It is then possible to enhance successively the solution (5.27) starting from a lower-order solution and using (5.35) by adding one basis polynomial at each time. As the lower-order coefficients are not modified along the procedure, this could lead to a successive built-up of error.

On an example application, Ghanem and Kruger (1996) found no significant discrepancy between the results obtained by this procedure and those obtained by a direct higher-order resolution. However, there is no proof or evidence that this is a general result. It is likely that the accuracy of the results obtained by the hierarchical approach decays when the coefficient of variation of the input field increases. A more exhaustive study should be carried out to assess the validity of this approach.

4 Extensions of SSFEM

4.1 Lognormal input random field

The use of Gaussian random fields is quite common in the context of probabilistic mechanics. However these fields are not well suited to modeling material properties (Young's modulus, yield stress, etc.) which are by their nature *positive* valued. Indeed for large coefficients of variation, realizations of the field could include negative outcomes that are physically meaningless. In contrast, the lognormal field appears attractive in this sense. A lognormal field can be defined by a transformation of a Gaussian field $g(\mathbf{x})$ as :

$$(5.36) \quad l(\mathbf{x}) = e^{g(\mathbf{x})}$$

The Karhunen-Loève expansion of a lognormal field, although possible, is of no practical interest since the probabilistic structure of the random variables $\{\xi_i\}$ appearing in the expansion cannot be determined. In order to be able to include lognormal fields in the SSFEM approach, Ghanem (1999b) proposed to expand them into the polynomial chaos. Due to the particular form of (5.36), this leads to closed-form expressions.

4.1.1 Lognormal random variable

Let us first consider a single lognormal random variable obtained as follows :

$$(5.37) \quad I = e^{\mu_g + \sigma_g \xi}$$

where ξ is a standard normal variable. The polynomial chaos expansion of I reads :

$$(5.38) \quad I = \sum_{i=0}^{\infty} I_i \Psi_i(\xi)$$

where $\Psi_i(\xi)$ is the i -th Hermite polynomial in this case. Due to the orthogonality properties of the Ψ_i 's, the coefficients I_i can be obtained as :

$$(5.39) \quad I_i = \frac{\mathbb{E}[\exp(\mu_g + \sigma_g \xi) \Psi_i(\xi)]}{\mathbb{E}[\Psi_i^2]}$$

which, after some algebra, reduces to :

$$(5.40) \quad I_i = \frac{\mathbb{E}[\Psi_i(\xi + \sigma_g)]}{\mathbb{E}[\Psi_i^2]} \exp\left[\mu_g + \frac{1}{2}\sigma_g^2\right]$$

The fraction in the above equation turns out to be $\frac{\sigma_g^i}{i!}$ after some algebra, whereas the exponential term is nothing but the mean value of I , denoted by μ_I . Thus the expansion of any lognormal random variable into the (one-dimensional) polynomial chaos reduces to :

$$(5.41) \quad I = \mu_I \sum_{i=0}^{\infty} \frac{\sigma_g^i}{i!} \Psi_i(\xi)$$

4.1.2 Lognormal random field

Let us now consider the approximate lognormal field $I(\mathbf{x})$ defined by exponentiating the following truncated Karhunen-Loève expansion of a Gaussian random field $g(\mathbf{x})$:

$$(5.42) \quad I(\mathbf{x}) = \exp\left[\mu_g(\mathbf{x}) + \sum_{i=1}^M g_i(\mathbf{x}) \xi_i\right] = \exp\left[\mu_g(\mathbf{x}) + \mathbf{g}(\mathbf{x})^T \cdot \boldsymbol{\xi}\right]$$

The polynomial chaos expansion now reads :

$$(5.43) \quad I(\mathbf{x}) = \sum_{i=0}^{\infty} I_i(\mathbf{x}) \Psi_i(\boldsymbol{\xi})$$

Closed-form expressions of the coefficients $I_i(\mathbf{x})$ are given in appendix A.2 at the end of this chapter.

To use SSFEM in conjunction with a lognormal input random field is now straightforward : the procedure described in Section 2 applies, where Eq.(5.4) is replaced by Eq.(5.38). The stochastic equilibrium equation (see Eq.(5.7)) now writes :

$$(5.44) \quad \left(\sum_{i=0}^{\infty} K_i \Psi_i(\theta) \right) \cdot U(\theta) = F$$

After truncation of the latter after P terms, the Galerkin minimization of error leads to a system of linear equations similar to (5.22), the coefficients c_{ijk} being now replaced by :

$$(5.45) \quad d_{ijk} = E[\Psi_i \Psi_j \Psi_k]$$

The polynomial chaos expansion of the input random field introduces a new approximation in SSFEM, which probably decreases the accuracy of the method. This accuracy has not been stated by Ghanem and his co-workers. Whether a fair accuracy could be obtained with a manageable number of terms in the series expansion is of crucial importance. Unfortunately no comparison with other methods (*e.g.* Monte Carlo simulation) are provided in Ghanem (1999*b,c*). Regarding reliability problems, the accuracy in the tails of PDFs is probably also affected by the use of the polynomial chaos expansion of the input random field.

4.2 Multiple input random fields

It is usual that more than one material property governs the evolution of a system. Consider for instance Young's modulus and Poisson's ratio in mechanical problems, conductivity and heat capacity in heat conduction, etc. In a probabilistic context, all these quantities have to be modeled as random fields⁶.

This is completed in the following manner : each field is discretized using different sets of standard normal variables, say $\{\xi_1, \dots, \xi_M\}$ for the first one, $\{\xi_{M+1}, \dots, \xi_{M'}\}$ for the second, etc. All these variables are then merged in a single list, the size of which determines the dimension of the polynomial chaos expansion of the response. This technique was applied in the heat conduction example presented by Ghanem (1999*c*).

Except from the point of view of data management, using multiple input random fields seems not a difficult task. However multiplying by 2 the length of vector ξ increases dramatically the size of the polynomial chaos basis (see for instance table 5.2, page 96), which basically controls the computation time.

⁶We suppose here the statistical independence of these fields

4.3 Hybrid SSFEM

4.3.1 Monte Carlo simulation

The SSFEM formalism consists in expanding the response process over a basis of $\mathcal{L}^2(\Theta, \mathcal{F}, P)$, namely the polynomial chaos. If the basis functions $\Psi_i(\theta)$ were *Dirac delta functions* $\delta(\theta - \theta_i)$, where θ_i denotes a particular sample in Θ , a collocation-like procedure along the random dimension would be obtained. Thus the response process is now considered as the *infinite* set of its realizations, and an approximation is defined by a finite set of θ_i 's. As stated in the introduction, this is in some sense the definition of Monte Carlo simulation.

Let Q be the number of samples. Practically speaking, a linear system $\mathbf{K}(\theta_i) \cdot \mathbf{U}(\theta_i) = \mathbf{F}$ is solved for each $\theta_i, i = 1, \dots, Q$. The whole simulation can be cast in the following linear system of size $NQ \times NQ$:

$$(5.46) \quad \begin{bmatrix} \mathbf{K}(\theta_1) & 0 & \dots & 0 \\ 0 & \mathbf{K}(\theta_2) & \dots & 0 \\ \vdots & 0 & \dots & \vdots \\ \vdots & \vdots & \dots & \vdots \\ 0 & 0 & \dots & \mathbf{K}(\theta_Q) \end{bmatrix} \cdot \begin{bmatrix} \mathbf{U}_1 \\ \mathbf{U}_2 \\ \vdots \\ \vdots \\ \mathbf{U}_Q \end{bmatrix} = \begin{bmatrix} \mathbf{F}_1 \\ \mathbf{F}_2 \\ \vdots \\ \vdots \\ \mathbf{F}_Q \end{bmatrix}$$

This system is similar in structure as that of Eq.(5.25), the size of which being $NP \times NP$. It is simpler because it can be solved by blocks resulting in Q systems of size $N \times N$. In practical applications, Q is much greater than P (3-4 orders of magnitude). However, depending on the matrix storage and solving scheme, there should exist a threshold level for which one procedure (SSFEM or Monte Carlo simulation) becomes more efficient than the other.

4.3.2 Coupling SSFEM and MCS

The *hybrid* SSFEM proposed by Ghanem (1998a) is a coupling of Monte Carlo simulation and SSFEM. Using a P -terms polynomial chaos expansion of the response, and expanding the residual in terms of a set of delta functions $\Phi_j(\theta) = \delta(\theta - \theta_j)$ results in :

$$(5.47) \quad \mathbf{U}(\theta) \approx \sum_{j=0}^{P-1} \mathbf{U}_j \Psi_j(\theta) + \sum_{j=0}^{Q-1} \mathbf{U}_j^* \Phi_j(\theta)$$

The above expansion is substituted for in the equilibrium equation, and the obtained residual is made orthogonal both to the Ψ_j 's and the Φ_j 's. This leads to a $N(P+Q) \times N(P+Q)$ linear system. Further assumptions resulting in the partial decoupling of the equations are introduced. The linear system is then solved iteratively at lower cost than by the direct approach.

4.3.3 Concluding remarks

Details of the hybrid method can be found in Ghanem (1998a). However no convincing application of these ideas has been published so far. Moreover, the delta functions do not form a numerable set, and their use as a basis of $\mathcal{L}^2(\Theta, \mathcal{F}, P)$ or a subspace of it is questionable. The decoupling assumption which leads to the iterative procedure mentioned above is not really argued. There is globally a lack of mathematical justification of the method. Further theoretical research as well as applications are needed to assess the validity of this approach.

5 Summary of the SSFEM applications

The main applications of SSFEM found in the literature can be summarized as follows :

- Early applications (Spanos and Ghanem (1989); Ghanem and Spanos (1991a,b)) dealt with one- and two dimensional linear elastic structures : a cantilever beam with Gaussian flexural rigidity EI subjected to a deterministic transverse load at its free end, a square plate clamped along one edge and subjected to a uniform in-plane tension along the opposite edge with Gaussian Young's modulus, a clamped curve plate for which the KL expansion had to be computed numerically. Coefficients of variation of the response as well as PDF's were determined and compared to those obtained by Monte Carlo simulation. The number of finite elements in these examples was limited to 16. The maximal accuracy adopted in these examples was a 3rd order - 4-dimensional polynomial chaos. For medium COV of the input (say 15-30%), only these most accurate results compare fairly well with the Monte Carlo simulation results.
- Ghanem and Brzkala (1996) addressed the problem of a two-layer soil mass with deterministic properties in each layer and Gaussian random interface, subjected to a constant pressure on part of its free surface. In this case, the random field representing the Young's modulus of the material is not Gaussian due to its non-linear relationship with the Gaussian field defining the interface. Thus the stiffness matrix had to be expanded over the polynomial chaos as in Eq.(5.44).
- Waubke (1996) addressed the problem of deterministic vibrations of a rigid plate over a two-layer soil mass with random elastic parameters.
- The application of SSFEM to transport of contaminant in unsaturated porous media was addressed by Ghanem (1998b). The permeability coefficients as well as the diffusion coefficient are modeled as Gaussian random fields and discretized using

Karhunen-Loève expansion. The effective head and the contaminant concentration are expanded into the polynomial chaos. The numerical results include the coefficients in the expansion of the concentration as well as the variance of the latter over the domain. No comparison with other approaches (*e.g.* Monte Carlo simulation) is given.

- The problem of heat conduction was addressed by Ghanem (1999c). In this case, both the conductivity and the heat capacity are modeled as Gaussian or lognormal random fields. As an example, a one-dimensional domain of unit length is subjected to a constant flux at one end and perfectly insulated at the other one. The initial temperature of the domain is uniform. It is divided in 10 elements. The COV of the input is up to 40%. The results are presented in terms of the coefficients of the polynomial chaos expansion. Neither post-processing of these results nor comparison with Monte Carlo simulation is provided in this paper. Due to the relatively small number of terms included in the expansions ($M = 2 - 3$), it is difficult to judge the accuracy of the results or even interpret them.
- The first application of SSFEM to elasto-plastic problems can be found in Anders and Hori (1999) introducing some simplifying assumptions. The elasto-plastic constitutive law indeed defines the plastic strain rate proportional to the derivative of the yield criterion with respect to the current stress. In a stochastic context, this would imply differentiation with respect to random variables, which is not an easy task (see Ghanem (1999a) for some theoretical developments and references on this topic). Moreover, it is not clear how to enforce the negativeness of the yield criterion when the stress is now a random quantity.

Thus the authors simplified the problem introducing two *bounding solids*, whose mechanical properties allow to bound the stresses. The plastic flow rule is thus applied with *deterministic* bounding stresses in each point. Although these assumptions are questionable, this is the only example of real non-linear application of SSFEM, which shows that a lot of work remains in this matter.

6 Advantages and limitations of SSFEM

In this chapter, SSFEM has been presented in a comprehensive way including the most recent developments. As an extension of the deterministic finite element method, this approach represents the response as a vector of random nodal displacements. Each component of this vector is characterized by its coefficients in a series of polynomials in standard normal variables. Due to this property, the representation of the response randomness is said to be *intrinsic*.

Formally, Eq.(5.27) can be interpreted as a polynomial response surface for the displacement field, defined by means of the basic random variables $\{\xi_i\}_{i=1}^M$. In contrast with usual response surface methods such as those described in Chapter 4, Section 5, SSFEM allows to define it at any order in a consistent framework.

Note that in all applications found in the literature, only the Karhunen-Loève expansion has been used to discretize the input Gaussian random field. The use of other schemes such as OSE or EOLE would however be possible and in some case more practical than KL (for instance when other correlation structures than that with exponential decay are dealt with).

The approximate solution Eq.(5.27) is obtained in the context of Galerkin minimization of residuals. General convergence properties to the exact solution are associated with this procedure : when the number of terms in the series tends to infinity, SSFEM tends to be "exact".

However the following limitations of the method have to be recognized :

- it is practically limited to *linear* problems. Material non linearity (*e.g.* plasticity) or geometrical non-linearity cannot be dealt with by SSFEM in its latest state of development.
- The amount of computation required for a given problem is much greater than that of the equivalent deterministic problem. Typically 15-35 coefficients are needed to characterize each nodal displacement. As a consequence a huge amount of output data is available. The question of whether this data is *really* useful for practical problems has not been addressed.
- The truncation of the series involved in SSFEM introduces approximation. So far, no *error estimator* has been developed and no real study of the accuracy of the method has been carried out, except some comparisons with Monte Carlo simulations presented in early papers by Ghanem and Spanos.
- Although it is claimed in different papers quoted above that the reliability analysis is a straightforward post-processing of SSFEM, no application could be found in the literature. The application of SSFEM to reliability analysis remains broadly an open problem. Important issues such as the accuracy of SSFEM in representing the tails of the PDFs of response quantities have to be addressed for this purpose.
- When lognormal random fields are used, another accuracy issue comes up. Even for a single variable, only an infinite number of terms in the expansion reproduces the lognormal characteristic. This means that the input field defined by using only a few terms in the polynomial chaos expansion (Eq.(5.38)) can be far from the actual lognormal field.

As a conclusion, it is noted that SSFEM is a quite new approach. Although limited for the time being, it deserves further investigation and comparisons with other approaches to assess its efficiency.

Appendix

A.1 Polynomial chaos expansion

A.1.1 Definition

The polynomial chaos is a particular basis of the space of random variables $\mathcal{L}^2(\Theta, \mathcal{F}, P)$ based on Hermite polynomials of standard normal variables.

Classically, the one-dimensional Hermite polynomials are defined by :

$$(5.48) \quad h_n(x) = (-1)^n \frac{d^n \left[e^{-\frac{1}{2}x^2} \right]}{dx^n} e^{\frac{1}{2}x^2}$$

Hermite polynomials of independent standard normal variables are orthogonal to each other with respect to the inner product of $\mathcal{L}^2(\Theta, \mathcal{F}, P)$ defined in (2.4-a), that is :

$$(5.49) \quad \mathbb{E} [h_m(\xi_i(\theta)) h_n(\xi_j(\theta))] = 0, \quad m \neq n$$

Multidimensional Hermite polynomials can be defined as products of Hermite polynomials of independent standard normal variables. To further specify their construction, let us consider the following integer sequences :

$$(5.50) \quad \alpha = \{\alpha_1, \dots, \alpha_p\} \quad \alpha_j \geq 0$$

$$(5.51) \quad i = \{i_1, \dots, i_p\} \quad i_j > 0$$

The multidimensional Hermite polynomial associated with the sequences (i, α) is :

$$(5.52) \quad \Psi_{i,\alpha}(\theta) = \prod_{k=1}^p h_{\alpha_k}(\xi_{i_k}(\theta))$$

It turns out that the set $\{\Psi_{i,\alpha}\}$ of all polynomials associated with all possible sequences (i, α) of any length p forms a basis in $\mathcal{L}^2(\Theta, \mathcal{F}, P)$.

For further convenience, let us denote by $\Gamma_p(\xi_{i_1}(\theta), \dots, \xi_{i_p}(\theta))$ the set of basis polynomials $\{\Psi_{i,\alpha}(\theta) \mid \sum_{k=1}^p \alpha_k = p\}$ and by Γ_p the space they span. Γ_p is a subspace of $\mathcal{L}^2(\Theta, \mathcal{F}, P)$, usually called *homogeneous chaos of order p*. The subspaces Γ_p are orthogonal to each other in $\mathcal{L}^2(\Theta, \mathcal{F}, P)$. This is easily proven by the fact that they are spanned by two sets of $\Psi_{i,\alpha}$ having null intersection. Thus the following relationship, known as the *Wiener Chaos decomposition*, holds :

$$(5.53) \quad \bigoplus_{k=0}^{\infty} \Gamma_k = \mathcal{L}^2(\Theta, \mathcal{F}, P)$$

where \oplus denotes the operator of orthogonal summation of subspaces in linear algebra. Consequently the expansion of any random variable $u(\theta)$ in the polynomial chaos can be written as :

$$(5.54) \quad u(\theta) = u_o \Gamma_o + \sum_{i_1=1}^{\infty} u_{i_1} \Gamma_1(\xi_{i_1}(\theta)) + \sum_{i_1=1}^{\infty} \sum_{i_2=1}^{\infty} u_{i_1 i_2} \Gamma_2(\xi_{i_1}(\theta), \xi_{i_2}(\theta)) + \dots$$

In this expression $u_o, u_{i_1}, u_{i_1 i_2}$ are the “coordinates” of $u(\theta)$ associated with 0-th, first and second order homogeneous chaoses respectively. The lower order homogeneous chaos have the following closed-form expression :

$$(5.55-a) \quad \Gamma_o = 1$$

$$(5.55-b) \quad \Gamma_1(\xi_i) = \xi_i$$

$$(5.55-c) \quad \Gamma_2(\xi_{i_1}, \xi_{i_2}) = \xi_{i_1} \xi_{i_2} - \delta_{i_1 i_2}$$

$$(5.55-d) \quad \Gamma_3(\xi_{i_1}, \xi_{i_2}, \xi_{i_3}) = \xi_{i_1} \xi_{i_2} \xi_{i_3} - \xi_{i_1} \delta_{i_2 i_3} - \xi_{i_2} \delta_{i_3 i_1} - \xi_{i_3} \delta_{i_1 i_2}$$

Remark The polynomial chaos can be related to the (non orthogonal) basis associated with the Neumann series expansion, see Eq.(5.13). For this purpose, let us introduce the *orthogonal projection* π_p of $\mathcal{L}^2(\Theta, \mathcal{F}, P)$ onto Γ_p . It can be shown that the following relationship holds⁷ :

$$(5.56) \quad \pi_p(\xi_{i_1}^{\alpha_1}(\theta) \dots \xi_{i_p}^{\alpha_p}(\theta)) = \Psi_{i, \alpha}$$

A.1.2 Computational implementation

For computational purposes, *finite dimensional* polynomial chaoses are constructed by means of a *finite number* M of orthonormal Gaussian random variables. These variables are for instance selected from the Karhunen-Loève expansion of the input random field. The polynomial basis formed by means of these M random variables is denoted by $\Gamma_p(\xi_1, \dots, \xi_M)$ and it is called *homogeneous chaos of dimension M and order p* .

Due to (5.52), the basis $\Gamma_p(\xi_1, \dots, \xi_M)$ is generated as follows. To each set of M integers $\{\alpha_1, \dots, \alpha_M\}$ ranging from 0 to p and summing up to p , the following basis vector is associated :

$$(5.57) \quad \Psi_{\alpha} = \prod_{i=1}^M h_{\alpha_i}(\xi_i)$$

This formula allows for a systematic construction of the polynomial chaoses of any order. It can be shown that the dimension of $\Gamma_p(\xi_1, \dots, \xi_M)$ is the binomial factor $\binom{M+p-1}{p}$.

⁷This relationship and other mathematical properties of the polynomial chaos can be found in Ghanem (1999a).

The lower-dimensional polynomial chaoses (up to $M = 4$) have been tabulated by Ghanem and Spanos (1991*b*, chap. 2) for different orders (up to $p = 4$). As an example, Table 5.1 gives the two-dimensional polynomial chaoses at different orders.

Table 5.1: Two-dimensional polynomial chaoses

j	p	j -th basis polynomial Ψ_j
0	$p = 0$	1
1	$p = 1$	ξ_1
2		ξ_2
3	$p = 2$	$\xi_1^2 - 1$
4		$\xi_1 \xi_2$
5		$\xi_2^2 - 1$
6	$p = 3$	$\xi_1^3 - 3\xi_1$
7		$\xi_2 (\xi_1^2 - 1)$
8		$\xi_1 (\xi_2^2 - 1)$
9		$\xi_2^3 - 3\xi_2$
10	$p = 4$	$\xi_1^4 - 6\xi_1^2 + 3$
11		$\xi_2 (\xi_1^3 - 3\xi_1)$
12		$(\xi_1^2 - 1)(\xi_2^2 - 1)$
13		$\xi_1 (\xi_2^3 - 3\xi_2)$
14		$\xi_2^4 - 6\xi_2^2 + 3$

When truncating Eq.(5.54) after order p , the total number of basis polynomials P is given by :

$$(5.58) \quad P = \sum_{k=0}^p \binom{M+k-1}{k}$$

Table 5.2 gives an evaluation of P for certain values of M and p . It is seen that P is increasing extremely fast with both parameters. Remembering that *each* scalar response quantity u (which was a single number in the deterministic finite element method) is now represented by P coefficients, it is easily seen that SSFEM will require a large amount of computation. This may be worthwhile, considering that the whole probabilistic structure of u is (approximately) contained in these P coefficients.

From a practical point of view, the choice of M is dictated by the discretization of the input random fields. In the original SSFEM, the Karhunen-Loève expansion (see chapter 2, Section 5.2) is used under the assumption that the input field is Gaussian. The choice of M is thus directly related to the accuracy requested in this random field discretization. The higher M , the better higher frequency random fluctuations of the input

Table 5.2: Number of basis polynomials P (M = number of basis random variables, p = order of homogeneous chaos expansion)

M	p=1	p=2	p=3	p=4
2	3	6	10	15
4	5	15	35	70
6	7	28	83	210

will be taken into account. Conversely, parameter p governs the order of non-linearity captured in describing the solution process. Typical values used in the applications are $M = 4$ and $p = 2, 3$.

A.2 Karhunen-Loève expansion of lognormal random fields

Let us consider the following truncated Karhunen-Loève expansion of a Gaussian random field $g(\mathbf{x})$:

$$(5.59) \quad \hat{g}(\mathbf{x}, \theta) = \mu_g(\mathbf{x}) + \sum_{i=1}^M g_i(\mathbf{x}) \xi_i(\theta)$$

Gathering the random variables $\xi_i(\theta)$ in a vector $\boldsymbol{\xi}$ and the deterministic functions $g_i(\mathbf{x})$ in a vector $\mathbf{g}(\mathbf{x})$, we can define the following approximate lognormal random field⁸ :

$$(5.60) \quad l(\mathbf{x}) = \exp[\hat{g}(\mathbf{x})] = \exp[\mu_g(\mathbf{x}) + \mathbf{g}(\mathbf{x})^T \cdot \boldsymbol{\xi}]$$

Its coefficients in the polynomial chaos expansion are obtained as in (5.39) by :

$$(5.61) \quad l_i(\mathbf{x}) = \frac{\mathbb{E}[\exp[\mu_g(\mathbf{x}) + \mathbf{g}(\mathbf{x})^T \cdot \boldsymbol{\xi}] \Psi_i]}{\mathbb{E}[\Psi_i^2]}$$

The first coefficient corresponding to $\Psi_0 \equiv 1$ is the mean value of $l(\mathbf{x})$, *i.e.* :

$$(5.62) \quad l_0(\mathbf{x}) = \mu_l(\mathbf{x}) = \exp[\mu_g(\mathbf{x}) + \frac{1}{2} \sum_{i=1}^M g_i(\mathbf{x})^2] = \exp[\mu_g(\mathbf{x}) + \frac{1}{2} \sigma_g^2(\mathbf{x})]$$

where $\sigma_g(\mathbf{x})$ is the standard deviation of $\hat{g}(\mathbf{x})$. The other ones simplify after some algebra to :

$$(5.63) \quad l_i(\mathbf{x}) = \mu_l(\mathbf{x}) \frac{\mathbb{E}[\Psi_i(\boldsymbol{\xi} + \mathbf{g}(\mathbf{x}))]}{\mathbb{E}[\Psi_i^2]}$$

⁸For the sake of simplicity, the dependency on θ is dropped in the sequel.

Referring to representation (5.57) of the polynomials $\Psi_i(\xi)$, the fraction in the above equation can be written as :

$$(5.64) \quad \frac{E[\Psi_i(\xi + g(x))]}{E[\Psi_i^2]} = \frac{\prod_{j=1}^M g_j(x)^{\alpha_j}}{\prod_{j=1}^M \alpha_j!}$$

Finally, letting M tend to ∞ , the polynomial chaos expansion of the lognormal field can be written as :

$$(5.65) \quad I(x) = \mu_l(x) + \sum_{i=1}^{\infty} I_i(x) \Psi_i(\xi) \equiv \mu_l(x) \sum_{\alpha} \frac{\prod_{j=1}^M g_j(x)^{\alpha_j}}{\prod_{j=1}^M \alpha_j!} \Psi_{\alpha}(\xi)$$

Chapter 6

Conclusions

1 Summary of the study

This report has presented several techniques using the finite element method coupled with probabilistic approaches. Methods for discretizing random fields, obtaining second moment statistics of the response, probabilities of failure, or approximations of the stochastic response process itself have been reviewed. In each case, advantages and limitations have been analyzed and examples of application taken from the literature have been reported.

So far, these examples deal with simple geometries (beams, square plates, sometimes plates with a hole) and few elements (up to one hundred). Thus the random field discretization obtained directly or indirectly from the finite element mesh involves a manageable number of variables. However, some work remains on the topic of treating in a really independent fashion the random field- and finite element meshes (both of them being for instance generated automatically with respect to their respective criteria), and connect them properly.

Perturbation-based approaches were presented in Chapter 3. From a practical point of view, they can easily give information about response variability (*i.e.* mean and standard deviation). They require gradient operators at the element level in the finite element code. For strongly non-linear limit state functions, they are expected to be accurate only with small coefficients of variation of the input variables. This could be a limitation when geomaterials are involved. The CPU time becomes very large when the number of random variables is medium (say 20-50). The second order approach may be intractable in this case.

The finite element reliability approach (see Chapter 4) is based on the *coupling* of finite element calculations and a reliability algorithm determining the design point. It allows to

compute the probability of failure of a system with respect to a given limit state function. Due to this coupled formulation, it is possible to use state-of-the-art finite element codes by linking them to the reliability program. It has been applied to general non-linear problems including plasticity, plane stress plasticity and damage. It is applicable to industrial problems in its current state of development. Current research on this topic is related to time- and space-variant reliability.

The spectral stochastic finite element method has been applied to linear problems, and it is not applicable to general non-linear problems yet. However, it is a rather new approach and deserves further exploration. The main idea of obtaining an approximation of the stochastic response process itself is definitely attractive due to the wide spectrum of byproducts it can yield. The SSFEM method is computationally demanding but, on the other hand, gives a full characterization of the output quantities. Whether this information is really needed for practical applications is an open question. So is also the question of the efficiency and accuracy of SSFEM in the context of reliability analysis.

2 Suggestions for further study

As mentioned in the introduction, the various approaches presented in this study are investigated by different communities of researchers, so that no real comparison of these methods has been made so far. Such a comparison would be of greatest importance to assess the relative advantages of each approach and compare the computational costs for a given problem. It should be emphasized that the examples presented in the literature do not provide a basis for comparison as themselves, because of the use of different parameters, computing platforms, etc.

In the context of two-dimensional elastic problems, it is proposed to implement the SSFEM method and compare it with :

- perturbation method and Monte Carlo simulation for second moment analysis,
- direct coupling between FORM analysis and a deterministic code for reliability problems.

The implementation issues and comparison results are presented in Part II of the present report.

Part II

Comparisons of
Stochastic Finite Element Methods
with MATLAB

Chapter 1

Introduction

1 Aim of the present study

Part I of the present report reviewed methods coupling finite element analysis with a probabilistic description of the input parameters. Emphasis has been put on taking into account the spatial variability of material properties. This has been done by introducing the concept of *random fields* and the related discretization techniques.

Second moment approaches (including the perturbation and the weighted integral methods) have been reviewed as well as the so-called finite element reliability methods. Finally, the spectral stochastic finite element method (SSFEM) has been presented, which is claimed to provide after post-processing second moment as well as reliability results.

As already stated in Part I, there has been little comparison of SSFEM with the other approaches, at least no comparison with the perturbation method in the context of second moment analysis, and no reliability study at all. The current part of this report aims at making these comparisons and thus evaluating the efficiency and accuracy of SSFEM with respect to more classical approaches.

As already discussed in Part I, Chapter 5, SSFEM is only well established for linear problems so far. Thus elastic two-dimensional mechanical problems have been chosen for the present study. The conclusions of the study should be understood only in this context. It is reminded that both the perturbation method and the finite element reliability methods can be and have already been applied to general non-linear problems (including large strains, plasticity) as well as dynamics. These approaches have a much larger scope than SSFEM, at least in its present stage of development. However, in the case when all these approaches are applicable (*i.e.* for linear problems), the present study will give some new lights about their respective advantages and shortcomings.

2 Object-oriented implementation in MATLAB

In order to carry out the comparisons mentioned above, numerical tools had to be implemented. The MATLAB environment was chosen for this purpose. The first reason is the ease of implementation due to the numerous toolboxes for numerical analysis provided by MATLAB. The second reason is the ability of developing software within the *object-oriented* paradigm. Although MATLAB is not by itself a fully object-oriented language, it possesses some special features (*e.g.* structures, “cell arrays”) that allow to pack information into some kinds of objects. Having adopted this way of programming, it should not be a hard task to transfer the MATLAB code into a true object-oriented language like C++¹.

In this sense, the computer code produced for the present study can be viewed as a paste-up for later more robust implementation in C++.

3 Outline

The second part of this report is divided into four chapters. The first two chapters are devoted to implementation issues, the last two chapters to the comparisons mentioned above.

Chapter 2 presents a new *random field discretization toolbox* within MATLAB. This toolbox is later used by the different programs required by the present study. It practically implements the spectral discretization schemes discussed in Part I, Chapter 2, Sections 5-6.

Chapter 3 presents the implementation of the SSFEM method. A detailed description of the implementation of the polynomial chaos expansion (see Part I, Chapter 5) is given. Post-processing techniques to get second-moment and reliability results are also detailed.

Chapter 4 is devoted to second-moment approaches. The formulation of the perturbation method is particularized to the situation when the randomness in the system is limited to a random field describing the Young’s modulus of the material. The problem of simulating random fields representing material properties is then addressed. Finally the various methods are compared on the example of computing the settlement of a foundation over an elastic soil mass with spatially varying Young’s modulus.

Chapter 5 is devoted to reliability analysis. The post-processing of SSFEM by FORM and importance sampling is compared to a direct coupling between FORM and a deter-

¹The MATLAB routines (“M-files”) can also be automatically translated to C++ and compiled, if desired.

ministic finite element code. The serviceability of a foundation over an elastic soil mass with spatially varying Young's modulus is investigated.

Chapter 2

Implementation of random field discretization schemes

1 Introduction

Taking into account material spatial variability in finite element analysis requires the introduction of random fields and the implementation of *discretization schemes* such as those presented in Part I, Chapter 2. In the present chapter, attention is focused on series expansion methods, *i.e.* Karhunen-Loève expansion (KL), Expansion Optimal Linear Estimation (EOLE), and Orthogonal Series Expansion (OSE). In order to get a versatile tool that can be used by itself, an object-oriented implementation in MATLAB is aimed at. All the input data defining the field, as well as all the quantities required to evaluate realizations are gathered in a *random field object*.

The three proposed discretization schemes are basically implemented for Gaussian random fields. As an extension, lognormal fields are dealt with by exponentiation.

2 Description of the input data

2.1 Gaussian random fields

The implementation is limited to homogeneous one- or two-dimensional random fields whose mean and standard deviation are denoted by μ and σ respectively. Following the notation in Part I, Chapter 2, the approximated random field is expressed as :

$$(2.1) \quad \hat{H}(\mathbf{x}, \theta) = \mu + \sum_{i=1}^M H_i(\mathbf{x}) \xi_i(\theta)$$

where $\{\xi_i(\theta), i = 1, \dots, M\}$ are independent standard normal variables and $\{H_i(\mathbf{x}), i = 1, \dots, M\}$ are deterministic functions. More precisely, depending on the discretization scheme, these functions are :

- related to the eigenfunctions of the covariance kernel in case of the Karhunen-Loève expansion (see Part I, Eq.(2.42)),
- related to the autocorrelation function of the field in case of EOLE (see Part I, Eq.(2.65)),
- related to a complete set of deterministic functions $\{h_i(\mathbf{x})\}_{i=0}^{\infty}$ (e.g. Legendre polynomials) in case of OSE (see Part I, Eq.(2.54)).

The parameters describing a homogeneous random field are stored in an object (e.g. RFinput), which is practically implemented as a *structure* having the following entries¹ :

- RFinput.Type : its value is 'Gaussian' in this case.
- RFinput.Mean : contains the mean value μ .
- RFinput.Stdv : contains the standard deviation σ .
- RFinput.CorrLength : contains the correlation length of the field, cast as a single scalar ℓ in case of 1D fields and as an array of length 2 (e.g. $[\ell_x, \ell_y]$) in case of 2D fields.
- RFinput.CorrType : contains the type of the autocorrelation function. Available options are 'exp' for exponential type :

$$(2.2) \quad \rho(\mathbf{x}, \mathbf{x}') = \begin{cases} \exp\left(-\frac{|\mathbf{x} - \mathbf{x}'|}{\ell}\right) & \text{for 1D fields} \\ \exp\left(-\frac{|\mathbf{x} - \mathbf{x}'|}{\ell_x} - \frac{|\mathbf{y} - \mathbf{y}'|}{\ell_y}\right) & \text{for 2D fields} \end{cases}$$

and 'exp2' for exponential square type :

$$(2.3) \quad \rho(\mathbf{x}, \mathbf{x}') = \begin{cases} \exp\left(-\left(\frac{\mathbf{x} - \mathbf{x}'}{\ell}\right)^2\right) & \text{for 1D fields} \\ \exp\left(-\left(\frac{\mathbf{x} - \mathbf{x}'}{\ell_x}\right)^2 - \left(\frac{\mathbf{y} - \mathbf{y}'}{\ell_y}\right)^2\right) & \text{for 2D fields} \end{cases}$$

¹In Matlab as in C, components of a *structure* type are usually called *fields* and accessed using the operator ".". In the sequel, the word "entry" is used instead of "field" in order to avoid any confusion with the random field under consideration.

- `RFinput.DiscScheme` : contains the name of the discretization scheme. Available options are 'KL' (only available for exponential autocorrelation function), 'EOLE' and 'OSE'.
- `RFinput.OrderExp` : contains the order of expansion, that is the number of terms M in the summation (2.1).
- `RFinput.NbPts` : This entry is required when the EOLE method is chosen and involves the definition of a grid. This entry contains the number of points along each direction, defining a uniform grid over the domain. This is a scalar in case of 1D fields and an array of length 2 in case of 2D fields.

2.2 Lognormal random fields

By exponentiating the approximate Gaussian field (2.1), one gets an approximate log-normal field :

$$(2.4) \quad \hat{I}(\mathbf{x}, \theta) = \exp \left[\mu + \sum_{i=1}^M H_i(\mathbf{x}) \xi_i(\theta) \right]$$

In the context of SSFEM, the latter equation is expanded over the polynomial chaos basis (Part I, Chapter 5, Section 4.1) as :

$$(2.5) \quad \hat{I}(\mathbf{x}, \theta) = \mu_l + \sum_{i=1}^P l_i(\mathbf{x}) \Psi_i(\theta)$$

The input parameters for such fields are the same as those for a Gaussian field except the following entries :

- `RFinput.Type` : its value is 'Lognormal' in this case.
- `RFinput.LNMean` : contains the mean value μ_l .
- `RFinput.LNStdv` : contains the standard deviation σ_l .

3 Discretization procedure

From the random field input and the geometry of the mechanical system (defined as an array containing the mesh nodal coordinates, *e.g.* `COORD`), a random field object (*e.g.* `RF`) is constructed. It contains both the input data provided by `RFinput` and the quantities required for evaluating realizations of the field.

3.1 Domain of discretization

The rectangular envelope of the system Ω is determined from the array of nodal coordinates. This envelope defines the *domain of discretization* of the random field, and is denoted by Ω_{RF} in the sequel. It is stored in `RF.Domain`.

As an alternative, this entry can be input in the form of the following list : `RF.Domain = {xmin, xmax}` for one-dimensional fields (resp. `RF.Domain = {[xmin, ymin], [xmax, ymax]}`) for two-dimensional fields. This option is useful when the random field toolbox is used by itself to numerically compare different discretization schemes.

3.2 The Karhunen-Loève expansion

The approximate random field in this case is defined by :

$$(2.6) \quad \hat{H}(\mathbf{x}, \theta) = \mu + \sum_{i=1}^M \sigma \sqrt{\lambda_i} \varphi_i(\mathbf{x}) \xi_i(\theta) \quad , \quad \mathbf{x} \in \Omega_{\text{RF}}$$

where (λ_i, φ_i) are the solution of the eigenvalue problem :

$$(2.7) \quad \int_{\Omega_{\text{RF}}} \rho(\mathbf{x}, \mathbf{x}') \varphi_i(\mathbf{x}') d\Omega_{\mathbf{x}'} = \lambda_i \varphi_i(\mathbf{x})$$

In case of an exponential autocorrelation function (see Eq.(2.2)) and rectangular domain, the latter equation can be solved in closed form.

3.2.1 One-dimensional case

Suppose $\Omega_{\text{RF}} = [-a, a]$. The eigenvalue problem (2.7) can be rewritten as :

$$(2.8) \quad \int_{-a}^a e^{-\frac{|x-x'|}{\ell}} \varphi_i(x') dx' = \lambda_i \varphi_i(x)$$

where ℓ is the correlation length. The solution of Eq.(2.8) is (Ghanem and Spanos, 1991b) :

- for i odd, $i \geq 1$:

$$(2.9-a) \quad \lambda_i = \frac{2\ell}{1 + \omega_i^2 \ell^2}$$

$$(2.9-b) \quad \varphi_i(x) = \alpha_i \cos \omega_i x \quad , \quad \alpha_i = \frac{1}{\sqrt{a + \frac{\sin 2\omega_i a}{2\omega_i}}}$$

where ω_i is the solution of :

$$(2.10) \quad \frac{1}{\ell} - \omega_i \tan \omega_i a = 0 \quad \text{in the range} \quad \left[(i-1)\frac{\pi}{a}, (i-\frac{1}{2})\frac{\pi}{a} \right]$$

• for i even, $i \geq 2$:

$$(2.11-a) \quad \lambda_i = \frac{2\ell}{1 + \omega_i^2 \ell^2}$$

$$(2.11-b) \quad \varphi_i(x) = \alpha_i \sin \omega_i x, \quad \alpha_i = \frac{1}{\sqrt{a - \frac{\sin 2\omega_i a}{2\omega_i}}}$$

where ω_i is the solution of :

$$(2.12) \quad \frac{1}{\ell} \tan \omega_i a + \omega_i = 0 \quad \text{in the range} \quad \left[(i-\frac{1}{2})\frac{\pi}{a}, i\frac{\pi}{a} \right]$$

All coefficients $\{\alpha_i, \omega_i\}$ are computed for $i = 1, \dots, M$ and stored as additional entries of RF.

3.2.2 Two-dimensional case

Following Ghanem and Spanos (1991b), the solution of the two-dimensional eigenvalue problem is simply obtained by products of one-dimensional solutions, *e.g.* :

$$(2.13) \quad \lambda_i = \lambda_{i_1}^{1D} \cdot \lambda_{i_2}^{1D}$$

$$(2.14) \quad \varphi(\mathbf{x}) \equiv \varphi(x, y) = \varphi_{i_1}(x) \cdot \varphi_{i_2}(y)$$

where superscript ^{1D} refers to the one-dimensional solution given in the above paragraph. In implementation, the products of the 1D eigenvalues are computed and sorted in descending order, and the M greatest products are stored together with the corresponding subscripts (i_1, i_2) as additional entries of RF.

3.2.3 Case of non symmetrical domain of definition

If Ω_{RF} is non symmetric, *e.g.* $\Omega_{\text{RF}} = [x_{\min}, x_{\max}]$, a *shift* parameter is computed :

$$(2.15) \quad \mathbf{T} = \frac{\mathbf{x}_{\min} + \mathbf{x}_{\max}}{2}$$

Then the eigenvalue problem is solved over :

$$(2.16) \quad \Omega'_{\text{RF}} = \Omega_{\text{RF}} - \mathbf{T} = \left[\frac{\mathbf{x}_{\min} - \mathbf{x}_{\max}}{2}, \frac{\mathbf{x}_{\max} - \mathbf{x}_{\min}}{2} \right]$$

which is symmetric, and Eq.(2.6) is replaced by :

$$(2.17) \quad \hat{H}(\mathbf{x}, \theta) = \mu + \sum_{i=1}^M \sigma \sqrt{\lambda_i} \varphi_i(\mathbf{x} - \mathbf{T}) \xi_i(\theta) \quad , \quad \mathbf{x} \in \Omega_{\text{RF}}$$

3.3 The EOLE method

The EOLE method requires the definition of a grid. In the current implementation, *uniform* grids are defined within the rectangular domain of discretization Ω_{RF} . The number of points defining the grid (in each direction for 2D problems) is specified in the entry `RFinput.NbPts`. First the coordinates of all the nodes of this grid are computed, say $\{\mathbf{x}_1, \dots, \mathbf{x}_N\}$. The array containing these coordinates is stored in the entry `RF.COORD`. It is emphasized that these nodes are *different* from the nodes of the structural mesh. In other words, a *completely* independent definition of the structural mesh and the random field mesh is possible.

In case of a homogeneous Gaussian field, it can be shown from (Part I, Eq.(2.65)) that the discretized random field reduces to :

$$(2.18) \quad \hat{H}(\mathbf{x}, \theta) = \mu + \sigma \sum_{i=1}^M \frac{\xi_i(\theta)}{\sqrt{\lambda_i}} \phi_i^T \mathbf{C}_{\mathbf{x}, \mathbf{x}_i}$$

where $\mathbf{C}_{\mathbf{x}, \mathbf{x}_i} = \{\rho(\mathbf{x} - \mathbf{x}_i), i = 1, \dots, M\}$, and (λ_i, ϕ_i) is the solution of the eigenvalue problem :

$$(2.19) \quad \mathbf{C}_{\text{XX}} \phi_i = \lambda_i \phi_i$$

\mathbf{C}_{XX} being the correlation matrix whose terms are given by :

$$(2.20) \quad \mathbf{C}_{\text{XX}}(k, l) = \rho(\mathbf{x}_k - \mathbf{x}_l)$$

In implementation, the correlation matrix Eq.(2.20) is first computed from the grid coordinates `RF.COORD`. Using a MATLAB built-in procedure, the M greatest eigenvalues λ_i and corresponding eigenvectors ϕ_i are then computed and stored as additional entries of `RF`. It is noted that the full eigenvalue problem does not have to be solved, if an algorithm computing the greatest eigenvalues one by one is available.

3.4 The OSE method

3.4.1 General formulation

The discretized random field in this case reads (see Eq.(2.54) in Part I) :

$$(2.21) \quad \hat{H}(\mathbf{x}, \theta) = \mu + \sum_{i=1}^M h_i(\mathbf{x}) \chi_i(\theta)$$

where $\boldsymbol{\chi} = \{\chi_1(\theta), \dots, \chi_M(\theta)\}$ is a zero-mean Gaussian vector, whose covariance matrix $\boldsymbol{\Sigma}_{\text{XX}}$ is defined by :

$$(2.22) \quad \boldsymbol{\Sigma}_{\text{XX}}(k, l) = \mathbb{E}[\chi_k \chi_l] = \int_{\Omega_{\text{RF}}} \int_{\Omega_{\text{RF}}} \sigma^2 \rho(\mathbf{x}, \mathbf{x}') h_k(\mathbf{x}) h_l(\mathbf{x}') d\mathbf{x} d\mathbf{x}'$$

The spectral decomposition of this covariance matrix is :

$$(2.23) \quad \Sigma_{xx} \cdot \Phi = \Phi \cdot \Lambda$$

where Λ is the diagonal matrix of eigenvalues and Φ contains the corresponding eigenvectors arranged in columns. Consequently, the correlated Gaussian vector \mathcal{X} can be transformed into an uncorrelated vector ξ as follows :

$$(2.24) \quad \mathcal{X} = \Phi \cdot \Lambda^{1/2} \cdot \xi$$

where $\Lambda^{1/2}$ is a diagonal matrix whose terms are the square roots of the diagonal terms of Λ . Substituting for (2.24) into (2.21) finally gives :

$$(2.25) \quad \hat{H}(x, \theta) = \mu + \sum_{i=1}^M \sqrt{\lambda_i} \left\{ \sum_{k=1}^M \Phi_k^i h_k(x) \right\} \xi_i(\theta)$$

3.4.2 Construction of a complete set of deterministic functions

Following Zhang and Ellingwood (1994), the set of deterministic functions $\{h_n(x)\}_{n=1}^{\infty}$ is based upon the Legendre polynomials $\{P_n(x)\}_{n=0}^{\infty}$, which can be defined by the recursive equations :

$$(2.26-a) \quad P_0(x) = 1 \quad ; \quad P_1(x) = x$$

$$(2.26-b) \quad P_{n+1}(x) = \frac{1}{n+1} [(2n+1)xP_n(x) - nP_{n-1}(x)] \quad n \geq 1$$

The Legendre polynomials have the following elementary properties :

$$(2.27-a) \quad P_n(-1) = (-1)^n$$

$$(2.27-b) \quad P_n(0) = \begin{cases} 0 & \text{if } n \text{ odd} \\ \frac{n!}{2^{n/2} \left(\frac{n}{2}\right)!} & \text{if } n \text{ even} \end{cases}$$

$$(2.27-c) \quad P_n(1) = 1$$

and satisfy the following orthogonality conditions :

$$(2.28) \quad \int_{-1}^1 P_m(x) P_n(x) dx = \begin{cases} 0 & \text{if } n \neq m \\ \frac{2}{2m+1} & \text{if } n = m \end{cases}$$

Considering the one-dimensional discretization domain $\Omega_{RF} = [x_{min}, x_{max}]$, it is possible to construct a set of orthonormal deterministic functions $\{h_n(x)\}_{n=1}^{\infty}$ based upon the Legendre polynomials as follows :

$$(2.29) \quad h_n(x) = \sqrt{\frac{2n-1}{2a}} P_{n-1}\left(\frac{x-T}{a}\right) \quad n = 1, 2, \dots$$

where :

$$(2.30-a) \quad T = \frac{x_{min} + x_{max}}{2}$$

$$(2.30-b) \quad a = \frac{x_{max} - x_{min}}{2}$$

are the *shift* and *scaling* parameters respectively.

The covariance matrix Σ_{xx} Eq.(2.22) in this case is given by :

$$(2.31) \quad \Sigma_{xx}(k, l) = \frac{\sigma^2}{2a} \sqrt{(2k-1)(2l-1)} \int_{x_{min}}^{x_{max}} \int_{x_{min}}^{x_{max}} \rho(x, x') P_{k-1}\left(\frac{x-T}{a}\right) P_{l-1}\left(\frac{x'-T}{a}\right) dx dx'$$

Introducing the mapping :

$$(2.32-a) \quad u = \frac{x-T}{a}$$

$$(2.32-b) \quad v = \frac{x'-T}{a}$$

Eq.(2.31) reduces to

$$(2.33) \quad \Sigma_{xx}(k, l) = \frac{a\sigma^2}{2} \sqrt{(2k-1)(2l-1)} \int_{-1}^1 \int_{-1}^1 \rho(au, av) P_{k-1}(u) P_{l-1}(v) du dv$$

Using a Gaussian integration procedure, the above equation is evaluated by

$$(2.34) \quad \Sigma_{xx}(k, l) = \frac{a\sigma^2}{2} \sqrt{(2k-1)(2l-1)} \sum_{i=1}^{NPG} \sum_{j=1}^{NPG} w_i w_j \rho(aX_i, aX_j) P_{k-1}(X_i) P_{l-1}(X_j)$$

where $\{(w_i, X_i), i = 1, \dots, NPG\}$ are the integration weights and points, respectively.

To get an invertible covariance matrix, the number of Gaussian points NPG should be greater than the number of random variables M . In implementation, NPG = 16 was used in the computation. To efficiently evaluate Eq.(2.34), two matrices are first computed :

- Matrix C of size $NPG \times NPG$, containing :

$$(2.35) \quad C(i, j) = \rho(aX_i, aX_j)$$

- Matrix LP of size $M \times \text{NPG}$, containing :

$$(2.36) \quad \text{LP}(k, l) = P_{k-1}(X_l)$$

After Σ_{xx} has been computed using Eqs.(2.34)-(2.36), the spectral decomposition is performed using a MATLAB built-in procedure. The correlation matrix, the eigenvalues and eigenvectors are stored as additional entries of the object RF. Subsequent evaluations of the field are obtained by Eq.(2.25).

3.5 Case of lognormal fields

Lognormal fields are treated as the result of the exponentiation of a discretized Gaussian field. From the mean value μ_l and standard deviation σ_l (stored in `RFinput.LNMean` and `RFinput.LNStdv`, respectively), the mean value λ and standard deviation ζ of the underlying Gaussian field are first computed from :

$$(2.37) \quad \zeta = \sqrt{\ln(1 + \sigma_l^2/\mu_l^2)}$$

$$(2.38) \quad \lambda = \ln \mu_l - \frac{1}{2}\zeta^2$$

They are stored in the entries `RF.Mean` and `RF.Stdv` respectively.

Then the underlying Gaussian field is discretized using one of the three methods described in the preceding sections.

4 Visualization tools

When dealing with Gaussian random fields, the accuracy of the discretization can be evaluated by means of the following *point estimator* :

$$(2.39) \quad \text{err}(\mathbf{x}) = \frac{\text{Var} [H(\mathbf{x}) - \hat{H}(\mathbf{x})]}{\text{Var} [H(\mathbf{x})]}$$

For homogeneous fields (*i.e.* $\text{Var} [H(\mathbf{x})] \equiv \sigma^2$), this estimator can be given closed form expressions depending on the discretization scheme :

KL method :

$$\begin{aligned}
 \varepsilon_{err}(\mathbf{x}) &= \frac{1}{\sigma^2} \text{Var} \left[\sum_{M+1}^{\infty} \sigma \sqrt{\lambda_i} \varphi_i(\mathbf{x}) \xi_i(\theta) \right] \\
 (2.40) \qquad &= \sum_{M+1}^{\infty} \lambda_i \varphi_i^2(\mathbf{x}) \\
 &= 1 - \sum_{i=1}^M \lambda_i \varphi_i^2(\mathbf{x})
 \end{aligned}$$

EOLE method (see Eq.(2.66) in Part I) :

$$(2.41) \qquad \varepsilon_{err}(\mathbf{x}) = 1 - \sum_{i=1}^M \frac{1}{\lambda_i} (\phi_i^T \mathbf{C}_{\mathbf{x}, \mathbf{x}_i})^2$$

OSE method Due to the independence of the basic random variables $\{\xi_i\}_{i=1}^{\infty}$ in the KL and EOLE expansions, it can be seen from Eqs.(2.40)-(2.41) that the variance of the error is simply the difference between the variances of $H(\mathbf{x})$ and $\hat{H}(\mathbf{x})$, leading to :

$$(2.42) \qquad \varepsilon_{err}(\mathbf{x}) = 1 - \frac{\text{Var} [\hat{H}(\mathbf{x})]}{\sigma^2}$$

Such a result does not hold when dealing with correlated variables. In the case of OSE method, the expression for error estimator (2.39) requires a little more algebra. Letting aside the mean value (*i.e.* assuming in the sequel that $\mu = 0$), and restricting to the one-dimensional case, one can write :

$$(2.43) \qquad \hat{H}(x, \theta) = \sum_{i=1}^M h_i(x) \chi_i(\theta)$$

where, due to the orthonormality of the deterministic basis functions :

$$(2.44) \qquad \chi_i(\theta) = \int_{\Omega} H(y, \theta) h_i(y) dy$$

The variance of the error can be written as :

$$\begin{aligned}
 (2.45) \qquad \text{Var} [H(x) - \hat{H}(x)] &= \text{E} \left[(H(x) - \hat{H}(x))^2 \right] \\
 &= \text{E} [H^2(x)] + \text{E} [\hat{H}^2(x)] - 2 \text{E} [H(x) \hat{H}(x)]
 \end{aligned}$$

From Eq.(2.43), one gets :

$$(2.46) \qquad \text{E} [\hat{H}^2(x)] = \sigma^2 \sum_{i=1}^M \sum_{j=1}^M h_i(x) h_j(x) \mathbf{C}_{\chi\chi}(i, j)$$

where C_{xx} is given in Eq.(2.22). From Eqs.(2.43)-(2.44), one can write :

$$(2.47) \quad E \left[H(x) \hat{H}(x) \right] = E \left[H(x) \sum_{i=1}^M h_i(x) \int_{\Omega} H(y) h_i(y) dy \right]$$

By regrouping the deterministic terms outside the expectation operation, one gets :

$$(2.48) \quad \begin{aligned} E \left[H(x) \hat{H}(x) \right] &= \sum_{i=1}^M h_i(x) \int_{\Omega} h_i(y) E[h(x)h(y)] dy \\ &= \sigma^2 \sum_{i=1}^M h_i(x) \int_{\Omega} h_i(y) \rho(x, y) dy \end{aligned}$$

Substituting for Eqs.(2.46),(2.48) in Eq.(2.45), and dividing by $E[H^2(x)] = \sigma^2$ gives eventually the error estimator :

$$(2.49) \quad \epsilon_{rr}(x) = 1 + \sum_{i=1}^M \sum_{j=1}^M h_i(x) h_j(x) C_{xx}(i, j) - 2 \sum_{i=1}^M h_i(x) \int_{\Omega} h_i(y) \rho(x, y) dy$$

where the integral in the above equation is numerically computed using Gaussian integration.

A routine plotting the error estimator over the domain Ω_{RF} has been implemented. In addition, the mean value $\bar{\epsilon}$ of this error estimator over the domain is computed, which gives an indication on the global accuracy of the discretization :

$$(2.50) \quad \bar{\epsilon} = \frac{1}{|\Omega_{RF}|} \int_{\Omega_{RF}} \epsilon_{rr}(x) d\Omega$$

This can be used for instance to determine the order of expansion M yielding a mean error smaller than a prescribed tolerance. Figure 2.1 shows an example of the output for different discretization schemes, in case of one-dimensional field. So does Figure 2.2 in case of two-dimensional fields and EOLE discretization scheme.

5 Conclusion

This chapter has presented the implementation of a random field discretization toolbox within MATLAB . Due to the object-oriented programming, this toolbox is easily extensible to other types of discretization (*e.g.* OSE based on other deterministic basis functions than the Legendre polynomials), autocorrelation functions (*e.g.* with triangular decay-ing) or three-dimensional fields. This toolbox has been used to compare the accuracy of the series expansion discretization methods in Part I, Chapter 2, Section 6.

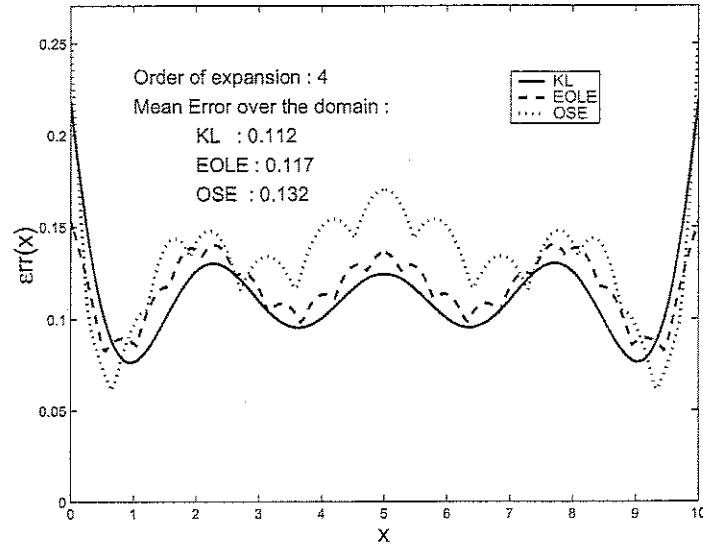


Figure 2.1: Error estimator computed for different discretization schemes - one-dimensional field

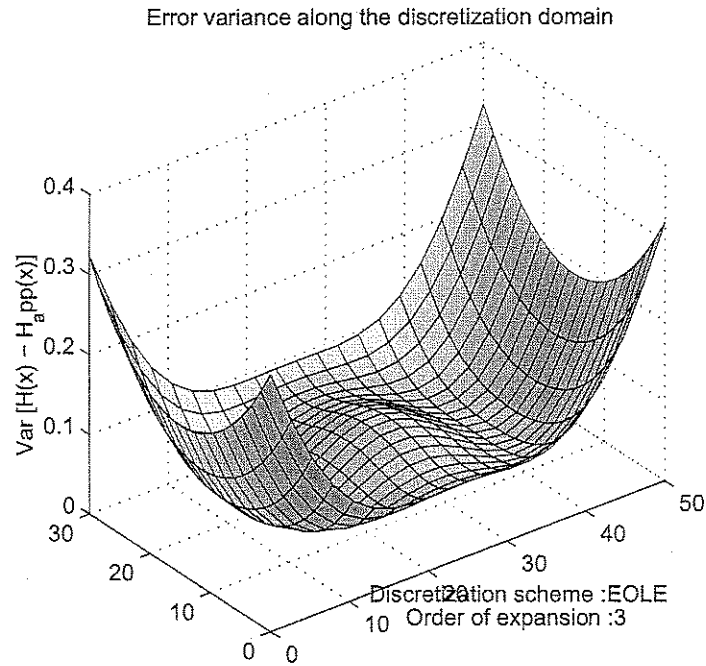


Figure 2.2: Error estimator computed for EOLE expansion - two-dimensional field

Chapter 3

Implementation of SSFEM

1 Introduction

1.1 Preliminaries

As presented in Part I, Chapter 5, the Spectral Stochastic Finite Element Method (SSFEM) aims at representing the mechanical response of a system (*e.g.* the vector of nodal displacements) through its coefficients over a basis of the space of random variables $\mathcal{L}^2(\Theta, \mathcal{F}, P)$. Any nodal displacement, now considered as a random variable, is described as a truncated series :

$$(3.1) \quad u(\theta) = \sum_{j=0}^{P-1} u_j \Psi_j (\{\xi_k(\theta)\}_{k=1}^M)$$

where $\{\Psi_j (\{\xi_k(\theta)\}_{k=1}^M)\}$ is the so-called *polynomial chaos basis* defined by means of M standard normal variables $\{\xi_k(\theta)\}_{k=1}^M$, and $\{u_j\}$ are the “coordinates” of the random variable u over this basis.

As already discussed in Chapter 1, SSFEM is practically applicable only to *linear problems*. Thus the current implementation is limited to *linear elastic two-dimensional* mechanical problems. Furthermore, the material Young’s modulus will be the only parameter considered as spatially variable, and consequently modeled as a random field.

1.2 Summary of the procedure

As with any finite element program, SSFEM is organized in three stages :

- **The pre-processing stage** : The data describing the mechanical model and the random field discretization are provided in the MATLAB workspace. In the context of an object-oriented implementation, this data is gathered in two objects called Model and RF respectively. Details of this construction are given in section 2.

The implementation of SSFEM also requires the representation of the polynomial chaos in a practical computational way. This is done by considering the polynomial chaos as the multidimensional Hermite polynomials. All data regarding the polynomial chaos is then stored in a single object called PC. Details are given in section 3.

- **The analysis stage** : Element stiffness matrices are computed, then assembled to form a global linear system of equations, on which boundary conditions are applied. The unknowns of this system are the set of coefficients $\{u_j^k\}$ describing the probabilistic structure of each nodal displacement u^k , see Eq.(3.1). Details regarding this stage are given in section 4.
- **The post-processing stage** : The set of coefficients $\{u_j^k\}$ are used either for second-moment or reliability analysis. Details are given in section 5.

Remark All along this chapter, MATLAB variable names (*e.g.* Model, RF, PC) are used for the sake of clarity. The user can of course choose any other name, provided there is consistency in the input file specifying the data to be put in the MATLAB workspace.

2 SSFEM pre-processing

2.1 Mechanical model

To get started with a finite element analysis, the following data describing the mechanical model has to be provided in the MATLAB workspace.

- A flag variable (*e.g.* TypeDef), set to 0 or 1 whether a plane stress or plane strain analysis is carried out.
- An array of nodal coordinates (*e.g.* COORD) of size NbNodes \times 2, where NbNodes is the number of nodes of the mesh.
- A connectivity array (*e.g.* CONEC) of size NbElts \times NbNodesElt, where NbElts is the number of elements and NbNodesElt the maximum number of nodes per element.

- An element data structure (*e.g.* `ELData`) containing the type of each element (`ELData.type`) and its constitutive material (`ELData.mat`). Each entry is an integer array of size `NbElts`. For instance 4-node isoparametric elements correspond to `ELData.type(i) = 1` for $i = 1, \dots, \text{NbElts}$.
- A material structure (*e.g.* `MATS`) containing the parameters of the material constitutive law. For linear elastic isotropic material, the entries corresponding to material `#i` are :
 - `MATS{i}.E` : Young's modulus
 - `MATS{i}.nu` : Poisson's ratio
 - `MATS{i}.initialstress` : an array describing the initial stress state in the structure (a linear variation with respect to coordinates can be specified.)
 - `MATS{i}.bodyforces` : an array of length 2 containing the prescribed body forces in x and y directions.
- A boundary conditions array (*e.g.* `BC`) of size `NbNodes` \times 2. For each node i and each degree of freedom $j = 1, 2$, `BC(i, j)` is set to 1 to impose a zero value of the corresponding nodal displacement (default value of `BC` is thus 0).
- A load vector (*e.g.* `LOADS`) of size `NbNodes` \times 2, allowing to prescribe nodal loads.

All the above arrays are gathered into a structure called `Model`. This allows passing all the parameters of the mechanical model as a single variable to subroutines. The input data described so far is sufficient to run a deterministic analysis. For each application, such an analysis is carried out systematically in order to check the data as well as the quality of the mesh with respect to the output quantity under consideration.

2.2 Random field definition

The parameters describing the random field and its discretization scheme are gathered in a structure (*e.g.* `RFinp`), see Chapter 2, Section 2. From this object and the mesh coordinates `COORD`, a random field object (*e.g.* `RF`) is created as described in Chapter 2, Section 3.

3 Polynomial chaos

3.1 Introduction

The M -th dimensional p -th order polynomial chaos consists in a set of multidimensional Hermite polynomials in $\{\xi_1, \dots, \xi_M\}$, whose degree does not exceed p (see Part I, Chapter 5). In implementation, each of these polynomials is completely defined by a sequence of M non-negative integers $\{\alpha_1, \dots, \alpha_M\}$ as follows :

$$(3.2) \quad \Psi_{\alpha} = \prod_{i=1}^M h_{\alpha_i}(\xi_i) \quad , \quad \alpha_i \geq 0$$

where $h_q(\cdot)$ is the q -th Hermite polynomial. Let us furthermore denote by $\partial_{\alpha} = \sum_{i=1}^M \alpha_i$ the degree of the list α .

The implementation of the polynomial chaos requires :

- computing and storing the (one-dimensional) Hermite polynomials,
- generating all the lists α , whose degree is less or equal than p . These lists are numbered from 0 to $P - 1$ and the polynomials simply denoted by $\{\Psi_j, j = 0, \dots, P - 1\}$ ¹.

In the context of SSFEM, the variables $\{\xi_1, \dots, \xi_M\}$ are standard normal variables. Furthermore, expectations of products of polynomials appear in the calculation (See Part I, Chapter 5, Section 2), namely :

- $E[\Psi_j^2]$, interpreted as the square norm of the basis function Ψ_j in $\mathcal{L}^2(\Theta, \mathcal{F}, P)$.
- $c_{ijk} = E[\xi_i \Psi_j \Psi_k]$. These coefficients are required when the input random field is Gaussian.
- $d_{ijk} = E[\Psi_i \Psi_j \Psi_k]$. These coefficients are required when the input random field is lognormal.

¹In the actual implementation, subscript j varies from 1 to P to comply with MATLAB requirements on array indexing.

3.2 Implementation of the Hermite polynomials

The Hermite polynomials can be defined by a recursive algorithm as follows :

$$(3.3-a) \quad h_0(x) = 1$$

$$(3.3-b) \quad \frac{d h_q(x)}{dx} = q h_{q-1}(x)$$

$$(3.3-c) \quad h_q(0) = \begin{cases} 0 & \text{if } q \text{ odd} \\ (-1)^{q/2} \frac{q!}{2^{q/2} (\frac{q}{2})!} & \text{if } q \text{ even} \end{cases}$$

Polynomial h_q is stored as an array of $q + 1$ coefficients computed from those of h_{q-1} by means of Eqs.(3.3-b)-(3.3-c). The set of polynomials is gathered in a single object using the *cell array* feature of MATLAB . A cell array Z is basically an array whose elements $Z\{i\}, i = 1, \dots$ can be of any kind (*i.e.* not necessarily the same for all of them). In the present example, this feature is mandatory, since the arrays representing the Hermite polynomials have different lengths.

3.3 Implementation of the polynomial basis

For each degree $q = 1, \dots, p$, the goal is to compute all the lists of non-negative integers whose sum equals q . This problem is equivalent to that of filling $(M + q - 1)$ boxes with $(M - 1)$ balls as illustrated in Figure 3.1. The correspondence between the integer sequences and the ball samples is as follows :

- for each integer α_i in the sequence, skip α_i boxes and put a ball in the next box;
- conversely, for each sample of ball positions, each integer equals the number of empty boxes (possibly 0) between two consecutive balls.

From this equivalence, the number of lists α of degree $\partial_\alpha = q$ is the number of the corresponding ball samples, that is the binomial factor $\binom{M+q-1}{M-1} = \binom{M+q-1}{q}$, which appears in (Part I, Eq.(5.58)).

The following recursive algorithm was used to generate all possible ball samples (see the complete generation in Figure 3.2 in case of $(M = 4, q = 2)$) :

- For a given q , the initial sample corresponds to all balls in the $(M - 1)$ first boxes, which corresponds to the list $\alpha = \{0, 0, \dots, 0, q\}$.



ball sample	Integer sequence	Polynomial basis
	1 0 1 0	$h_1(\xi_1) \cdot h_1(\xi_3) = \xi_1 \xi_3$
	0 0 0 2	$h_2(\xi_4) = \xi_4^2 - 1$

Figure 3.1: Correspondance between ball samples and integer sequences α ($M = 4$, $q = 2$)


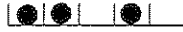






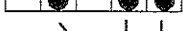

Ball sample	Integer sequence	Polynomial basis
	0 0 0 2	$\xi_4^2 - 1$
	0 0 1 1	$\xi_3 \xi_4$
	0 0 2 0	$\xi_3^2 - 1$
	0 1 0 1	$\xi_2 \xi_4$
	0 1 1 0	$\xi_2 \xi_3$
	0 2 0 0	$\xi_2^2 - 1$
	1 0 0 1	$\xi_1 \xi_4$
	1 0 1 0	$\xi_1 \xi_3$
	1 1 0 0	$\xi_1 \xi_2$
	2 0 0 0	$\xi_1^2 - 1$

Figure 3.2: Recursive generation of the polynomial chaos ($M = 4$, $q = 2$)

- From the current sample, the next one is recursively obtained by shifting the rightmost ball by one box to the right. If this is not possible (*i.e.* the ball is already in the rightmost box), then the rightmost ball that can be shifted by one box to the right is found. This ball is shifted, and all the balls lying to its right are brought back to its immediate right.

For each ball sample, the corresponding integer sequence α is computed and stored as an array of length M .

- The set of all polynomials is finally gathered in a cell array.

3.4 Computation of expectation of products

3.4.1 Products of two polynomials

By definition, Hermite polynomials in standard normal variables are orthogonal with respect to the expectation operator :

$$(3.4) \quad E[h_p(\xi)h_q(\xi)] = \delta_{pq} p!$$

where δ_{pq} is the Kronecker symbol. By extension, the polynomials $\{\Psi_j, j = 0, \dots, P-1\}$ are also orthogonal and satisfy :

$$(3.5) \quad E[\Psi_\alpha \cdot \Psi_\beta] = \delta_{\alpha\beta} \cdot \prod_{i=1}^M \alpha_i!$$

where $\delta_{\alpha\beta}$ is the Kronecker symbol, whose value is 1 if sequences α and β are identical and 0 otherwise.

3.4.2 The product of two polynomials and a standard normal variable

When dealing with Gaussian random fields within SSFEM, the coefficients $c_{ijk} = E[\xi_i \Psi_j \Psi_k]$ are required. For further derivation, let us consider that Ψ_j (resp. Ψ_k) corresponds to the integer sequence α (resp. β), see Eq.(3.2). From the independence of the standard normal variables $\{\xi_1, \dots, \xi_M\}$, it follows that :

$$(3.6) \quad c_{ijk} \equiv E[\xi_i \Psi_\alpha \Psi_\beta] = E[\xi_i h_{\alpha_i}(\xi_i) h_{\beta_i}(\xi_i)] \cdot \prod_{l \neq i} E[h_{\alpha_l}(\xi_l) h_{\beta_l}(\xi_l)]$$

Thus if for any given $j_0 \neq i$, α_{j_0} and β_{j_0} are different, the above product vanishes due to the orthogonality of $h_{\alpha_{j_0}}$ and $h_{\beta_{j_0}}$. Otherwise, α and β differ only by their i -th component and Eq.(3.6) reduces to :

$$(3.7) \quad c_{ijk} \equiv E[\xi_i \Psi_\alpha \Psi_\beta] = E[\xi_i h_{\alpha_i}(\xi_i) h_{\beta_i}(\xi_i)] \cdot \prod_{l \neq i} \alpha_l!$$

The problem is now reduced to that of computing $E[\xi h_p(\xi)h_q(\xi)]$, when ξ is a standard normal variable, and h_p, h_q are Hermite polynomials in ξ .

Introducing the probability density function of ξ , one gets :

$$(3.8) \quad E[\xi h_p(\xi)h_q(\xi)] = \int_{\mathbb{R}} \frac{1}{\sqrt{2\pi}} h_p(x) h_q(x) x e^{-\frac{1}{2}x^2} dx$$

By partial integration, the above expression becomes :

$$(3.9) \quad E[\xi h_p(\xi)h_q(\xi)] = E\left[\frac{d}{d\xi}\{h_p(\xi)h_q(\xi)\}\right] = E\left[\frac{dh_p(\xi)}{d\xi}h_q(\xi) + \frac{dh_q(\xi)}{d\xi}h_p(\xi)\right]$$

Using Eq.(3.3-b), one finally gets :

$$(3.10) \quad E[\xi h_p(\xi)h_q(\xi)] = p! \delta_{p-1,q} + q! \delta_{p,q-1}$$

This result is substituted for in Eq.(3.7) to eventually get c_{ijk} .

3.4.3 Products of three polynomials

When dealing with lognormal random fields within SSFEM, the coefficients $\{d_{ijk} = E[\Psi_i\Psi_j\Psi_k]\}$ are required. From Eq.(3.2) and the independence of the standard normal variables $\{\xi_1, \dots, \xi_M\}$, it follows that :

$$(3.11) \quad d_{ijk} = \prod_{l=1}^M E[h_{\alpha_l}(\xi_l)h_{\beta_l}(\xi_l)h_{\gamma_l}(\xi_l)]$$

which requires the expectation of a product of three Hermite polynomials in ξ_l . Unfortunately, no simple formula similar to Eq.(3.10) can be derived in this case. Thus the rather inefficient following algorithm is used :

- The coefficients of the polynomial product is algebraically computed using a MATLAB built-in function :

$$(3.12) \quad Q_l(\xi_l) \equiv h_{\alpha_l}(\xi_l)h_{\beta_l}(\xi_l)h_{\gamma_l}(\xi_l) = \sum_{r=0}^{\alpha_l+\beta_l+\gamma_l} a_{rl} \xi_l^r$$

- Using the linearity of the expectation operator and the closed form solution for the moments of the standard normal variable ξ_l , one obtains :

$$(3.13) \quad E[Q_l(\xi_l)] = E[h_{\alpha_l}(\xi_l)h_{\beta_l}(\xi_l)h_{\gamma_l}(\xi_l)] = \sum_{\substack{r=0 \\ r \text{ even}}}^{\alpha_l+\beta_l+\gamma_l} a_{rl} \frac{r!}{2^{r/2} \left(\frac{r}{2}\right)!}$$

- Eq.(3.13) is used for $l = 1, \dots, M$ and the results are multiplied according to Eq.(3.11).

Due to the symmetry in the subscripts of the coefficients subscripts, only those d_{ijk} that are associated with $0 \leq i \leq j \leq k \leq P - 1$ are computed and stored.

3.5 Conclusion

This technical section has described the practical implementation of the polynomial chaos. All the basis polynomials and related coefficients are eventually gathered in a single object called PC, defined as a MATLAB structure. It is emphasized that except in Ghanem and Spanos (1991b), no details about the implementation of SSFEM could be found in the literature. The method proposed by Ghanem and Spanos used symbolic calculus, which is much more complicated to implement than the approach proposed in the present report. It is believed that the present chapter provides new solutions to this problem.

4 SSFEM Analysis

As any finite element software, the core of the SSFEM program consists in computing element stiffness matrices and nodal forces, assembling element contributions and solving the obtained linear system. These different steps are described in detail in the sequel.

4.1 Element stochastic stiffness matrix

In the context of two-dimensional elastic problems with spatially variable Young's modulus, the element stiffness matrix is given by (Chapter 5, Section 2) :

$$(3.14) \quad \mathbf{k}^e(\theta) = \int_{\Omega_e} H(\mathbf{x}, \theta) \mathbf{B}^T \cdot \mathbf{D}_o \cdot \mathbf{B} d\Omega_e$$

where $H(\mathbf{x}, \theta)$ is the random field representing the material Young's modulus and \mathbf{D}_o is the elasticity matrix computed with unit Young's modulus. Substituting for the truncated series expansion (2.1) into (3.14) leads to computing the following *deterministic* matrices :

- the mean element stiffness matrix :

$$(3.15) \quad \bar{\mathbf{k}}^e = \int_{\Omega_e} \mu \mathbf{B}^T \cdot \mathbf{D}_o \cdot \mathbf{B} d\Omega_e$$

- M weighted element stiffness matrices :

$$(3.16) \quad \mathbf{k}_i^e = \int_{\Omega_e} H_i(\mathbf{x}) \mathbf{B}^T \cdot \mathbf{D}_o \cdot \mathbf{B} d\Omega_e \quad i = 1, \dots, M$$

For 4-node isoparametric elements, a 2×2 Gaussian integration scheme was used to compute these integrals².

Equivalent nodal forces resulting from initial stresses σ_o and body forces b were computed as follows :

$$(3.17) \quad f^e = \int_{\Omega_e} -B^T \cdot \sigma_o d\Omega_e + \int_{\Omega_e} N^T \cdot b d\Omega_e$$

where N stands for the matrix of the element shape functions and B for the matrix yielding the strain components from the nodal displacements.

4.2 Assembly procedures

A standard assembling technique is used to get the mean and weighted *global* stiffness matrices, *i.e.* :

$$(3.18-a) \quad \bar{K} = \bigcup_e \bar{k}^e = \bigcup_e \int_{\Omega_e} \mu B^T \cdot D_o \cdot B d\Omega_e$$

$$(3.18-b) \quad K_i = \bigcup_e k_i^e = \bigcup_e \int_{\Omega_e} H_i(x) B^T \cdot D_o \cdot B d\Omega_e$$

This step is called the *first level* of assembly.

The Galerkin technique associated with SSFEM then leads to the following system of equations using the above matrices (see Part I, Eq.(5.22)) :

$$(3.19) \quad \sum_{i=0}^M \sum_{j=0}^{P-1} c_{ijk} K_i \cdot U_j = F_k \quad k = 0, \dots, P-1$$

where the terms corresponding to $i = 0$ are the mean quantities, *i.e.*, $K_o \equiv \bar{K}$ and $U_o \equiv \bar{U}$. Moreover, in case of deterministic loading, the vectors F_k appearing in the right hand side of Eq.(3.19) are all zero except the first one F_o . Introducing the notation :

$$(3.20) \quad K_{jk} = \sum_{i=0}^M c_{ijk} K_i = c_{ojk} \bar{K} + \sum_{i=1}^M c_{ijk} K_i \quad j, k = 0, \dots, P-1$$

Eqs.(3.19) can be cast in the following form :

$$(3.21) \quad \begin{bmatrix} K_{00} & \dots & K_{0,P-1} \\ K_{10} & \dots & K_{1,P-1} \\ \vdots & & \vdots \\ K_{P-1,0} & \dots & K_{P-1,P-1} \end{bmatrix} \cdot \begin{bmatrix} U_0 \\ U_1 \\ \vdots \\ U_{P-1} \end{bmatrix} = \begin{bmatrix} F_o \\ 0 \\ \vdots \\ 0 \end{bmatrix}$$

²A 3×3 scheme was tried but gave practically the same result for larger computation time, and was thus abandoned.

which may be rewritten formally as :

$$(3.22) \quad \mathcal{K} \cdot \mathcal{U} = \mathcal{F}$$

Building the above matrix \mathcal{K} from the \mathbf{K}_{jk} matrices is called the *second level* of assembly. In implementation, the matrices \mathbf{K}_{jk} are first computed using (3.20). Attention is paid to summing up only those terms associated with $c_{ijk} \neq 0$. Then \mathbf{K}_{jk} is plugged into the large matrix \mathcal{K} as indicated in (3.21). The number of unknowns in the system (3.21) is $N \times P$, where N is the number of degrees of freedom of the structure (*i.e.* twice the number of nodes in two-dimensional continuum analysis), and P is the size of the polynomial chaos basis.

4.3 Application of the boundary conditions

The boundary conditions are assumed to be *deterministic* and given in terms of a set of *fixed* degrees of freedom \mathcal{I} (*i.e.* for which the nodal displacement is set to zero). Considering Eq.(3.21), this writes :

$$(3.23) \quad u_j^k = 0 \quad \forall k \in \mathcal{I}, \forall j = 0, \dots, P-1$$

where u_j^k is the k -th component of vector \mathbf{U}_j in (3.21).

The Lagrange multiplier technique is used, where a partial back-substitution of the constraints equations $\{u_j^k = 0\}$ leads to the following operations onto the global stiffness matrix \mathcal{K} :

- $\forall k \in \mathcal{I}, \forall j = 0, \dots, P-1$, row and column $\#(jN + k)$ are all set to zero, then the diagonal term is set equal to 1.
- The corresponding right-hand side component F_j^k is set equal to 0.

However the same result can be obtained with greater computational efficiency by applying the boundary conditions onto the \mathbf{K}_{pq} matrices *before* the second level of assembly. Precisely, the following operations are applied on each \mathbf{K}_{pq} :

- if $p \neq q$, for each $k \in \mathcal{I}$, row and column $\#k$ of \mathbf{K}_{pq} are set equal to 0.
- if $p = q$, the same operation is applied, then the diagonal term $\mathbf{K}_{pq}(k, k)$ is set equal to 1.

4.4 Storage and solver

As in deterministic finite element analysis, all the matrices involved in the calculation (*i.e.* \bar{K} , K_i , K_{jk}) are *sparse*, that is, contain a great number of zeros. Thus the sparse storage option in MATLAB is used in their declaration. In this case, only the non zero terms of are stored together with the indices of their position.

After having declared these matrices as sparse, the user can perform any operation without worrying about the storage issues, which greatly simplifies the implementation. The solution of the problem, *i.e.* $\mathcal{U} = \{U_o, \dots, U_{P-1}\}$ is finally obtained using a MATLAB built-in solver.

By running examples, it appeared that the most time consuming step in the analysis is the second level of assembly. The solving step itself usually represented a small fraction of the total computation time. This can be explained by the fact that an interpreted code is used for the assembly steps, whereas the solver is a compiled MATLAB routine. A different behavior would be expected if the program were to be fully compiled.

5 SSFEM post-processing

The crude output of the SSFEM analysis is a set of nodal displacement coefficients $\mathcal{U} = \{U_o, \dots, U_{P-1}\}$ which allow to represent the random vector of nodal displacements as :

$$(3.24) \quad \mathcal{U}(\theta) = \sum_{j=0}^{P-1} U_j \Psi_j (\{\xi_k(\theta)\}_{k=1}^M)$$

5.1 Strain and stress analysis

For any given element Ω_e , let us gather the nodal displacements into a vector :

$$(3.25) \quad \mathbf{u}^e(\theta) = \sum_{j=0}^{P-1} \mathbf{u}_j^e \Psi_j (\{\xi_k(\theta)\}_{k=1}^M)$$

The strain- and stress components at a given point \mathbf{x} are random variables obtained as :

$$(3.26) \quad \epsilon(\mathbf{x}, \theta) = \mathbf{B}(\mathbf{x}) \sum_{j=0}^{P-1} \mathbf{u}_j^e \Psi_j (\{\xi_k(\theta)\}_{k=1}^M)$$

$$(3.27) \quad \sigma(\mathbf{x}, \theta) = \left[\mu + \sum_{i=1}^M \xi_i(\theta) \right] D_o \mathbf{B}(\mathbf{x}) \sum_{j=0}^{P-1} \mathbf{u}_j^e \Psi_j (\{\xi_k(\theta)\}_{k=1}^M)$$

5.2 Second moment analysis

The second order statistics of the nodal displacements are given by :

$$(3.28) \quad \mathbb{E}[\mathbf{U}] = \bar{\mathbf{U}} \equiv \mathbf{U}_o$$

$$(3.29) \quad \text{Cov}[\mathbf{U}, \mathbf{U}] = \sum_{i=1}^{P-1} \mathbb{E}[\Psi_i^2] \mathbf{U}_i \cdot \mathbf{U}_i^T$$

Similar results can be obtained for strain and stress components by means of Eqs.(3.26)-(3.27).

5.3 Reliability analysis

As described in Part I, Chapter 4, reliability analysis is based on the definition of a limit state function depending on the output of the mechanical analysis. For the sake of simplicity, only displacement-based limit state functions are considered in the sequel :

$$(3.30) \quad g(\mathbf{U}(\theta)) = u - u^{i_o}(\theta)$$

where $u^{i_o}(\theta)$ is a (random) nodal displacement under consideration and u is a prescribed threshold. Substituting the i_o -th component of the vectorial equation (3.24) in (3.30) yields the following *analytical* polynomial expression of the limit state function in terms of M standard normal variables $\{\xi_k(\theta)\}_{k=1}^M$:

$$(3.31) \quad g(\mathbf{U}(\theta)) = u - \sum_{j=0}^{P-1} u_j^{i_o} \Psi_j(\{\xi_k(\theta)\}_{k=1}^M)$$

In the latter equation, the coefficients $u_j^{i_o}$ are known from the analysis stage, see section 4.

A FORM analysis using the iHLRF algorithm can be carried out to determine the design point ξ^* and the corresponding values of the reliability index β and the probability of failure. Thereafter, importance sampling around the design point can be performed in order to get a more accurate value of the probability of failure. This is computationally cheap since the expression of the limit state function is analytical.

It is emphasized that the limit state function is already defined in terms of standard normal variables, which avoids any probabilistic transformation within the iHLRF algorithm (see Part I, Chapter 4, Section 2.4).

Moreover, the gradient of $g(\mathbf{U}(\theta))$ can be given a closed form expression. Indeed, recalling the integer sequence representation (3.2) of $\Psi_j \equiv \Psi_\alpha$, one gets :

$$(3.32) \quad \frac{\partial \Psi_\alpha}{\partial \xi_k} = \begin{cases} 0 & \text{if } \alpha_k = 0 \\ \alpha_k h_{\alpha_k-1}(\xi_k) \cdot \prod_{l \neq k} h_{\alpha_l}(\xi_l) & \text{otherwise} \end{cases}$$

5.4 Probability density function of a response quantity

The probability density function (PDF) of u^{i_0} can also be determined using sensitivity analysis. From (3.31) one gets :

$$(3.33) \quad P_f = P(u \leq u^{i_0}) = 1 - F_{i_0}(u)$$

where F_{i_0} is the cumulative distribution function (CDF) of random variable u^{i_0} . Using now Eq.(4.84) of Part I, the PDF of u^{i_0} is :

$$(3.34) \quad f_{i_0}(u) = \frac{dF_{i_0}}{du} = -\frac{dP_f}{du} = \varphi(\beta(u)) \frac{d\beta}{du}$$

Using Eq.(4.82) of Part I, one has :

$$(3.35) \quad \frac{d\beta}{du} = \frac{1}{\|\nabla_{\xi} g(\mathbf{U}(\xi^*(u)), u)\|} \cdot \frac{\partial g(\xi, u)}{\partial u}$$

In this expression, the derivative of g with respect to u is simply 1 due to the form of (3.31). Thus substituting for (3.35) in (3.34) finally yields :

$$(3.36) \quad f_{i_0}(u) = \frac{\varphi(\beta(u))}{\|\nabla_{\xi} g(\mathbf{U}(\xi^*(u)), u)\|}$$

To compute the entire PDF of a nodal displacement, a FORM analysis is carried out for different thresholds u , for which Eq.(3.36) is evaluated.

6 Conclusions

This chapter has presented the implementation of the Spectral Stochastic Finite Element Method (SSFEM) in the MATLAB environment. Object-oriented programming was aimed at, first to allow a versatile utilization of the code, second to build a base for later implementation in a true object-oriented language like C++.

An original implementation of the polynomial chaos basis was proposed, which is believed to be simpler than the only other implementation found in the literature, *i.e.* that by Ghanem and Spanos (1991*b*).

The SSFEM procedure was described in detail from data pre-processing to solution and to post-processing. Results obtained from the second moments (resp. reliability) post-processing should now be compared with other approaches, *i.e.* perturbation method and Monte Carlo simulation (resp. direct coupling between a deterministic finite element code and the FORM procedure). This is the goal of Chapter 4 (resp. Chapter 5).

Chapter 4

Second moment analysis

1 Introduction

The aim of this chapter is to compare second moment methods for elastic two-dimensional mechanical problems involving spatial variability of material properties. Precisely, modeling the Young's modulus of the material as a random field, the mean value and standard deviation of response quantities such as nodal displacements are computed. Three different methods have been implemented.

- The crude *Monte-Carlo simulation* consists in simulating samples of the random field, then carrying out a deterministic finite element analysis of the mechanical problem, and finally, statistically treating the response quantities of interest.
- The *perturbation method* presented in Part I, Chapter 3, Section 2 is applied at first and second order, the specific formulation associated with random fields being first discussed.
- The SSFEM method is applied followed by the post-processing procedure described in Chapter 3, Section 5.2.

These three approaches are applied to compute the statistics of the settlement of a foundation over an elastic layer, whose heterogeneity is accounted for by modeling its Young's modulus as a random field.

2 Monte Carlo simulation

2.1 Introduction

The principle of the Monte Carlo method is to simulate a large number of samples (here realizations of the random field) then compute for each sample the response quantity under consideration (here a given nodal displacement) and then perform a statistical treatment of the sample population.

This approach requires being able to analyze by finite elements a structure whose material properties (*e.g.* Young's modulus) are realizations of a random field. To properly take into account the spatial variability, a *deterministic* finite element code called FEMRF was implemented for two-dimensional elastic problems.

2.2 The finite element code FEMRF

The only difference between FEMRF and a standard finite element code is in the way the element stiffness matrices are computed. Considering a realization $H(\mathbf{x}, \theta_o)$ of the random field modeling the material Young's modulus, the element stiffness matrix is given by (See Eq.3.14) :

$$(4.1) \quad \mathbf{k}^e(\theta_o) = \int_{\Omega_e} H(\mathbf{x}, \theta_o) \mathbf{B}^T(\mathbf{x}) \cdot \mathbf{D}_o \cdot \mathbf{B}(\mathbf{x}) d\Omega_e$$

Using the isoparametric formulation, this integral is recast over a reference domain $\Omega_{\mathcal{R}}$ (unit square in the case of 4-node quadrangles) as follows :

$$(4.2) \quad \mathbf{k}^e(\theta_o) = \int_{\Omega_{\mathcal{R}}} H(\mathbf{x}(\boldsymbol{\eta}), \theta_o) \mathbf{B}^T(\boldsymbol{\eta}) \cdot \mathbf{D}_o \cdot \mathbf{B}(\boldsymbol{\eta}) |\mathcal{J}_{\mathbf{x},\boldsymbol{\eta}}| d\Omega_{\mathcal{R}}$$

where $\mathcal{J}_{\mathbf{x},\boldsymbol{\eta}}$ is the determinant of the mapping $\mathbf{x}(\boldsymbol{\eta})$.

Using Gaussian integration, the latter equation becomes :

$$(4.3) \quad \mathbf{k}^e(\theta_o) \approx \sum_{i=1}^{\text{NPG}} w_i H(\mathbf{x}(\boldsymbol{\eta}_i), \theta_o) \mathbf{B}^T(\boldsymbol{\eta}_i) \cdot \mathbf{D}_o \cdot \mathbf{B}(\boldsymbol{\eta}_i) |\mathcal{J}_{\mathbf{x},\boldsymbol{\eta}}|$$

where NPG is the number of integration points, whose coordinates are $\boldsymbol{\eta}_i$ and related weights are w_i . Thus Eq.(4.3) requires the evaluation of the current realization θ_o of the random field at point $\mathbf{x}(\boldsymbol{\eta}_i)$.

In practical calculations, $H(\mathbf{x}(\boldsymbol{\eta}_i), \theta_0)$ is replaced by a truncated series expansion as follows :

$$(4.4) \quad \hat{H}(\mathbf{x}(\boldsymbol{\eta}_i), \theta_0) = \mu + \sum_{i=1}^M H_i(\mathbf{x}(\boldsymbol{\eta}_i)) \xi_i(\theta_0) \quad \text{if } H(\cdot) \text{ Gaussian}$$

$$(4.5) \quad \hat{H}(\mathbf{x}(\boldsymbol{\eta}_i), \theta_0) = \exp \left[\lambda + \sum_{i=1}^M H_i(\mathbf{x}(\boldsymbol{\eta}_i)) \xi_i(\theta_0) \right] \quad \text{if } H(\cdot) \text{ lognormal, } \lambda \text{ being the mean value of the underlying Gaussian field in this case.}$$

Adequate routines have been implemented to compute Eqs.(4.4)-(4.5) depending on the nature of the random field. They are called by the routine computing the element stiffness matrix Eq.(4.3).

In the context of Monte-Carlo simulation, θ_0 corresponds to the generation of M random numbers $\boldsymbol{\xi} = \{\xi_1(\theta_0), \dots, \xi_M(\theta_0)\}$ according to a standard normal distribution. This is done using the MATLAB built-in random number generator.

2.3 Statistical treatment of the response

Unbiased estimates of the mean and variance of a given statistical sample are given by

$$(4.6) \quad E^{\text{MC}} [U] = \frac{1}{N_{\text{sim}}} \sum_{i=1}^{N_{\text{sim}}} U(\theta_i)$$

$$(4.7) \quad \text{Var}^{\text{MC}} [U] = \frac{1}{N_{\text{sim}} - 1} \left[\sum_{i=1}^{N_{\text{sim}}} U^2(\theta_i) - N_{\text{sim}} (E^{\text{MC}} [U])^2 \right]$$

where N_{sim} is the number of samples considered, $U(\theta_i)$ is the nodal displacement vector associated with sample θ_i , and $U^2(\theta_i)$ is the vector containing the square values of the nodal displacements.

In implementation, the sums $\sum_i U(\theta_i)$ and $\sum_i U^2(\theta_i)$ are updated continuously after each finite element run. The accuracy of the Monte-Carlo simulation is estimated by the coefficient of variation of the empirical mean (4.6), which is given by :

$$(4.8) \quad \text{COV}^{\text{MC}} = \frac{\sqrt{\text{Var}^{\text{MC}} [U]}}{\sqrt{N_{\text{sim}}} E^{\text{MC}} [U]}$$

Typical values for COV^{MC} are 0.01 - 0.05.

2.4 Remarks on random fields representing material properties

A number of papers published on stochastic finite element methods including random fields (*e.g.* Liu *et al.* (1986*b,a*); Ghanem and Spanos (1991*a,b*); Deodatis and Shinozuka (1991); Anders and Hori (1999)) assess the validity of the proposed approach by comparing the results with those obtained by a Monte Carlo simulation. In practice, these authors use Gaussian random fields.

When material properties are modeled, the use of Gaussian random fields is questionable. Indeed realizations of Gaussian random variables can be negative valued, whereas the material properties are positive in nature. The results obtained by Monte Carlo simulation in this case are definitely doubtful due to the possible negative outcomes. Either these negative outcomes have to be discarded, which introduces a bias in the simulation, or non physical results (*e.g.* corresponding to negative Young's modulus) are included. Moreover, the general result, which says that Monte Carlo simulation is asymptotically exact (the more samples, the best result) does no longer hold : in this case indeed, the more samples, the more non physical outcomes.

This problem has not received much attention in the literature, the authors of the papers mentioned above do not even bring up the question. From the remarks above, the following strategy will be adopted in the present study : Monte Carlo simulation of Young's modulus will only be performed with lognormal distributions.

3 Perturbation method for structures with spatially varying materials properties

3.1 Introduction

The perturbation method is based on a Taylor series expansion of the quantities involved in the equilibrium equation $\mathbf{K} \cdot \mathbf{U} = \mathbf{F}$. In this chapter, the randomness in the input is limited to spatial variability of the material Young's modulus. Thus the basic variables used in the Taylor series expansion are M independent standard normal variates $\boldsymbol{\xi} = \{\xi_1, \dots, \xi_M\}$ used in the random field discretization, and the formulation of the perturbation method presented in a general context in Part I, Chapter 3, Section 2 can be simplified.

The second order Taylor series expansions of $K(\xi)$ and $U(\xi)$ respectively are :

$$(4.9) \quad K(\xi) \approx K_o + \sum_{i=1}^N K_i^I \xi_i + \frac{1}{2} \sum_{i=1}^N \sum_{j=1}^N K_{ij}^{II} \xi_i \xi_j$$

$$(4.10) \quad U(\xi) \approx U^o + \sum_{i=1}^N U_i^I \xi_i + \frac{1}{2} \sum_{i=1}^N \sum_{j=1}^N U_{ij}^{II} \xi_i \xi_j$$

where the notation used in the above equations has been introduced in Part I, Chapter 3, Section 2. Moreover, the load vector F is assumed deterministic in the sequel.

3.2 Derivatives of the global stiffness matrix

The perturbation method is "distribution-free" in essence, which means that the input should be limited to the second moments of the basic random variables. However, when random fields are used, the Taylor series expansion depends on the discretization scheme implicitly selected.

In the following derivations, the series expansion discretization schemes of a Gaussian random field are implicitly considered. Under this assumption, the global stiffness matrix has the form :

$$(4.11) \quad K(\xi) = \bigcup_e \int_{\Omega_e} \left[\mu + \sum_{i=1}^M H_i(x) \xi_i \right] B^T \cdot D_o \cdot B d\Omega$$

Thus the derivative of K with respect to ξ_i is :

$$(4.12) \quad K_i^I \equiv \frac{\partial K}{\partial \xi_i} \Big|_{\xi=0} = \bigcup_e \int_{\Omega_e} H_i(x) B^T \cdot D_o \cdot B d\Omega$$

that is, the *global weighted stiffness matrix* K_i , see Eqs.(3.16)-(3.18-b). Furthermore, the second derivatives K_{ij}^{II} are all zero.

From Eqs.(4.9)- (4.10), the Taylor series expansion of the equilibrium equation is :

$$(4.13) \quad \left(K_o + \sum_{i=1}^M K_i^I \right) \left(U^o + \sum_{i=1}^M U_i^I \xi_i + \frac{1}{2} \sum_{i=1}^M \sum_{j=1}^M U_{ij}^{II} \xi_i \xi_j \right) = F$$

By identifying the coefficients of ξ_i and $\xi_i \xi_j$ on both sides, one finally gets :

$$(4.14) \quad U^o = K_o^{-1} \cdot F$$

$$(4.15) \quad U_i^I = -K_o^{-1} \cdot K_i \cdot U = -L_i \cdot U \quad \text{where} \quad L_i = K_o^{-1} \cdot K_i$$

$$(4.16) \quad U_{ij}^{II} = U_{ji}^{II} = -K_o^{-1} [K_i^I \cdot U_j^I + K_j^I \cdot U_i^I] = -(L_i \cdot U_j^I + L_j \cdot U_i^I) \\ = (L_i \cdot L_j + L_j \cdot L_i) \cdot U^o$$

3.3 Second moments of the response

The second-order statistics of the response can be now computed from Eqs.(4.10),(4.14)-(4.16). Recalling that $\{\xi_1, \dots, \xi_M\}$ are independent standard normal variables, it follows that :

$$(4.17-a) \quad E[\xi_i] = 0$$

$$(4.17-b) \quad \text{Cov}[\xi_i, \xi_j] = \delta_{ij} \quad (\text{Kronecker symbol})$$

Thus the first- and second-order estimates of the nodal displacement mean values are :

$$(4.18-a) \quad E^I[\mathbf{U}] = \mathbf{U}^o$$

$$(4.18-b) \quad E^{II}[\mathbf{U}] = \mathbf{U}^o + \frac{1}{2} \sum_{i=1}^M \mathbf{L}_i^2 \cdot \mathbf{U}^o$$

The first-order approximation of the covariance matrix of \mathbf{U} is :

$$(4.19) \quad \text{Cov}^I[\mathbf{U}, \mathbf{U}] = \sum_{i=1}^M \mathbf{U}_i^I \cdot \mathbf{U}_i^{IT}$$

The second-order approximation of the covariance matrix of \mathbf{U} can be easily derived using the following properties :

$$(4.20-a) \quad E[\xi_i \xi_j \xi_k] = 0$$

$$(4.20-b) \quad E[\xi_i \xi_j \xi_k \xi_l] = \delta_{ij} \delta_{kl} + \delta_{ik} \delta_{jl} + \delta_{il} \delta_{jk}$$

After some algebra, one finally obtains :

$$(4.21) \quad \text{Cov}^{II}[\mathbf{U}, \mathbf{U}] = \text{Cov}^I[\mathbf{U}, \mathbf{U}] + \frac{1}{4} \sum_{i=1}^M \sum_{j=1}^M \mathbf{U}_{ii}^{II} \cdot \mathbf{U}_{jj}^{II T} + \frac{1}{2} \sum_{i=1}^M \sum_{j=1}^M \mathbf{U}_{ij}^{II} \cdot \mathbf{U}_{ij}^{II T}$$

3.4 Remark on another possible Taylor series expansion

In the above derivations, the random field was implicitly considered as Gaussian to carry out the Taylor series expansion of \mathbf{K} . If it were to be considered as lognormal (which, in some sense, corresponds to selecting a different point around which the expansions are carried out), the global stiffness matrix would write :

$$(4.22) \quad \mathbf{K}(\boldsymbol{\xi}) = \bigcup_e \int_{\Omega_e} \exp \left[\lambda + \sum_{i=1}^M H_i(\mathbf{x}) \xi_i \right] \mathbf{B}^T \cdot \mathbf{D}_o \cdot \mathbf{B} \, d\Omega$$

In this case, the derivatives of K with respect to ξ_i are :

$$(4.23) \quad K_i^I \equiv \left. \frac{\partial K}{\partial \xi_i} \right|_{\xi=0} = \bigcup_e \int_{\Omega_e} e^\lambda H_i(\mathbf{x}) B^T \cdot D_o \cdot B d\Omega$$

$$(4.24) \quad K_{ij}^{II} \equiv \left. \frac{\partial^2 K}{\partial \xi_i \partial \xi_j} \right|_{\xi=0} = \bigcup_e \int_{\Omega_e} e^\lambda H_i(\mathbf{x}) H_j(\mathbf{x}) B^T \cdot D_o \cdot B d\Omega$$

It is emphasized that the value of the random field computed for $\xi = 0$ (i.e. e^λ) is *not* the mean value of the field. The latter is indeed $\mu = e^{\lambda + \zeta^2/2}$, where ζ is the standard deviation of the approximate underlying Gaussian field. This means that the expansion in this case would not be carried out around the mean value K_o . Thus the accuracy of the results is expected to be worse than that obtained in the previous section. Moreover, the computation of the second order terms U_{ij}^{II} now involves the non zero matrices K_{ij}^{II} , which makes the whole computation much more time consuming. This type of expansion will not be used in the numerical applications.

4 Settlement of a foundation on an elastic soil mass

4.1 Deterministic problem statement

Consider an elastic soil layer of thickness t lying on a rigid substratum. A superstructure to be founded on this soil mass is idealized as a uniform pressure P applied over a length $2B$ of the free surface (see Figure 4.1). The soil is modeled as an elastic linear isotropic material. A plane strain analysis is carried out.

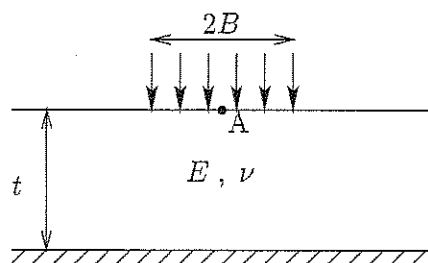


Figure 4.1: Settlement of a foundation - problem statement

Due to the symmetry, half of the structure is modeled by finite elements. Rigorously speaking, there is no more symmetry in the system when random material properties are introduced. However, it is believed that this simplification does not significantly influence the results. The parameters selected for the computation are gathered in Table 4.1.

A refined mesh was first used to get the “exact” maximum displacement under the foundation (point A in Figure 4.1). Then different meshes were tried in order to design an optimal mesh, *i.e.* allowing to get 1% accuracy in the maximum settlement using the smallest number of elements. The mesh displayed in Figure 4.2-a was eventually chosen. It contains 99 nodes and 80 elements.

Table 4.1: Settlement of a foundation - Parameters of the deterministic model

Soil layer thickness	t	30 m
Foundation width	$2B$	10 m
Applied pressure	P	0.2 MPa
Soil Young's modulus	E	50 MPa
Soil Poisson's ratio	ν	0.3
Mesh width	L	60 m

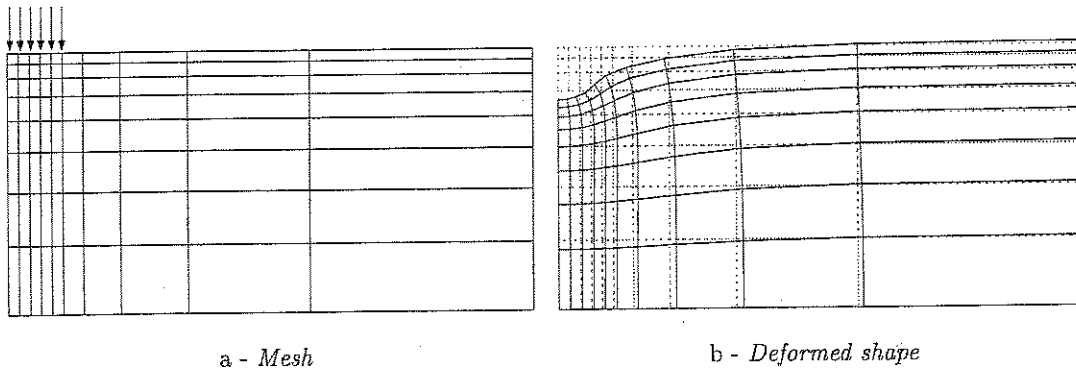


Figure 4.2: Settlement of a foundation - Mesh and deformed shape obtained by a deterministic analysis

For the input parameters given in Table 4.1, the maximum displacement obtained with the most refined mesh is $u_A^{exact} = 5.49$ cm, the value obtained with the mesh in Figure 4.2-a is $u_o = 5.43$ cm. The deformed shape is plotted in Figure 4.2-b.

4.2 Case of homogeneous soil layer

4.2.1 Closed form solution for lognormal Young's modulus

In this section, the Young's modulus E of the soil layer is assumed to be *homogeneous* and follow a lognormal distribution $LN(\lambda, \zeta)$, that is :

$$(4.25) \quad E = e^{\lambda + \zeta \xi} \quad \xi = N(0, 1)$$

where the parameters (λ, ζ) can be computed from the mean μ_E and coefficient of variation $\delta_E = \sigma_E/\mu_E$ of E by :

$$(4.26) \quad \zeta = \sqrt{\ln(1 + \delta_E^2)}$$

$$(4.27) \quad \lambda = \ln \mu_E - \frac{1}{2}\zeta^2$$

Due to the linearity of the problem, the maximum settlement U_A corresponding to any value E of the Young's modulus can be computed as :

$$(4.28) \quad U_A(E) = u_o \frac{\mu_E}{E}$$

Using Eq.(4.25), the above equation rewrites :

$$(4.29) \quad U_A(E) = e^{\ln(u_o \mu_E) - \lambda - \zeta \xi}$$

Thus the maximum settlement U_A follows a lognormal distribution $LN(\ln(u_o \mu_E) - \lambda, -\zeta)$, whose mean value and standard deviation, after some basic algebra, are given by :

$$(4.30) \quad \mu_{U_A} = u_o (1 + \delta_E^2)$$

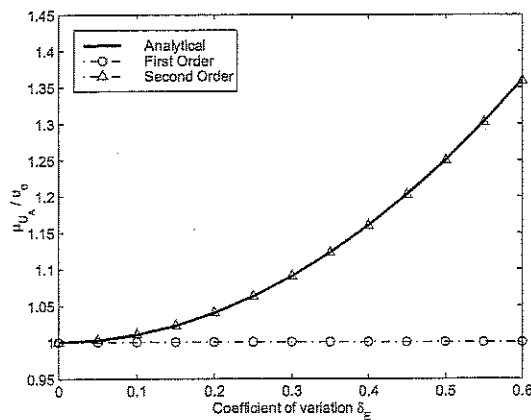
$$(4.31) \quad \sigma_{U_A} = \mu_{U_A} \cdot \delta_E = u_o \delta_E (1 + \delta_E^2)$$

These analytical expressions are used in the sequel to assess the validity of the first- and second order- perturbation and SSFEM methods. Results are presented for different coefficients of variation δ_E .

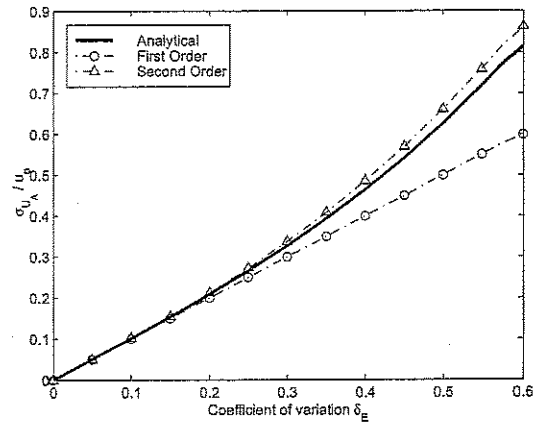
4.2.2 Numerical results

The different softwares developed for dealing with random fields are used in this example by setting the correlation length of the random field equal to $\ell = 10000$ m, and by choosing only one random variable ($M = 1$) in the discretization procedure. SSFEM is applied considering the random field as *lognormal*. The perturbation method corresponds to the derivation in Section 3.3, *i.e* assuming implicitly a Gaussian representation of the random field.

Perturbation method Results regarding the perturbation method are given in Figure 4.3. Considering a "good" approximation as one giving less than 5% discrepancy from the exact result, it appears that the (constant) first-order estimate of the mean is acceptable only for $\delta_E < 0.2$. In contrast, the second-order estimate is almost the exact value, whatever δ_E in the range under consideration. This can be partially explained by

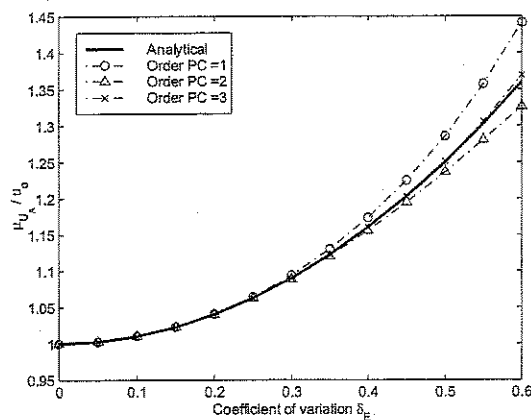


a - Mean value of maximum settlement

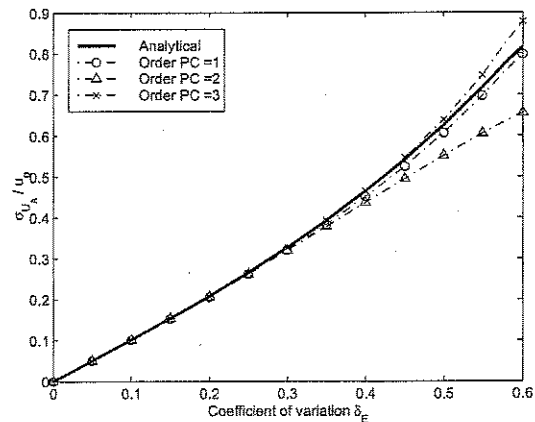


b - Standard deviation of maximum settlement

Figure 4.3: Settlement of a foundation - Homogeneous Young's modulus with lognormal distribution - Perturbation results



a - Mean value of maximum settlement



b - Standard deviation of maximum settlement

Figure 4.4: Settlement of a foundation - Homogeneous Young's modulus with lognormal distribution - SSFEM results

the fact that the *exact* Taylor series expansion of the stiffness matrix has only constant and linear terms.

The first-order estimate of the standard deviation is linearly increasing with δ_E , which is a fair approximation as long as $\delta_E < 0.2$. The second-order estimate gives much better accuracy for larger COV δ_E .

As a conclusion, it is seen on this example that the first-order perturbation method can-

not be expected to give satisfactory results for medium to large coefficients of variation of the input random field. In contrast, the second-order approach is much more accurate, whatever the value of δ_E . Furthermore, using the expansion described in Section 3.3, the latter is inexpensive to apply due to the fact that the second-order derivatives K_{ij}^{II} are all zero.

SSFEM method Results regarding the SSFEM approach are given in Figure 4.4 for different orders of expansion. As only one random variable is used to discretize the underlying random field, the size of the polynomial chaos of order p is $P = p + 1$. The polynomial chaos is used to expand both the global stiffness matrix and the vector of nodal displacements, as described in Part I, Chapter 5, Section 4.1.

It appears that a good accuracy is obtained with $p = 3$ for any COV of the Young's modulus, whereas $p = 2$ is enough if the COV δ_E is less than 0.3. It can be seen in Figure 4.4-b that the first order result is closer to the exact solution than the second order. No satisfactory explanation to this behavior could be found.

4.3 Case of heterogeneous soil layer

4.3.1 Problem statement

To account for the heterogeneity in the soil, the Young's Modulus is now modeled as a homogeneous *lognormal* random field having the following properties :

- mean value : $\mu_E = 50$ MPa,
- standard deviation : $\sigma_E = \mu_E \times \delta_E$ where the coefficient of variation δ_E varies within $[0, 0.5]$,
- *exponential square* correlation structure with correlation length $\ell = 30$ m.

The discretized lognormal field is obtained by exponentiation of an EOLE expansion of the underlying Gaussian field.

Different EOLE grids were tried, each of them corresponding to a uniform mesh, whose element size L_{RF} satisfies $L_{RF}/\ell = 1/2 - 1/10$. The mean of the error variance (2.50) has been computed in each case for different orders of expansion M , the results are reported in Table 4.2.

If selecting a tolerance of 10% for the accuracy in the discretization, it appears from Table 4.2 that $M = 4$ should be selected. For our choice of parameters, the refinement

Table 4.2: Settlement of a foundation - Mean error $\bar{\epsilon}$ in the EOLE discretization (See Eq.(2.50))

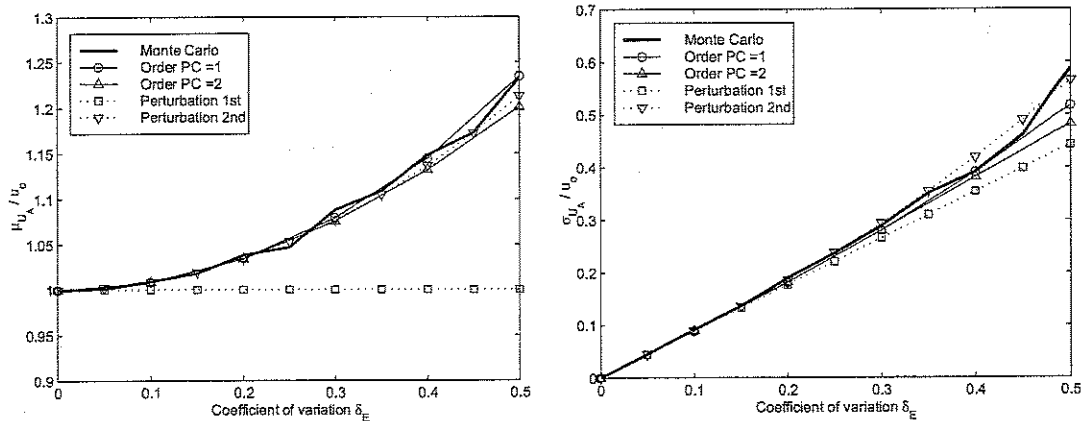
M	$L_{RF}/\ell = 1/2$	$L_{RF}/\ell = 1/3$	$L_{RF}/\ell = 1/4$	$L_{RF}/\ell = 1/5$	$L_{RF}/\ell = 1/10$
1	0.467	0.462	0.461	0.460	0.459
2	0.236	0.228	0.226	0.225	0.224
3	0.151	0.143	0.140	0.139	0.138
4	0.085	0.078	0.076	0.075	0.074
5	0.048	0.041	0.038	0.037	0.036

of the EOLE grid does not significantly improve the accuracy, for a given M . Thus $L_{RF}/\ell = 1/2$ is selected in the computations, which corresponds to a 5×3 point grid.

As there is no closed form solution to the statistics of the response, a Monte Carlo simulation is performed. For each coefficient of variation δ_E , 1000 samples are used (the obtained simulation error measured by Eq.(4.8) is increasing from 0.1% to 1.5% when the COV of the input random field varies from 0.05 to 0.5)

4.3.2 Numerical results

The mean value μ_{U_A} and the standard deviation σ_{U_A} of the maximum settlement U_A are plotted in Figure 4.5 as a function of the COV of the input.



a - Mean value of maximum settlement

b - Standard deviation of maximum settlement

Figure 4.5: Settlement of a foundation - Young's modulus modeled by a lognormal random field

For any COV, μ_{U_A} and σ_{U_A} are smaller than the values they take in case of homogeneous Young's modulus (See Figures 4.3-4.4). As in the case of homogeneous Young's modulus, the first-order estimate of the mean has acceptable accuracy only if $\delta_E < 0.2$. The first-order estimate of the standard deviation is reasonably accurate for the range of δ_E considered. Both the second-order perturbation and the second-order SSFEM methods give good accuracy for any COV in the range under consideration.

4.4 Efficiency of the approaches

In order to fully compare the three methods used in this chapter, computation times have been reported in Table 4.3. The time unit corresponds to a deterministic analysis with constant Young's modulus.

Table 4.3: Settlement of a foundation - Comparison of computation times

Method	CPT
Deterministic finite element analysis with constant Young's modulus	1
Deterministic finite element analysis with Young's modulus obtained from discretized random field	4.47
Monte Carlo simulation (1000 samples)	4508
1st order perturbation method	11.8
2nd order perturbation method	21
1st order SSFEM	19.5
2nd order SSFEM	1446

Regarding the Monte Carlo simulation, the computation time comes almost only from the successive deterministic finite element runs. The second order perturbation method requires about twice as much time as the first order.

As far as SSFEM is concerned, there is a huge difference between the computational cost of the first- and the second-order methods. Higher order computations could not be carried out. This can be explained by the fact that the discretization of the random field required $M = 4$ random variables to get an acceptable accuracy, leading to a large size of the polynomial chaos basis even for small order (*e.g.*, $p = 3$). Completely different computation times would have been observed in the first example (*i.e.* in case of lognormal Young's modulus), where only one random variable was used.

It is emphasized that the computed times reported in Table 4.3 are related to the discretization scheme employed (here EOLE) and would be different if another discretization scheme was chosen. They are of course related to the MATLAB implementation, *i.e.*, in an interpreted language. They would probably be completely different in a fully compiled implementation.

5 Conclusions

In this chapter, three second moment methods have been presented in the context of spatial variability of material properties and applied to a geomechanical problem.

The particular formulation of each method in the present context has been derived. It appears that the perturbation method is inexpensive to apply up to second order, due to the fact that the second-order derivatives of the stiffness matrix with respect to the basic random variables are zero.

The accuracy of each method has been investigated for different values of the coefficient of variation of the input random field. The cost of each approach has been finally evaluated.

After compiling all the results, it appears that the second-order perturbation method is the most attractive for problems involving random fields, because it is inexpensive and accurate even for large coefficients of variation of the input. The SSFEM approach also gives accurate results when applied at second and higher orders. The computation time may however blow up when more than 2 or 3 random variables are used to discretize the random field.

Chapter 5

Reliability analysis of mechanical problems involving random spatial variability

1 Introduction

The aim of this chapter is to compare two different approaches for solving reliability problems based on elastic two-dimensional analyses involving random spatial variability of material properties.

- The first approach called *direct coupling* consists in coupling a *deterministic* finite element code with the iHLRF algorithm presented in Part I, Chapter 4. To take into account the spatial variability, the deterministic code FEMRF described in Chapter 4, Section 2.2 is used. Details are given in Section 2.
- The second approach consists in post-processing the results of a SSFEM analysis as described in Chapter 3, Section 5.3.

Both approaches are applied to compute the reliability index associated with the maximum settlement of a foundation lying on an elastic soil layer.

A parametric study is carried out using a Gaussian (resp. lognormal) random field in Section 3 (resp. Section 4). Comparisons of the two approaches described above are made by varying successively :

- the order of expansion in the random field discretization as well as that of the polynomial chaos expansion,

- the admissible threshold in the limit state function,
- the correlation length of the random field,
- the coefficient of variation of the input.

Efficiency is investigated by comparing the computation time required by each approach.

Remark As already stated in Chapter 4, Gaussian random fields are not well suited to model material properties, due to possible negative outcomes. In the context of reliability analysis, even the computed design point could happen to correspond to non physical values, for instance when large coefficients of variation of the input are considered. However, as Gaussian random fields have been used extensively in the literature together with the Karhunen-Loève expansion, they will be used for comparison purposes in Section 3.

2 Direct coupling approach : key points of the implementation

2.1 Utilization of the finite element code FEMRF

In the context of FORM analysis, a given realization of the basic random variables $\xi(\theta_o) = \{\xi_1(\theta_o), \dots, \xi_M(\theta_o)\}$ is provided by the iHLRF algorithm at each iteration. A deterministic finite element analysis is carried out with FEMRF, where $\xi(\theta_o)$ is used in the computation of the element stiffness matrices, see Eqs.(4.3)-(4.5).

2.2 Direct differentiation method for gradient computation

The FORM analysis requires the computation of the gradient of the limit state function. As already described in Part I, Chapter 4, Section 3, the most effective method for this purpose is the so-called *direct differentiation method*. The general formulation presented in that section is now applied to problems for which the randomness is limited to random fields describing the material's Young's modulus.

The limit state function under consideration in the present study is :

$$(5.1) \quad g(\mathbf{U}(\xi)) = u - u^{i_o}(\xi)$$

where u^{i_o} is the nodal displacement under consideration and u is a prescribed threshold. Accordingly, the gradient of the limit state function with respect to the basic random

variables $\xi = \{\xi_1, \dots, \xi_M\}$ is given by :

$$(5.2) \quad \nabla_{\xi} g^T(U(\xi)) = \nabla_U^T g(U) \cdot \nabla_{\xi} U(\xi)$$

Furthermore, due to the form of (5.1), one has :

$$(5.3) \quad \nabla_U^T g(U) = [0, \dots, 0, -1, 0, \dots]$$

where the only non zero component is the i_o -th one. The gradient of U with respect to ξ is obtained from Eqs.(4.57)-(4.60) of Part I :

$$(5.4) \quad \frac{\partial U}{\partial \xi_i} = -K^{-1} \cdot \bigcup_e \left\{ \int_{\Omega_e} B^T \cdot \frac{\partial D}{\partial \xi_i} \cdot B \, d\Omega \cdot u_e \right\}$$

where K is the global elastic stiffness matrix, B the matrix yielding the strain components from the nodal displacements u_e , and D is the elasticity matrix. In case of Gaussian random fields, the latter has the form :

$$(5.5) \quad D = H(x) D_o \approx (\mu + \sum_{i=1}^M H_i(x) \xi_i) D_o$$

Hence the partial derivative is :

$$(5.6) \quad \frac{\partial D}{\partial \xi_i} = \frac{\partial H(x)}{\partial \xi_i} D_o = H_i(x) D_o$$

Substituting (5.6) in (5.4) yields :

$$(5.7) \quad \frac{\partial U}{\partial \xi_i} = -K^{-1} \cdot \bigcup_e \left\{ \int_{\Omega_e} H_i(x) B^T \cdot D_o \cdot B \, d\Omega \cdot u_e \right\}$$

Comparing the latter equation with (3.18-b), one finally obtains :

$$(5.8) \quad \frac{\partial U}{\partial \xi_i} = -K^{-1} \cdot K_i \cdot U$$

where K_i is the i -th global weighted stiffness matrix. Substituting for Eqs.(5.3) and (5.8) in (5.2) finally gives the following closed-form expression for the gradient of the limit state function :

$$(5.9) \quad \nabla_{\xi} g^T(U(\xi)) = [0, \dots, 0, 1, 0, \dots] \cdot K^{-1} \cdot [K_1 \cdot U, \dots, K_M \cdot U]$$

For optimal efficiency, the leftmost product $\Lambda = [0, \dots, 0, 1, 0, \dots] \cdot K^{-1}$ is carried out first. Then the products $K_i \cdot U$ are evaluated and arranged column-wise in a matrix of size $N \times M$. This matrix is eventually multiplied by Λ . This procedure is the so-called adjoint method described in Part I, Chapter 4, Section 3.2.

3 Settlement of a foundation on an elastic soil mass - Gaussian input random field

3.1 Introduction

The deterministic problem under consideration has been described in Chapter 4, Section 4.1. The assessment of the serviceability of the foundation is now investigated. The limit state function considered in the sequel is defined in terms of the maximum settlement U_A at the center of the foundation :

$$(5.10) \quad g(U(\xi)) = u - U_A(\xi)$$

where u is a given threshold.

In this section, the random field modeling the Young's modulus of the soil is supposed to be Gaussian, and has the following properties :

- mean value $\mu_E = 50$ MPa,
- variable standard deviation σ_E , corresponding to a coefficient of variation $\delta_E = \sigma_E/\mu_E \in [0, 0.5]$,
- *exponential* autocorrelation function. As all the applications of SSFEM found in the literature make use of this kind of correlation structure together with the Karhunen-Loève discretization scheme, this form is assumed in this section. To get a fair representation of the random field (*i.e.*, $\bar{\epsilon} \leq 10\%$) with a manageable number of terms in the expansion (*i.e.*, $M \leq 4$), the random field is assumed to be *one-dimensional* along the depth. This corresponds to a *layered* structure for the soil mass, which is physically meaningful. In actual computations, the two-dimensional random field toolbox is used with a different correlation length in each direction (see Chapter 2, Section 2.1), *i.e.* $\ell_x = 10000$ m, $\ell_y = 30$ m.
- variable admissible maximum settlement u .

3.2 Influence of the order of expansion

In this section, the coefficient of variation of the random field is set equal to 0.2, and the threshold in the limit state function is set to 10 cm. It is noted that the maximum settlement u_o obtained from a deterministic finite element analysis with homogeneous Young's modulus equal to 50 MPa is $u_o = 5.42$ cm.

3.2.1 Direct coupling

The reliability index β_{direct} is computed for different orders of expansion M of the input random field. Results are reported in Table 5.1 together with the accuracy of the discretization (estimator $\bar{\epsilon}$ defined in Eq.(2.50)).

Table 5.1: Influence of the accuracy in the random field discretization - Direct coupling approach

M	$\bar{\epsilon}$	β_{direct}
1	0.269	2.694
2	0.129	2.631
3	0.082	2.627
4	0.060	2.627
5	0.048	2.627

3.2.2 SSFEM +FORM

When applying the SSFEM method, the order p of the polynomial chaos expansion has to be specified. Together with the order of expansion M , this defines the size P of the polynomial chaos basis (see Eq.(5.58) in Part I).

The reliability index β_{SSFEM} is computed for different values of M and p , the results are reported in Table 5.2 together with the value β_{direct} obtained by direct coupling.

3.2.3 Analysis of the results

For our choice of parameters, it appears that the direct coupling allows to get 2-digit accuracy in the reliability index β_{direct} as soon as $M \geq 2$, which corresponds approximately to $\bar{\epsilon} \leq 10\%$.

For each value of M , β_{SSFEM} converges to β_{direct} when the order p of the polynomial chaos expansion is increased. At least $p = 3$ should be selected to have 5% accuracy in the reliability index.

It is noted that for the finite element model under consideration (which has 198 degrees of freedom), the maximum size of the polynomial chaos basis that leads to reasonable computation times is $P=21$. This corresponds to $(M = 2, p = 5)$. The size of the resulting SSFEM system of equations is $198 \times 21 = 4148$.

Table 5.2: Influence of the orders of expansion M and p - SSFEM approach

M	β_{direct}	p	P	β_{SSFEM}
1	2.694	1	2	4.665
		2	3	3.008
		3	4	2.741
		4	5	2.685
		5	6	2.681
2	2.631	1	3	4.510
		2	6	2.904
		3	10	2.656
		4	15	2.611
		5	21	2.614
3	2.627	1	4	4.487
		2	10	2.889
		3	20	2.645
4	2.627	1	5	4.480
		2	15	2.885

3.3 Influence of the threshold in the limit state function

In this section, the accuracy of SSFEM for increasing values of the reliability index is investigated. The order of expansion is $M = 2$ ($\bar{\varepsilon} = 0.129$) and the coefficient of variation of the input is 0.2. The reliability index is computed for different thresholds of maximum settlement u by means of direct coupling and SSFEM (different orders of polynomial chaos expansion are used in this case). Results are reported in Table 5.3.

When direct coupling is used, it is observed that the number of iterations required by the iHLRF algorithm to get the design point increases with β_{direct} . However the accuracy of the results does not depend on the value of β (the same computations have been carried out using 3 terms in the Karhunen-Loève expansion; the results are equal to those given in Table 5.3 with less than 1% discrepancy).

When using SSFEM up to order 5, it appears that fair results (*i.e.* less than 5% discrepancy between β_{SSFEM} and β_{direct}) are obtained only for $u \leq 20$ cm ($\beta \approx 4$). For $\beta \geq 5$, a good accuracy using SSFEM would require higher orders of expansion ($p > 5$), which becomes intractable in our example. Moreover, the example was cooked up so that $M = 2$ provides a sufficient accuracy in the discretization, which then allows to use up to 5-th order polynomial chaos expansions. Usually, the number of random variables necessary to get a good discretization is larger (*e.g.* ≥ 4), and only the second

order SSFEM method would be practically applicable. From Table 5.3, it is seen that, on the present example, the *second order* SSFEM method gives a fair estimation of the reliability index only if the latter is less or equal then 4.

It is noticed that, if the SSFEM program was implemented in a fully compiled language, and thus much faster than the current implementation in MATLAB, one or two additional orders in the polynomial chaos expansion may be affordable. In any case, there would be a limit value for β for which the results are no more accurate.

As a conclusion, the estimation of large reliability indices by direct coupling requires possibly additional iterations, but this corresponds to a constant order of magnitude of the computer processing time. In contrast, using SSFEM in this context requires increasing the order of expansion p , leading rapidly to intractable calculations.

Table 5.3: Influence of the threshold in the limit state function - Direct coupling and SSFEM results

u (cm)	β_{direct}	# Iterations	p	β_{SSFEM}
6	0.553	4	1	0.392
			2	0.504
			3	0.564
			4	0.564
			5	0.552
8	1.856	6	1	2.451
			2	1.859
			3	1.821
			4	1.842
			5	1.858
10	2.631	7	1	4.509
			2	2.904
			3	2.655
			4	2.610
			5	2.614
12	3.143	7	1	6.568
			2	3.787
			3	3.298
			4	3.161
			5	3.126
15	3.648	10	1	9.656
			2	4.926
			3	4.065
			4	3.782
			5	3.674
20	4.139	12	1	14.803
			2	6.523
			3	5.054
			4	4.535
			5	4.304
30	4.601	13	1	25.096
			2	9.093
			3	6.498
			4	5.564
			5	5.118

3.4 Influence of the correlation length of the input

In this section, the case of short correlation length of the input random field is investigated. The random field representing the Young's modulus is one-dimensional along the depth and its correlation length is 10 m. The coefficient of variation of the field is 0.2 and the threshold in the limit state function is $u_o = 10$ cm. The reliability index is computed for different orders of expansion M (direct coupling) and different orders of polynomial chaos expansion p (SSFEM). Results are reported in Table 5.4 together with the mean of the error variance $\bar{\epsilon}$ of the discretized field.

Table 5.4: Influence of the correlation length of the input random field ($\ell = 10$ m) - Direct coupling and SSFEM results

M	$\bar{\epsilon}$	β_{direct}	p	β_{SSFEM}
1	0.550	3.441	1	6.198
			2	3.978
			3	3.583
			4	3.474
			5	3.443
2	0.335	3.215	1	5.778
			2	3.690
			3	3.327
			4	3.232
			5	3.208
3	0.232	3.181	1	5.671
			2	3.625
			3	3.277
4	0.175	3.180	1	5.646
			2	3.608
5	0.140	3.179	-	-
10	0.071	3.179	-	-

When comparing column#2 of Table 5.4 with column#2 of Table 5.1 (which corresponds to $\ell = 30$ m), it is seen that, in order to get an acceptable discretization error, a larger number of terms M is now required. However, as soon as $M \geq 5$, *i.e.*, $\bar{\epsilon} < 14\%$, a two-digit accuracy on the reliability index is obtained when direct coupling is used.

When using SSFEM, it appears that fair results (*i.e.* less than 5% discrepancy between β_{SSFEM} and β_{direct}) are obtained as soon as $M \geq 2-3$, and $p \geq 3$. Higher orders of polynomial chaos expansion are intractable.

As a conclusion, the direct coupling approach is applicable whatever the correlation length of the field, because it is still computationally inexpensive even when $M = 10$ or more. In contrast, it would not be possible to apply SSFEM with $p > 2$ when M is more than 10, which means that the obtained reliability index would probably be inaccurate.

3.5 Influence of the coefficient of variation of the input

In this section, the order of expansion M is set equal to 2 and the threshold in the limit state function is $u = 20$ cm. The reliability index is computed for different coefficients of variation of the input random field. Results are reported in Table 5.5.

When the direct coupling is used, convergence of the iHLRF algorithm is always obtained, the number of iterations required varying from 4 to 12 depending on the level of β (the higher β , the more iterations). The values obtained are within 1% of those obtained with $M = 3$. It is observed that the reliability index strongly decreases when the variability of the input increases.

When SSFEM is used, bad results are obtained for $\delta_E = 0.1$ as expected, because this value induces a relatively large reliability index (see Section 3.3). For larger δ_E however, the results are not very good either. Some FORM analyses carried out after SSFEM do not converge, some others converge to a wrong design point, especially when the order of the polynomial chaos is large. This may be explained by the fact that the polynomial response surface associated with SSFEM is undulatory in this case (due to higher order polynomials) and may have several local design points. As an example, for the case of $\delta_E = 0.4$, it is observed that the convergence to the true reliability index is not monotonic with increasing p . Thus the result obtained for a given order cannot be *a priori* positioned with respect to the true value.

From these examples, it appears that SSFEM coupled with FORM cannot be applied safely for large coefficients of variation of the input (*e.g.* $\delta_E > 0.3$), whereas the results obtained by the direct coupling are reliable whatever δ_E .

3.6 One-dimensional vs. two-dimensional random fields

As mentioned in Section 3.1, the random field modeling of the Young's modulus was *one-dimensional* in the previous applications. This was necessary to get an acceptable discretization error $\bar{\epsilon}$ with a manageable number of terms in the expansion ($M = 2-3$).

The random field is now considered to be *two-dimensional* and *isotropic*, with a correlation length $\ell = 30$ m. The coefficient of variation of the field is set equal to 0.2 and the threshold in the limit state function is $u = 10$ cm. The direct coupling and the SSFEM

Table 5.5: Influence of the coefficient of variation of the input random field - Direct coupling and SSFEM results ($M = 2$)

δ_E	β_{direct}	p	β_{SSFEM}
0.1	8.277	1	30.706
		2	13.769
		3	10.702
		4	9.578
		5	9.043
0.2	4.132	1	14.803
		2	6.523
		3	5.054
		4	4.535
		5	4.303
0.3	2.759	1	9.257
		2	3.925
		3	2.994
		4	2.666
		5	2.467
0.4	2.069	1	6.301
		2	2.455
		3	1.708
		4	0.807 [†]
		5	2.045 [†]
0.5	1.655	1	4.380
		2	1.370
		3	3.062
		4	1.592 [†]
		5	1.227

[†] For these values, the iHLRF algorithm applied after SSFEM has not converged after 30 iterations.

method are applied with different orders of expansion M and p . Results are reported in Table 5.6

It can be seen from column #2 that the discretization error $\bar{\epsilon}$ is much larger than that obtained for a one-dimensional random field. For instance, even 50 terms in the Karhunen-Loève expansion do not allow to have $\bar{\epsilon} < 5\%$.

The direct coupling can still be applied up to this order of expansion though. In-

Table 5.6: Influence of the choice of a one-dimensional *vs.* two-dimensional input random field - Direct coupling and SSFEM results

M	$\bar{\epsilon}$	β_{direct}	p	β_{SSFEM}
1	0.586	4.212	1	7.647
			2	4.924
			3	4.427
			4	4.281
			5	4.232
2	0.442	3.271	1	5.823
			2	3.748
			3	3.387
			4	3.293
			5	3.269
3	0.362	3.239	1	5.736
			2	3.692
			3	3.343
4	0.303	3.019	1	5.303
			2	3.414
			3	3.098
5	0.273	2.946	-	-
10	0.177	2.876	-	-
50	0.059	2.826	-	-

deed, as it will be explained in Section 3.7, the computation time for direct coupling is approximately linear with M . The best result obtained with direct coupling here is $\beta_{direct} = 2.826$, which is probably a slight over-estimate of the true reliability index.

In contrast, as already mentioned above, SSFEM is limited to a rather small order of expansion in practice, and thus gives poor results in the case under consideration in this section: the best result obtained by the method is here for $M = 4$ and $p = 3$ yielding $\beta_{SSFEM} = 3.098$, which means at best 10% accuracy in the reliability index.

3.7 Evaluation of the efficiency

In this section, a comparison between the computer processing time (CPT) required by the direct coupling and the SSFEM methods is carried out. CPT corresponding to the set of parameters used in Section 3.2 are reported in Table 5.7. The bold characters correspond to choices of parameters (M, p) giving a fair estimation of the reliability

index.

Table 5.7: Computer processing time required by direct coupling and SSFEM methods - Gaussian random fields

M	CPT † Direct Coupling (")	p	CPT† SSFEM (")
1	20.6	1	2.3
		2	2.5
		3	3.2
		4	4.0
		5	4.8
2	33.6	1	3.9
		2	8.0
		3	22.6
		4	58.2
		5	129.0
3	43.7	1	4.7
		2	30.3
		3	296.4
		4	1888.7
4	53.8	1	8.7
		2	127.4
5	65.8	1	11.4

† The CPT for a deterministic finite element run with constant Young's modulus was 0.57".

From column #2 of Table 5.7, one can see that the CPT required by the direct coupling is increasing linearly with the order of expansion M . This can be easily explained: the only step that is modified in the finite element analysis when M is changed is the computation of the element stiffness matrices. Each of these matrices requires the evaluation of the random field realization at four points (the Gauss points), and each evaluation takes a time exactly proportional to the order of expansion M (See Eq.(4.4)). The number of gradients computed is also proportional to M .

In contrast, when using SSFEM, the CPT increases extremely fast with the order of the polynomial chaos expansion. Thus the method can be efficiently applied only when a small number of terms M allows to describe the random field accurately, and when the reliability index under consideration is sufficiently small so that the second order SSFEM already gives a fair estimate.

3.8 Application of importance sampling

3.8.1 Introduction

The SSFEM approach allows to get an approximation of the random response of the structure in terms of polynomials in standard normal variables, see Eq.(3.1). In the context of reliability analysis, this allows to define *analytical* limit state functions, as described in Chapter 3, Section 5.3.

With such an expression, all kinds of methods can be used to determine the probability of failure of the system. So far, only the first-order reliability method (FORM) has been applied. It could be argued that FORM is not the better way of post-processing the SSFEM results, since:

- the analytical polynomial expression of the limit state function contains information that is lost when the linearization resulting from FORM is used.
- the limit state surface obtained from SSFEM could be globally accurate, however not necessarily around the true design point, which means that applying FORM could give poor results.

Moreover, since the limit state function is inexpensive to evaluate due to its analytical expression, simulation methods such as importance sampling become attractive.

3.8.2 Numerical results

An importance sampling routine has been developed in MATLAB in order to post-process the SSFEM results after FORM analysis. The sampling probability density function is Gaussian with unit standard deviation and it is centered on the design point determined by FORM.

The same choice of parameters as in Section 3.2 is made in the current section. For each order of expansion M (resp. p), importance sampling is applied using 10,000 samples. The obtained probability of failure is then transformed into the reliability index β_{SSFEM}^{IS} for comparison purposes. The results are gathered in Table 5.8.

The first-order reliability method is exact for $M = 1$ whatever p (because the limit state surface is reduced to a single point), and when $p = 1$ whatever M (because the limit state surface is an hyperplane). For all these cases, it can be seen in Table 5.8 that importance sampling gives exactly the same results as FORM (the last-digit discrepancy being explained by the fact that only 10,000 samples are used in the simulation).

Table 5.8: Post-processing of the SSFEM results - Comparison between FORM and importance sampling

M	p	β_{SSFEM}^{FORM}	β_{SSFEM}^{IS}
1	1	4.665	4.669
	2	3.008	3.012
	3	2.741	2.738
	4	2.685	2.689
2	1	4.510	4.515
	2	2.904	2.891
	3	2.656	2.633
	4	2.611	2.578
	5	2.614	2.580
3	1	4.487	4.490
	2	2.889	2.872
	3	2.645	2.608

Significant discrepancies between the two approaches appear only for higher orders of polynomial chaos expansion, *e.g.*, $p \geq 3$. In any case, they do not exceed 2% of the value of the reliability index, which means that the FORM result is satisfactory in all cases.

From this short study, the following conclusions can be drawn :

- for the example under consideration, the limit state surface defined analytically after the SSFEM analysis is sufficiently smooth so that the first-order reliability method gives good results.
- after having determined the design point by FORM, importance sampling allows to evaluate more accurately the probability of failure at low cost, due to the analytical definition of the limit state function.
- the fact that β_{SSFEM}^{FORM} and β_{SSFEM}^{IS} are close indicates that errors observed in the reliability estimates by SSFEM in the previous sections are due to the truncation of the polynomial chaos expansions and not due to the FORM approximation.

3.9 Probability distribution function of a response quantity

As already mentioned, after the SSFEM solution is obtained, any additional reliability analysis is computationally inexpensive due to the fact that the limit state function is

defined analytically and thus easy to evaluate. This allows to compute at low cost the probability density function of a response quantity, as described in Chapter 3, Section 5.4.

As an example, the PDF of the nodal displacement U_A (corresponding to the maximum settlement) is plotted in Figure 5.1. 200 points are used, *i.e.*, 200 reliability problems are solved¹. To improve the efficiency, the starting point of each analysis is chosen as the design point of the previous analysis. This allows convergence of the iHLRF algorithm within 3 iterations.

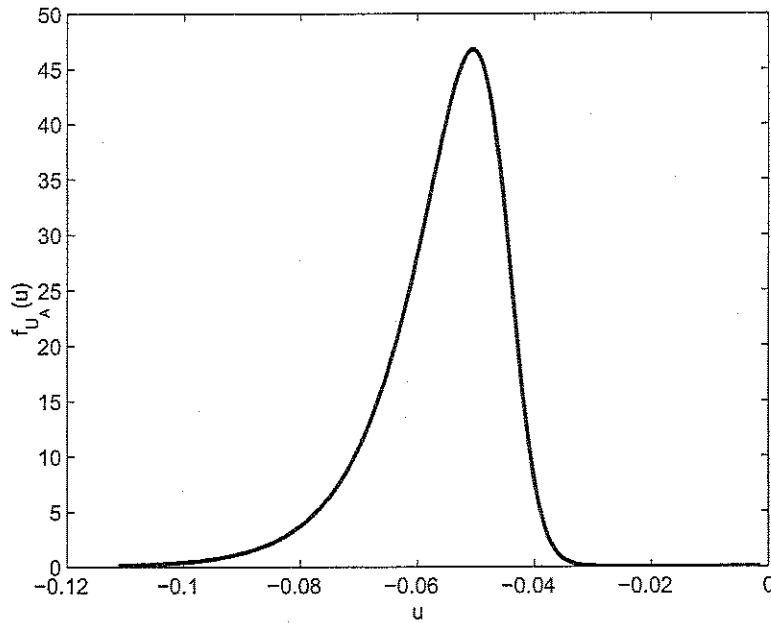


Figure 5.1: Probability density function of the maximum displacement obtained by multiple FORM analyses after SSFEM

It can be seen that the obtained PDF has its mode close to $u_o = -5.42$ cm (which is the value obtained from a deterministic finite element analysis) and that it looks like a lognormal distribution, in agreement with the results of Chapter 4, Section 4.2. It should be emphasized that the far tails of the PDF computed by this method may be inaccurate, as observed in Section 3.3.

3.10 Conclusions

From the above comprehensive parametric study, the following conclusions can be drawn :

¹This is done in a matter of seconds on a personal computer.

- The reliability index β_{direct} obtained by direct coupling of the iHLRF algorithm and a deterministic finite element code converges to a limit when the discretization error $\bar{\epsilon}$ tends to zero. This convergence is always obtained by upper values. As soon as $\bar{\epsilon} \leq 10\%$, the method gives a 2-digit accuracy for β , whatever its value (at least in the range $[0.5, 8]$ that has been considered).

The CPT for each iteration is increasing linearly with the order of expansion M . When an accurate discretization of the random field requires a large order of expansion (*e.g.* $M = 50$), the method is still applicable.

The number of iterations in the iHLRF algorithm tends to increase with the value of β (from 4 to 13 in our examples).

The accuracy of the first-order reliability index is insensitive to the coefficient of variation of the field.

- Generally speaking, the reliability index β_{SSFEM} obtained for a given discretization error $\bar{\epsilon}$ (*i.e.* a given M) converges to β_{direct} when the order p of the polynomial chaos increases. This means that SSFEM may be applicable in some cases to solve reliability problems. However, this convergence presents an unstable behavior, which makes the method unreliable.

When $\beta \approx 2 - 3$, the value $p = 3$ is required to get 5% accuracy on the result (Section 3.2). When β is larger ($\beta \approx 4 - 8$, Section 3.3), the convergence is much slower and $p = 3$ yields more than 15% error on β .

In practice, the size of the polynomial chaos basis was limited to $P = 21$ to get reasonable computer processing times². This makes the method inapplicable :

- when the correlation length of the input random field is small to medium, because of the large number of terms required in the Karhunen-Loève expansion for a fair discretization (Section 3.6).
- when the reliability index is large, because of the high order of the polynomial chaos expansion required.

Furthermore, when large coefficients of variation of the input are used ($\delta_E \geq 0.3$), the SSFEM approach followed by FORM may not converge or may converge to a wrong result (Section 3.5).

Finally, it is noted that importance sampling after FORM analysis is inexpensive to carry out due to the analytical expression of the limit state function. Thus it allows to refine the evaluation of the probability of failure of the system at low cost.

²Slightly greater values can certainly be obtained in a fully compiled implementation. However, this does not change fundamentally the conclusions.

- When both methods are employed and give the same results, the SSFEM analysis can be post-processed to compute the PDF of the response quantity appearing in the limit state function (see derivations in Chapter 3, Section 5.4). It can also be used to perform several FORM analyses with different limit-state functions. This seems to be the only case where SSFEM could give something more than the direct coupling approach. The direct coupling results are needed however in order to check the validity of the SSFEM solution.

4 Settlement of a foundation over an elastic soil mass - Lognormal input random field

4.1 Introduction

In this section, the direct coupling and SSFEM methods are applied together with a *one-dimensional lognormal* random field modeling the Young's modulus of the material.

As far as direct coupling is concerned, the only difference with the preceding section is the way the random field realizations are evaluated in FEMRF: Eq.(4.5) is now used instead of Eq.(4.4). As far as SSFEM is concerned, the introduction of lognormal fields requires the stiffness matrices to be expanded into the polynomial chaos, as explained in Part I, Chapter 5, Section 4.1.

It is emphasized that the discretization of the random field is not exactly identical for the two approaches. When using the direct coupling, it corresponds to the exponentiation of a truncated series expansion of a Gaussian field. When using SSFEM, it corresponds to a truncated polynomial chaos expansion such as that described in Part I, Chapter 5, Section 4.1.

The deterministic problem under consideration is the same as in Section 3. The mean value and coefficient of variation of the Young's modulus are $\mu_E = 50$ MPa and $\delta_E = 0.2$ respectively. The autocorrelation function is exponential, the correlation length in each direction being $\ell_x = 10000$ m and $\ell_y = 30$ m respectively. The threshold in the limit state function is $u = 10$ cm.

The parametric study presented in this section is limited to the influence of the orders of expansion on the reliability index, as well as the threshold in the limit state function. Indeed, it is believed that the poor results obtained in Section 3 for small correlation length and/or large coefficient of variation of the field would not be better when a lognormal field is considered.

4.2 Influence of the orders of expansion

The reliability index is computed by both approaches for different orders of expansion M and p , the results are reported in Table 5.9.

Table 5.9: Influence of the orders of expansion M and p - Lognormal input random field

M	β_{direct}	p	P	β_{SSFEM}
1	3.528	1	2	4.717
		2	3	3.714
		3	4	3.569
		4	5	3.561
		5	6	3.560
2	3.452	1	3	4.562
		2	6	3.617
		3	10	3.474
		4	15	3.467
3	3.447	1	4	4.539
		2	10	3.606
4	3.447	1	5	4.532
		2	15	3.603

Focusing on column #2, it appears that the direct approach gives a 2-digit accuracy for the reliability index as soon as $M \geq 2$, as in the case of Gaussian input random field.

Broadly speaking, β_{SSFEM} tends to β_{direct} when the order of the polynomial chaos expansion p increases. However, there seems to be a slight discrepancy in the limit. For instance, for $M=1$, β_{SSFEM} converges to 3.560 instead of 3.528. This comes from the fact that the representations of the lognormal field are not identical in the two approaches, as mentioned above.

4.3 Influence of the threshold in the limit state function

In this section, the accuracy of SSFEM for increasing values of the reliability index is investigated. The order of expansion of the input random field is $M = 2$. The reliability index is computed for different thresholds of maximum settlement u by means of direct coupling and SSFEM (different orders of polynomial chaos expansion are used in this case). Results are reported in Table 5.10.

Table 5.10: Influence of the threshold in the limit state function - Lognormal input random field

u (cm)	β_{direct}	# Iterations	p	β_{SSFEM}
6	0.473	4	1	0.401
			2	0.477
			3	0.488
			4	0.488
8	2.152	6	1	2.481
			2	2.195
			3	2.165
			4	2.166
10	3.452	6	1	4.562
			2	3.617
			3	3.474
			4	3.467
12	4.514	6	1	6.642
			2	4.858
			3	4.559
			4	4.534
15	5.810	7	1	9.763
			2	6.494
			3	5.918
			4	5.846
20	7.480	7	1	14.964
			2	8.830
			3	7.737
			4	7.561
30	9.829	8	1	25.367
			2	12.655
			3	10.475
			4	10.044

When direct coupling is used, it is observed that the number of iterations required by the iHLRF algorithm to get the design point increases slightly with β_{direct} , however not as much as in the case of Gaussian fields (see Table 5.3). The accuracy of the results does not depend on the value of β (the same computations have been carried out using 3 terms in the Karhunen-Loève expansion; the results are equal to those given in Table 5.10 with less than 1% discrepancy).

As far as SSFEM is concerned, there is convergence of β_{SSFEM} to a limit when p increases. This limit is always slightly greater than β_{direct} because of the difference in the random field discretization schemes. It is noted that the convergence rate related to increasing p is better than in the Gaussian case. When using a 4-th order polynomial chaos expansion, the reliability index is obtained within 1-2% accuracy whatever its value.

In other words, SSFEM applied with lognormal random fields appears to be more reliable than in the case when it is applied with Gaussian fields. This is an interesting property, since lognormal fields are more suited to modeling material properties. The fact that the polynomial chaos expansion has to be used also for representing the input field seems not deteriorate the accuracy of the results.

4.4 Evaluation of the efficiency

The computer processing time required by both approaches is reported in Table 5.11 for different values of the orders of expansion M and p .

Table 5.11: Computer processing time required by direct coupling and SSFEM methods - Lognormal random fields

M	CPT Direct Coupling (")	p	CPT SSFEM (")
1	22.4	1	3.5
		2	5.5
		3	8.8
		4	16.6
		5	36.3
2	31.2	1	6.6
		2	23.1
		3	324.2
		4	2952.6
3	40.5	1	8.2
		2	188.2
4	49.8	1	11.6
		2	829.0
5	58.8	1	13.4

By comparing the results in Table 5.11 with those in Table 5.7, the following conclusions can be drawn :

- As far as direct coupling is concerned, almost the same CPT is observed, whether the random field is Gaussian or lognormal. This is explained by the fact that the only difference between the two calculations is an exponentiation operation each time the random field is evaluated.
- As far as SSFEM is concerned, the CPT reported in Table 5.11 are much greater than those reported in Table 5.7. There are two main reasons explaining this difference:
 - if N_e is the number of finite elements in the structural model, the Gaussian SSFEM method requires computing $(M + 1) \times N_e$ element stiffness matrices and assembling at first level $(M + 1)$ global stiffness matrices. In the lognormal case, these numbers are $P \times N_e$ and P respectively (P is the size of the polynomial chaos basis, see Eq.(5.58) in Part I). As it has been mentioned already, $P \gg M$ as soon as the order of the polynomial chaos expansion p is large.
 - The second level of assembling requires more computational effort since, for a given pair (M, p) , there are much more non zero d_{ijk} -coefficients (related to the lognormal case) than c_{ijk} coefficients (related to the Gaussian case) in the summations (See Eq.(3.20)).

As a conclusion, for values of M and p for which β_{SSFEM} is a fair estimate of the true reliability index, the computer processing time is so large that the SSFEM method is not efficient at all (see numbers printed in bold characters in Table 5.11).

4.5 Conclusions

The parametric study carried out using lognormal input random fields has shown that :

- the direct coupling gives accurate results, whatever the value of the reliability index, at a cost similar to that obtained when using Gaussian fields.
- the SSFEM method gives better results with lognormal fields than with Gaussian random fields. Using a 4-th order polynomial chaos expansion allows to get 1-2% accuracy on the reliability index. However, the computation time in this case is huge compared to that of the direct coupling (about 100 times when $M = 2$). Practically the method could be applied only when the correlation length is large, so that the Karhunen-Loève expansion with $M = 1 - 2$ terms would be sufficiently accurate. Otherwise, SSFEM is inappropriate due to the huge computation required for obtaining a fair estimate of the reliability index.

5 Conclusions

In this chapter, reliability problems have been solved using two different methods, namely the direct coupling between the iHLRF algorithm and a deterministic finite element code, and the SSFEM method post-processed by the same algorithm. Both methods have been applied to assess the serviceability of a foundation lying on an elastic heterogeneous soil layer. The Young's modulus of the soil was successively modeled as a Gaussian and lognormal random field.

The case of Gaussian random fields with exponential autocorrelation function has been investigated first, because this type of fields has been extensively used in the literature, however without convincing comparisons or appreciation of the results. It appears that a fair discretization of the field may require more than a few terms, even when the correlation length is not small. The accuracy in the discretization turns out to be a key issue. It is noted that this point is never discussed in the papers making use of this kind of expansions together with SSFEM.

Whatever the parameters, the direct coupling appears robust and fast, the cost of the analysis increasing linearly with the order of expansion of the input random field.

As far as SSFEM is concerned, fair results can sometimes be obtained, usually using a high order polynomial chaos expansion ($p = 3 - 5$). When more than 2 terms are used in the random field discretization, the cost becomes rapidly prohibitive. Consequently, only results obtained with a low order polynomial chaos expansion are available in this case. They appear poor compared to those obtained by direct coupling. In some cases, the computed reliability index may not even be correct (for instance when large coefficients of variation of the input are considered).

The case of lognormal random fields has been investigated as well. The direct coupling provides reliable results, approximately at the same cost as in the Gaussian case. The SSFEM approach appears more stable than in the Gaussian case. However the computation cost for a given choice of (M, p) is even greater than in the Gaussian case (practically, the size of the polynomial chaos basis was limited to $P = 15$ in our calculations).

As a conclusion, the direct coupling appears far better than the SSFEM approach for solving reliability problems, because it is robust and fast. The SSFEM approach could however be applied *together with* the direct coupling in some cases (*i.e.* when it has proven accurate for the selected parameters) to compute probability distribution functions of response quantities in an efficient way, or to determine reliability indices for multiple response quantities.

Chapter 6

Conclusion

The goal of the second part of the present study was to compare different methods taking into account spatial variability of the material properties in the mechanical analysis. In order to be able to compare a broad spectrum of methods, attention has been focused on elastic two-dimensional problems. For this purpose, different routines have been developed in the MATLAB environment, namely :

- a random field discretization toolbox,
- a deterministic finite element code called FEMRF, which takes into account the spatial variability of the Young's modulus in elastic mechanical analysis,
- a software implementing the SSFEM method (including an original implementation of the polynomial chaos),
- the iHLRF algorithm for finding the design point in FORM analysis,
- additional routines for perturbation analysis, Monte Carlo simulation and importance sampling.

The detailed implementation of the programs has been presented in Chapters 2-3. An object-oriented programming was aimed at, in order to get easily extensible code.

The different programs were applied to compute the moments of the response of a foundation lying on an elastic soil layer (up to second order), as well as to assess its serviceability with respect to a maximum settlement criterion.

As far as second moment analysis is concerned, both the second-order perturbation and SSFEM methods provide good results, whatever the coefficient of variation of the input

random field. However, the former turns out to be computationally more efficient because of the special form it takes for the considered application.

As far as reliability analysis is concerned, the direct coupling turns out to be far better than SSFEM, because it provides excellent accuracy whatever the type of random field and the selected parameters. SSFEM can give fair results in some cases, but usually at a cost much greater than that of the direct coupling. Unfortunately, in some cases, it converges to a wrong solution, which makes it unreliable.

It is noted that the perturbation method and the direct coupling approach have a far larger scope than SSFEM, since they have been applied to all kinds of non-linear problems, whereas SSFEM is still more or less limited to linear problems.

As a conclusion, it is noted that the present study is the first attempt to compare a broad spectrum of stochastic finite element methods on a given application. Throughout the description of the implementation, it has been seen that these methods have more in common than what the different research communities involved in their development sometimes think, at least from a computational point of view. Of course, a single example (*i.e.*, the problem of the settlement of a foundation) cannot be used to draw general conclusions of the superiority of some methods over others, but it gives at least a new light on their respective advantages and shortcomings.

Bibliography

- Abdo, T. and Rackwitz, R., 1990, A new β -point algorithm for large time invariant and time-variant reliability problems, in *Reliability and Optimization of Structures, Proc. 3rd WG 7.5 IFIP conference, Berkeley*.
- Anders, M. and Hori, M., 1999, Stochastic finite element method for elasto-plastic body, *Int. J. Num. Meth. Eng.*, **46**, 11, 1897–1916.
- Baecher, G.-B. and Ingra, T.-S., 1981, Stochastic finite element method in settlement predictions, *J. Geotech. Eng. Div., ASCE*, **107**, 4, 449–463.
- Baldeweck, H., 1999, Méthodes des éléments finis stochastiques - applications à la géotechnique et à la mécanique de la rupture, Ph.D. thesis, Université d'Evry-Val d'Essonne, France, 195 pages.
- Breitung, K., 1984, Asymptotic approximation for multinormal integrals, *J. Eng. Mech., ASCE*, **110**, 3, 357–366.
- Brenner, C. and Bucher, C., 1995, A contribution to the SFE-based reliability assessment of non linear structures under dynamic loading, *Prob. Eng. Mech.*, **10**, 4, 265–273.
- Bucher, C.-G. and Bourgund, U., 1990, A fast and efficient response surface approach for structural reliability problems, *Struct. Safety*, **7**, 57-66.
- Cornell, C.-A., 1969, A probability-based structural code, *J. American Concrete Institution*, **66**, 974-985.
- Das, P.-K. and Zheng, Y., 2000, Cumulative formation of response surface and its use in reliability analysis, *Prob. Eng. Mech.*, **15**, 4, 309–315.
- Defaux, G. and Heinfing, G., 2000, Reliability of natural-draught hyperbolic cooling towers using a 3D finite element analysis coupled with probabilistic methods, in *Proc. 8th ASCE specialty Conference on Probabilistic Mechanics and Structural Reliability*.
- Demmel, J.-W., 1997, *Applied numerical linear algebra*, Society for Industrial and Applied Mathematics (SIAM), Philadelphia.

- Deodatis, G., 1990, Bounds on response variability of stochastic finite element systems, *J. Eng. Mech., ASCE*, **116**, 3, 565–585.
- Deodatis, G., 1991, The weighted integral method, I : stochastic stiffness matrix, *J. Eng. Mech.*, **117**, 8, 1851–1864.
- Deodatis, G. and Shinozuka, M., 1991, The weighted integral method, II : response variability and reliability, *J. Eng. Mech.*, **117**, 8, 1865–1877.
- Der Kiureghian, A. and de Stefano, M., 1991, Efficient algorithms for second order reliability analysis, *J. Eng. Mech., ASCE*, **117**, 12, 2906–2923.
- Der Kiureghian, A. and Ke, J.-B., 1985, Finite element based reliability analysis of frame structures, in *Proc. 4th Int. Conf. Structural Safety and Reliability*, 385–404.
- Der Kiureghian, A. and Ke, J.-B., 1988, The stochastic finite element method in structural reliability, *Prob. Eng. Mech.*, **3**, 2, 83–91.
- Der Kiureghian, A., Lin, H.-Z., and Hwang, S.-J., 1987, Second order reliability approximations, *J. Eng. Mech., ASCE*, **113**, 8, 1208–1225.
- Der Kiureghian, A. and Liu, P.-L., 1986, Structural reliability under incomplete probability information, *J. Eng. Mech., ASCE*, **112**, 1, 85–104.
- Der Kiureghian, A. and Taylor, R.-L., 1983, Numerical methods in structural reliability, in *Proc. 4th Int. Conf. on Appl. of Statistics and Probability in Soil and Structural Engineering*, 769–784.
- Der Kiureghian, A. and Zhang, Y., 1999, Space-variant finite element reliability analysis, *Comp. Meth. Appl. Mech. Eng.*, **168**, 173–183.
- Ditlevsen, O., 1996, Dimension reduction and discretization in stochastic problems by regression method, in F. Casciati and B. Roberts, Editors, *Mathematical models for structural reliability analysis, CRC Mathematical Modelling Series*, 2, 51–138.
- Ditlevsen, O. and Madsen, H., 1996, *Structural reliability methods*, J. Wiley and Sons, Chichester.
- Faravelli, L., 1989, Response surface approach for reliability analysis, *J. Eng. Mech.*, **115**, 12, 2763–2781.
- Ghanem, R.-G., 1998a, Hybrid stochastic finite elements and generalized Monte Carlo simulation, *J. Appl. Mech., ASME*, **65**, 1004–1009.
- Ghanem, R.-G., 1998b, Probabilistic characterization of transport in heterogeneous media, *Comp. Meth. Appl. Mech. Eng.*, **158**, 199–220.

- Ghanem, R.-G., 1999a, Ingredients for a general purpose stochastic finite elements implementation, *Comp. Meth. Appl. Mech. Eng.*, **168**, 19–34.
- Ghanem, R.-G., 1999b, The nonlinear gaussian spectrum of log-normal stochastic processes and variables, *J. Appl. Mech., ASME*, **66**, 964–973.
- Ghanem, R.-G., 1999c, Stochastic finite elements with multiple random non-Gaussian properties, *J. Eng. Mech., ASCE*, **125**, 1, 26–40.
- Ghanem, R.-G. and Brzkala, V., 1996, Stochastic finite element analysis of randomly layered media, *J. Eng. Mech.*, **122**, 4, 361–369.
- Ghanem, R.-G. and Kruger, R., 1996, Numerical solution of spectral stochastic finite element systems, *Comp. Meth. Appl. Mech. Eng.*, **129**, 3, 289–303.
- Ghanem, R.-G. and Spanos, P.-D., 1990, Polynomial chaos in stochastic finite elements, *J. App. Mech., ASME*, 197–202.
- Ghanem, R.-G. and Spanos, P.-D., 1991a, Spectral stochastic finite-element formulation for reliability analysis, *J. Eng. Mech.*, **117**, 10, 2351–2372.
- Ghanem, R.-G. and Spanos, P.-D., 1991b, *Stochastic finite elements - A spectral approach*, Springer Verlag.
- Grandhi, R.-V. and Wang, L., 1999, Higher-order failure probability calculation using non linear approximations, *Comp. Meth. Appl. Mech. Eng.*, **168**, 185–206.
- Haldar, A. and Mahadevan, S., 2000, *Reliability Assessment Using Stochastic Finite Element Analysis*, John Wiley and Sons.
- Handa, K. and Andersson, K., 1981, Application of finite element methods in the statistical analysis of structures, in *Proc. 3rd Int. Conf. Struct. Safety and Reliability, ICOSSAR'81*, 409–420.
- Hasofer, A.-M. and Lind, N.-C., 1974, Exact and invariant second moment code format, *J. Eng. Mech., ASCE*, **100**, 1, 111–121.
- Hisada, T. and Nakagiri, S., 1981, Stochastic finite element method developed for structural safety and reliability, in *Proc. 3rd Int. Conf. Struct. Safety and Reliability, ICOSAR'81*, 395–408.
- Hisada, T. and Nakagiri, S., 1985, Role of stochastic finite element method in structural safety and reliability, in *Proc. 4th Int. Conf. Struct. Safety and Reliability, ICOSAR'85*, 385–395.
- Hohenbichler, M. and Rackwitz, R., 1981, Non normal dependent vectors in structural safety, *J. Eng. Mech., ASCE*, **107**, 6, 1227–1238.

- Hornet, P., Pendola, M., and Lemaire, M., 1998, Failure probability calculation of an axisymmetrically cracked pipe under pressure and tension using a finite element code, *PVP, Fatigue, Fracture and Residual Stresses*, **373**, 3-7.
- Hurtado, J.-E. and Alvarez, D.-A., 2000, Reliability assessment of structural systems using neural networks, in *Proc. European Congress on Computational Methods in Applied Sciences and Engineering, ECCOMAS 2000 (Barcelona, 11-14 Sept. 2000)*, paper #290.
- Kim, S.-H. and Na, S.-W., 1997, Response surface method using vector projected sampling points, *Struct. Safety*, **19**, 1, 3-19.
- Kleiber, M., Antúnez, H., Hien, T.-D., and Kowalczyk, P., 1997, *Parameter sensitivity in nonlinear mechanics*, J. Wiley and sons, Chichester.
- Kleiber, M. (Editor), 1999, Computational stochastic mechanics, *Comp. Meth. Appl. Mech. Eng.*, **168**, (special issue).
- Knabe, W., Przewłócki, J., and Różyński, 1998, Spatial averages for linear elements for two-parameter random fields, *Prob. Eng. Mech.*, **13**, 3, 147-167.
- Lawrence, M., 1987, Basis random variables in finite element analysis, *Int. J. Num. Meth. Eng.*, **24**, 1849-1863.
- Lemaire, M., 1997, Finite element and reliability : combined methods by surface response, in G.-N. Frantziskonis, Editor, *Probamat-21st Century, Probabilities and Materials : Tests, Models and Applications for the 21st century*, 317-331, Kluwer Academic Publishers.
- Lemaire, M., 1998, Eléments finis et fiabilité : un mariage à la mode, in A. Mebarki, D. Boissier, and D. Breysse, Editors, *Fiabilité des matériaux et des structures - FIAB'98*.
- Lemaitre, J. and Chaboche, J., 1990, *Mechanics of solid materials*, Cambridge University Press.
- Li, C.-C. and Der Kiureghian, A., 1993, Optimal discretization of random fields, *J. Eng. Mech.*, **119**, 6, 1136-1154.
- Lin, Y.-K., 1967, *Probabilistic theory of structural dynamics*, McGraw-Hill, chap. 1-4.
- Liu, P. and Liu, K., 1993, Selection of random field mesh in finite element reliability analysis, *J. Eng. Mech., ASCE*, **119**, 4, 667-680.
- Liu, P.-L. and Der Kiureghian, A., 1986, Multivariate distribution models with prescribed marginals and covariances, *Prob. Eng. Mech.*, **1**, 2, 105-112.

- Liu, P.-L. and Der Kiureghian, A., 1989, Finite element reliability methods for geometrically non linear stochastic structures, Tech. Rep. n° UCB/SEMM/89-05, University of California, Berkeley.
- Liu, P.-L. and Der Kiureghian, A., 1991a, Finite element reliability of geometrically non linear uncertain structures, *J. Eng. Mech., ASCE*, **117**, 8, 1806-1825.
- Liu, P.-L. and Der Kiureghian, A., 1991b, Optimization algorithms for structural reliability, *Struct. Safety*, **9**, 161-177.
- Liu, P.-L., Lin, H.-Z., and Der Kiureghian, A., 1989, CALREL user's manual, Tech. Rep. n° UCB/SEMM/89-18, University of California, Berkeley.
- Liu, W.-K., Belytschko, T., and Mani, A., 1986a, Probabilistic finite elements for non linear structural dynamics, *Comp. Meth. App. Mech. Eng.*, **56**, 61-86.
- Liu, W.-K., Belytschko, T., and Mani, A., 1986b, Random field finite elements, *Int. J. Num. Meth. Eng.*, **23**, 10, 1831-1845.
- Loève, M., 1977, *Probability theory*, Springer Verlag, New-York, 4th ed.
- Luenberger, D., 1986, *Introduction to linear and non linear programming*, Addison & Wesley, Reading, MA.
- Madsen, H.-O., 1988, Omission sensitivity factors, *Struct. Safety*, **5**, 35-45.
- Mahadevan, S. and Haldar, A., 1991, Practical random field discretization in stochastic finite element analysis, *Struct. Safety*, **9**, 283-304.
- Matthies, G., Brenner, C., Bucher, C., and Guedes Soares, C., 1997, Uncertainties in probabilistic numerical analysis of structures and solids - stochastic finite elements, *Struct. Safety*, **19**, 3, 283-336.
- Neveu, J., 1992, *Introduction aux probabilités*, Cours de l'Ecole Polytechnique.
- Pellisetti, M. and Ghanem, R.-G., 2000, Iterative solution of systems of linear equations arising in the context of stochastic finite elements, *Advances in Engineering Software*, **31**, 8-9, 607-616.
- Pendola, M., Châtelet, E., and Lemaire, M., 2000a, Finite element and reliability: combined method by response surface using neural networks, *Struct. Safety*, submitted for publication.
- Pendola, M., Hornet, P., and Mohamed, A., 2000b, Parametric study of the reliability of a cracked pipe using a non-linear finite element analysis, in R.E Melchers and M.G Stewart, Editor, *Proc. ICASP8 "Applications of Statistics and Probability to Civil Engineering Reliability and Risk Analysis"*, 1135-1141.

- Pendola, M., Mohamed, A., Lemaire, M., and Horner, P., 2000c, Combination of finite element and reliability methods in nonlinear fracture mechanics, *Reliability Engineering & System Safety*, **70**, 1, 15-27.
- Phoon, K., Quek, S., Chow, Y., and Lee, S., 1990, Reliability analysis of pile settlements, *J. Geotech. Eng., ASCE*, **116**, 11, 1717-1735.
- Rackwitz, R. and Fiessler, B., 1978, Structural reliability under combined load sequences, *Comput. Struct.*, **9**, 489-494.
- Rajashekhar, M.-R. and Ellingwood, B.-R., 1993, A new look at the response surface approach for reliability analysis, *Struct. Safety*, **12**, 205-220.
- Schuëller, G. (Editor), 1997, A state-of-the-art report on computational stochastic mechanics, *Prob. Eng. Mech.*, **12**, 4, IASSAR report.
- Spanos, P.-D. and Ghanem, R.-G., 1989, Stochastic finite element expansion for random media, *J. Eng. Mech., ASCE*, **115**, 5, 1035-1053.
- Takada, T., 1990a, Weighted integral method in multidimensional stochastic finite element analysis, *Prob. Eng. Mech.*, **5**, 4, 158-166.
- Takada, T., 1990b, Weighted integral method in stochastic finite element analysis, *Prob. Eng. Mech.*, **5**, 3, 146-156.
- Vanmarcke, E., 1983, *Random fields : analysis and synthesis*, The MIT Press, Cambridge, Massachusetts.
- Vanmarcke, E.-H. and Grigoriu, M., 1983, Stochastic finite element analysis of simple beams, *J. Eng. Mech., ASCE*, **109**, 5, 1203-1214.
- Waubke, H., 1996, Dynamische Berechnungen für den Halbraum mit streuenden Parametern mittels orthogonaler Polynome, Ph.D. thesis, Technische Universität, München.
- Wong, F.-A., 1985, Slope reliability and response surface method, *J. Geotech., ASCE*, **111**, 1, 32-53.
- Yamazaki, F. and Shinozuka, M., 1990, Simulation of stochastic fields by statistical preconditioning, *J. Eng. Mech., ASCE*, **116**, 2, 268-287.
- Zeldin, B.-A. and Spanos, P.-D., 1998, On random field discretization in stochastic finite elements, *J. App. Mech., ASME*, **65**, 320-327.
- Zhang, J. and Ellingwood, B., 1994, Orthogonal series expansion of random fields in reliability analysis, *J. Eng. Mech., ASCE*, **120**, 12, 2660-2677.

- Zhang, Y. and Der Kiureghian, A., 1993, Dynamic response sensitivity of inelastic structures, *Comp. Meth. Appl. Mech. Eng.*, **108**, 23-36.
- Zhang, Y. and Der Kiureghian, A., 1995, Two improved algorithms for reliability analysis, in R. Rackwitz, G. Augusti, and A. Borr, Editors, *Proc. 6th IFIP WG7.5 "Reliability and optimization of structural systems"*.
- Zhang, Y. and Der Kiureghian, A., 1997, Finite element reliability methods for inelastic structures, Tech. Rep. n° UCB/SEMM-97/05, University of California, Berkeley - Dpt of Civil Engineering.
- Zienkiewicz, O.-C. and Taylor, R.-L., 1989, *The finite element method*, McGraw-Hill, London.